Ph.D. Thesis

Université de Limoges

Université de Limoges

ED 609 - Sciences et Ingénierie des Matériaux, Mécanique, Énergétique (SIMME)

Institut de Recherche sur les Céramiques (IRCER) - UMR CNRS 7315

A thesis presented to obtain the degree of Doctor of the University of Limoges
Speciality: Matériaux céramiques et traitements de surface

Presented and defended by
Henrique SCHAPPO
On October 18, 2021

SELECTIVE LASER SINTERING OF UHMWPE/HA BIOCOMPOSITES FOR BONE TISSUE ENGINEERING

Advisors: **Chantal DAMIA et Dachamir HOTZA**

Co-advisors: **Karine GIRY et Gean SALMORIA**

JURY:

Reporters:

M David GROSSIN, Maitre de Conférences HDR, Institut National Polytechnique de Toulouse, France
M Wilson ACCHAR, Professeur des universités, Universidade Federal do Rio Grande do Norte, Brésil

Examiners:

M Bruno HENRIQUES, Professeur des universités, Universidade Federal de Santa Catarina, Brésil
Mme Chantal DAMIA, Maitresse de conférences HDR, Université de Limoges, France
Mme Cynthia WIRTH, PhD, Siemens Energy Global Allemagne
M Dachamir HOTZA, Professeur des universités, Universidade Federal de Santa Catarina, Brésil
M Fabrice ROSSIGNOL, Directeur de recherche CNRS, IRCER Limoges

Henrique Schappo

SELECTIVE LASER SINTERING OF UHMWPE/HA BIOCOMPOSITES FOR BONE TISSUE ENGINEERING

Joint Supervision thesis presented to the Graduate Program in Materials Science and Engineering of the Federal University of Santa Catarina (UFSC) and the Limoges University (UL) as a requirement to obtain the PhD title.

Advisors:
Prof. Dr. Dachamir Hotza (UFSC)
Prof. Dr. Chantal Damia (UL)

Co-advisors:
Prof. Dr. Gean Vitor Salmoria (UFSC)
Prof. Dr. Karine Giry (UL)

Limoges
2021

Henrique Schappo

SELECTIVE LASER SINTERING OF UHMWPE/HA BIOCOMPOSITES FOR BONE TISSUE ENGINEERING

Tese submetida ao Programa de Pós-Graduação em Ciência e Engenharia de Materiais da Universidade Federal de Santa Catarina e pela Instituição Université de Limoges em regime de cotutela para a obtenção do título de Doutor em Ciência e Engenharia de Materiais.

Orientadores:
Prof. Dr. Dachamir Hotza (UFSC)
Prof. Dr. Chantal Damia (UL)

Co-orientadores:
Prof. Dr. Gean Vitor Salmoria (UFSC)
Prof. Dr. Karine Giry (UL)

Limoges
2021

Ficha de identificação da obra elaborada pelo autor,
através do Programa de Geração Automática da Biblioteca Universitária da UFSC.

Schappo, Henrique
Selective laser sintering of UHMWPE/HA biocomposites for bone tissue engineering / Henrique Schappo ; orientador, Dachamir Hotza, orientadora, Chantal Damia, coorientador, Gean Vitor Salmoria, coorientador, Karine Giry, 2021.
149 p.

Tese (doutorado) - Universidade Federal de Santa Catarina, Centro Tecnológico, Programa de Pós-Graduação em Ciência e Engenharia de Materiais, Florianópolis, 2021.

Inclui referências.

1. Ciência e Engenharia de Materiais. 2. spray drying. 3. hydroxyapatite. 4. UHMWPE. 5. selective laser sintering. I. Hotza, Dachamir. II. Damia, Chantal III. Vitor Salmoria, Gean. IV. Giry, Karine. V. Universidade Federal de Santa Catarina. Programa de Pós-Graduação em Ciência e Engenharia de Materiais. VI. Título.

Henrique Schappo

Título: Selective laser sintering of UHMWPE/HA biocomposites for bone tissue engineering

O presente trabalho em nível de doutorado foi avaliado e aprovado por banca examinadora composta pelos seguintes membros:

Prof. Dr. Bruno HENRIQUES, Universidade Federal de Santa Catarina

Dr. Cynthia WIRTH, Siemens Energy Global

Prof. Dr. David GROSSIN, Institut National Polytechnique de Toulouse

Prof. Dr. Fabrice ROSSIGNOL, IRCER Limoges

Prof. Dr. Wilson ACCHAR, Universidade Federal do Rio Grande do Norte

Certificamos que esta é a **versão original e final** do trabalho de conclusão que foi julgado adequado para obtenção do título de doutor em Doutor em Ciência e Engenharia de Materiais.

_____

Coordenação do Programa de Pós-Graduação em Ciência e Engenharia de Materiais

_____

Prof. Dachamir Hotza, Dr.

Orientador

Florianópolis, 2021.

For all those who care about me

ACKNOWLEDGEMENTS

Firstly, I would like to thank my advisors, Prof. Dr. Dachamir Hotza (UFSC) and Prof. Dr. Chantal Damia (UL) and co-advisors Prof. Dr. Gean Vitor Salmoria (UFSC) and Prof. Dr. Karine Giry (UL), for their contribution on my academic and professional path, and for their important contributions for the present work.

To *Fundação de Amparo à Pesquisa e Inovação do Estado de Santa Catarina* (FAPESC), for the PhD fellowship (FAPESC/287/2018, Edital 03/2017) and to *Coordenação de Aperfeiçoamento de Pessoal de Nível Superior* (CAPES) – CAPES PrInt (*Programa Institucional de Internacionalização*) program for the fellowship in France and to the *Agence Nationale de Recherche* (ANR) for the financial support to carry out this research.

To my friends and lab co-workers from Limoges, which were essential to the conclusion of this thesis, especially to Emeline for the continuous help, and Paul, Arthur, Antoine and Charlotte for the nice moments spent together.

To the technicians from the *Laboratório Central de Microscopia Eletrônica* (LCME/UFSC) and the technicians from the *Institut de Recherche sur les Céramiques* (IRCER) for the help different kinds of analysis.

To my friends from Brazil, Filipe, Gustavo, Matheus, Levi and NIMMA colleagues.

To my family Leo, Viviane, Filipe, Sissa, Zeca, Iolita, Juliana and Guillaume and especially to Katina for always motivating me in my decisions and for the unconditional love.

ABSTRACT

In this work, an investigation on the manufacturing of 3D parts using composite biomaterials, additive manufacturing and targeting bone tissue applications is presented. The employed manufacturing process was selective laser sintering (SLS) and the feedstock powder was commercial UHMWPE and self-synthesized hydroxyapatite (HA). First, a step-by-step approach to use spray drying (SD) for obtaining HA particles with suitable morphological characteristics for SLS processing was employed. Varying processing parameters it was possible to produced SDHA particles the within mean diameter range of 15 to 25 μm. A major influence of atomization pressure variation was identified, a greater pressure value resulted in smaller particle size. Desirability function was employed to determine the optimal SD processing parameters and the selected parameters have considered the processing efficiency. The SDHA powder was mixed, at 5 and 10% weight content, with sieved UHMWPE and several SLS processing parameters were evaluated. Powder characteristics were assessed, samples' dimensional and mechanical properties were measured, likewise, preliminary *in vitro* essays were conducted. Warping effect and dimensional variation were observed with the employed parameters combination. Results indicated that the addition of SDHA particles have favoured the processability and biological response, nevertheless, a greater amount of SDHA has hindered samples' mechanical properties so a compromise must be found.

Keywords: spray drying; hydroxyapatite; UHMWPE; selective laser sintering; bone tissue engineering.

TABLE OF CONTENTS

TABLE OF FIGURES

CHAPTER 4

INDEX OF TABLES

LIST OF ABBREVIATIONS, ACRONYMS AND SYMBOLS

AM	Additive manufacturing
a-PC	Aliphatic polycarbonate
BIS-GMA	Bisphenol A glycidyl methacrylate
C	Carbon
CAD	Computer-assisted design
Ca-P	Calcium phosphates
CF	Carbon fiber
C-HA	2-Carboxyethylphosphonic acid-modified hydroxyapatite
CHA	Carbonated hydroxyapatite
GF	Glass fibers
HA	Hydroxyapatite
HDPE	High-density polyethylene
KF	Kevlar fibers
LCP	Liquid crystalline polymer
PA	Polyamide
PBF	Powder bed fusion
PC	Polycarbonate
PCL	Polycaprolactone
PDLA	Poly(d-lactic acid)
PEA	Polyethylacrylate
PEEK	Polyetheretherketone
PEG	Polyethylene glycol
PELA	Block co-polymer of lactic acid and polyethylene glycol
PET	Polyethyleneterephthalate
PGA	Poly(glycolic acid)
PHB	Polyhydroxybutyrate
PHBV	Poly(3-hydroxybutyrate-co-3-hydroxyvalerate)
PHEMA	Poly(2-hydroxyethyl methacrylate)
PLGA	Poly(lactic-co-glycolic acid)
PLLA	Poly(l-lactic acid)
PMA	Polymethylacrylate
PMMA	Polymethyl methacrylate
PP	Polypropylene
PS	Polysulfone
PTFE	Polytetrafluoroethylene
PU	Polyurethane
S/O/W	Solid-in-oil-in-water
SBA	Santa barbara amorphous
SDHA	Spray-dried HA
SLS	Selective laser sintering
SR	Silicone rubber

TCP	Tricalcium phosphate
TE	Tissue engineering
UHMWPE	Ultra-High-Molecular-Weight Polyethylene
β-TCP	Beta-tricalcium phosphate

This thesis is divided into five chapters. **Chapter 1** provides a general overview of the current work along with its objectives. The Chapters 2 to 4 are the manuscripts that resulted from this PhD thesis. **Chapter 2** presents a literature review of polymer/calcium phosphate biocomposites manufactured by selective laser sintering. **Chapter 3** provides a screening method for producing suitable spray-dried HA powder for SLS applications. **Chapter 4** details SLS processing of spray-dried HA and UHMWPE powder composites. Finally, **Chapter 5** contains the general conclusions and final considerations.

CHAPTER 1
General Introduction

1. General Introduction

Personalized medical devices have improved quality of life and welfare, also favouring faster recovering and being useful for a wide range of applications. Over the past decades, great development has been done in devices for bone repairs and substitution. Bone tissue engineering is a field of study that comprises techniques and treatments to overcome the limitations of conventional treatments of bone diseases [1]. Composite materials have been used in different parts of the human body (Figure 1), the implanted devices must match the local mechanical properties requirements and bone morphology.

Progress in biomedicine, material science, surgical techniques and other related fields have favoured faster healing and minimally invasive procedures, increasing patient's welfare. The employed materials must avoid pathological reactions after implantation and ideally restore the functionality of the damaged area.

Essentially, human bone is a complex vascularized structure, composed of organic collagen fibrils and inorganic calcium phosphate (Ca-P) crystals [3]. In terms of proportion, the Ca-P phase comprises to 65-70%, water to 5-8% and the remaining portion is the organic phase of the bone [4]. Figure 2 illustrates the bone composition and its morphological features from the macro to the nanostructure, whereas the portion of compact and spongy bone can vary according to the bone's location the body.

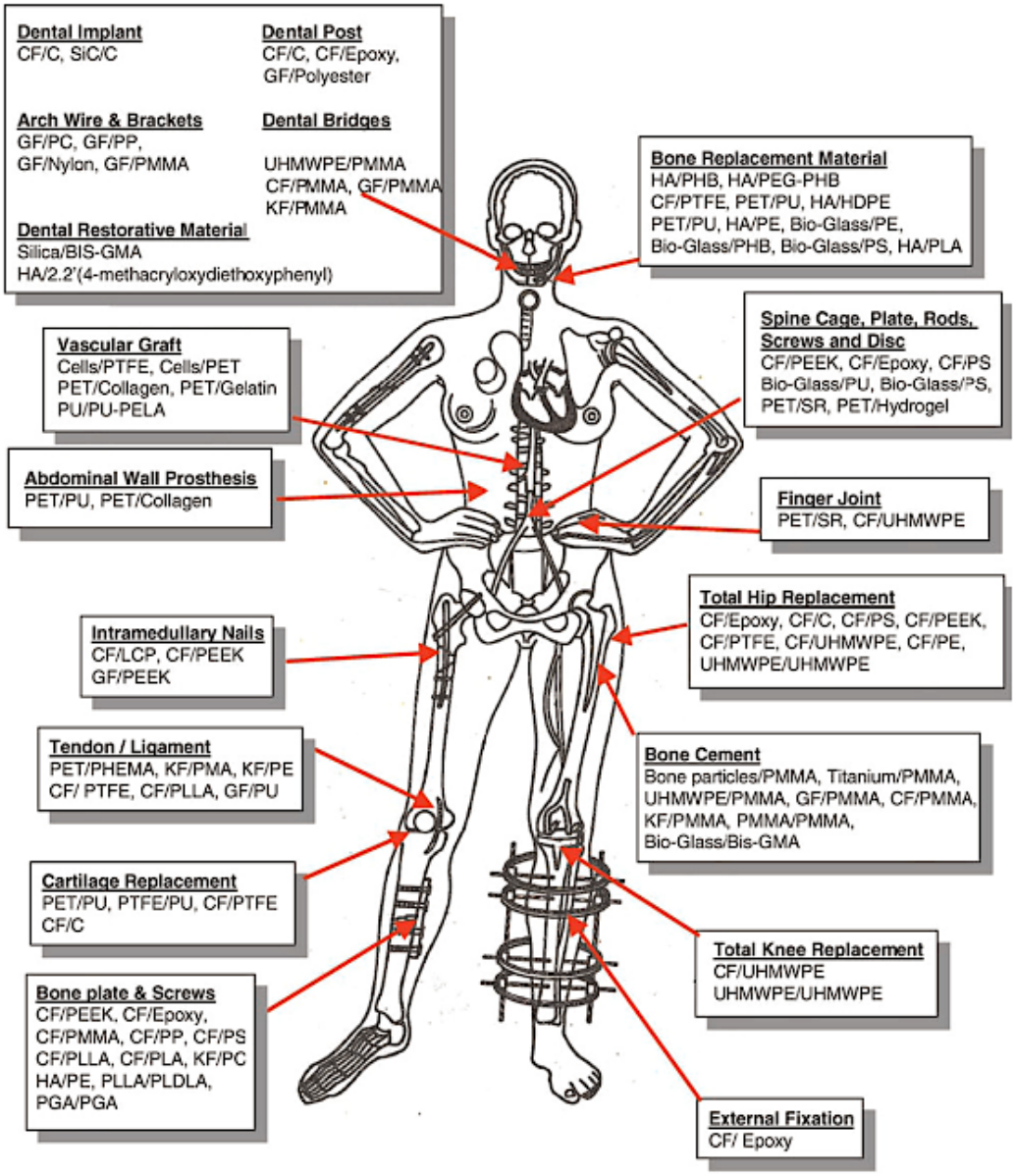

Figure 1: Composite materials and their applications in different body parts, adapted from Ramakrishna *et al.* [2].

The optimization of bone structure is interrelated with Wolff's law: "Mechanical stress placed upon a bone is responsible for determining the architecture and the external form of the bone" [5]. Consequently, bones can be considered as an anisotropic material and this aspect must be considered in the product development for the medical device. Fabricating a device using the combination of a matrix composed of a more flexible material (*i.e.,* polymers) and the addition of a mineral filler (*i.e.,* Ca-P) is suitable to mimic the bone structure and chemical

compatibility. Therefore, the feasibility of manufacturing complex geometries, combining composite biomaterials, matches with the requirements of implantable devices used for human tissue recovery.

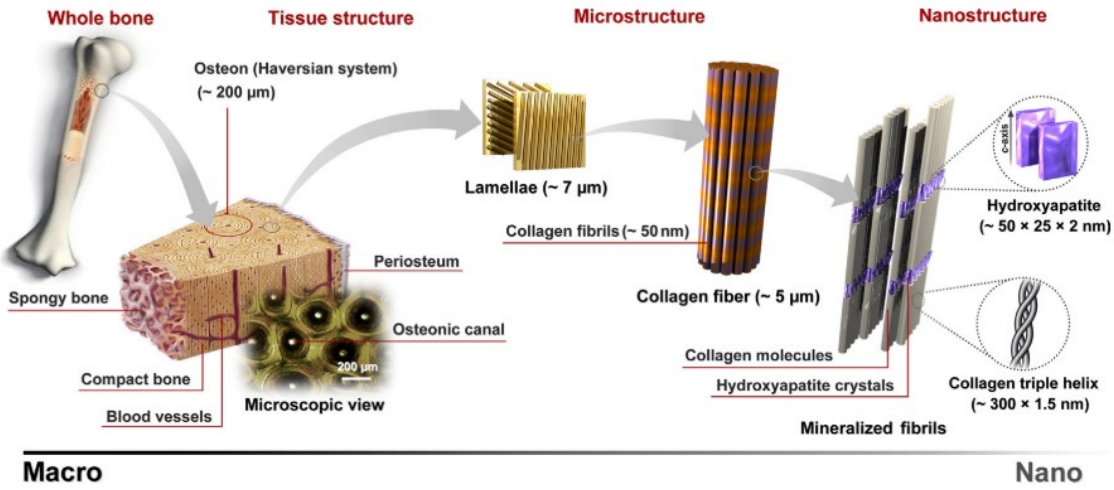

Figure 2: Hierarchical macro to nanostructure and composition of a typical human bone [4].

Additive manufacturing (AM) is a breakthrough technology that allowed significant progress for tissue engineering applications, and still reveals promising solutions for custom-made bone scaffolds [6–9]. Powder bed fusion, frequently referred to as selective laser sintering (SLS) is one of the commercially available AM processes [10]. In this process, particulate materials are fused layer by layer via heat supplied by an infrared laser source, creating 3D parts that were originally designed using computer-assisted design (CAD) tools.

The SLS fabricated parts are supported by a powder bed during manufacturing. It can achieve printing resolution up to 0.09 mm [11], which is dependent on the type of material employed. On the other hand, during SLS processing high temperatures can be achieved and the manufactured parts are characterized by a rough surface finish [12]. Nevertheless, SLS can be considered one of the most versatile AM techniques in terms of different material usage and structural stability.

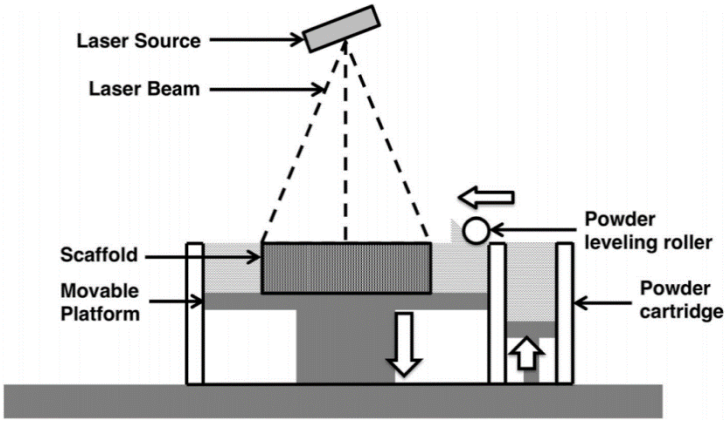

Figure 3: Simplified SLS scheme [12].

When using the SLS technique multiple parameters influence the outcome of the product. The parameters involved in this AM technique include, but are not limited to the following: part bed temperature, laser energy density, layer thickness, scan speed and hatch distance affect the mechanical and structural properties of fabricated parts [13]. Currently, many researchers are trying to find a correlation between these parameters, their adjustments, and material selection [13,14]. However, while different properties vary amongst the material, the correlation between the laser parameters and materials are currently being investigated. A challenging aspect of this technique is establishing material's processing within the optimal sintering window, which varies amongst different materials.

SLS processing with proper materials selection can contribute to enhancing the scaffold's final properties, particularly bioactivity [15,16]. When processing composite materials (*i.e.,* bioceramic fillers in a polymeric matrix) an association of properties can be achieved, enhancing the fabricated piece performance. Either, in terms of particle size, a substantial difference between each material is beneficial, allowing the filler to occupy voids in the interstices of matrix particles.

Concerning polymer SLS feedstock, there are preferable powder characteristics that improve the sinterability and final properties of the fabricated piece [17,18]. Related literature has indicated better processing and geometry accuracy when using spherical particles and narrow particle size distribution with an average size below 150 μm or equivalent to the laser beam diameter [17,19].

Polyethylene (PE) is one of the most common plastic in use and its variations have been used alone or in combination with other types of materials for medical devices. In terms of implantable devices, it is illustrated in Figure 2 different applications of the PE are shown: face bone replacement material, finger joint, tendon/ligament and total hip/knee replacement.

Concerning ultra-high-molecular-weight polyethylene (UHMWPE), it has also been used in different industries due to its outstanding physical and mechanical properties, such as: chemical inertness, lubricity, impact resistance, and abrasion resistance [20]. Its low friction coefficient and chemical inertness contributed to extensive use in orthopedics, mainly as bearing material in artificial joints. Given the widespread use of UHMWPE for medical applications, its processability using SLS equipment was also investigated. Rimell and Marquis [21] observed considerable shrinkage-induced warpage while fabricating multilayer parts of UHMWPE. Using a precise combination of processing conditions, including preheated powder Goodridge *et al.* [22] have successfully produced multilayer parts with relative accurate dimensions. Similarly, using optimized SLS processing parameters, Song *et al.* [23] minimized the warpage effect, achieving 83.25% density and tensile strength up to 14.1 MPa.

Ca-P materials [24,25] such as hydroxyapatite (HA) and beta-tricalcium phosphate (β-TCP) are widely used as bone substitutes and are commercially found in a few different geometries (*e.g.*, granules and sticks). Manufacturing customized scaffolds from these materials remains a challenge, therefore, the use of SLS processing also shows to be advantageous.

When compared to HA, β-TCP is degraded and absorbed quite rapidly by the body often occurring before new bone formation, therefore, discrepancies can be generated between new bone formation and material absorption [26]. Advantages of HA [$Ca_{10}(PO_4)_6(OH)_2$] is its chemical similarity with natural bone, possessing non-immunogenic properties, good biocompatibility and bone conductivity, it is considered one of the most suitable materials for bone scaffold fabrication [27]. In terms of biomedical applications, HA can correspond to different needs and has been used as an implant coating, drug delivery system and as bone scaffold and filler [28]. According to its application, appropriate HA morphological features must be fulfilled and specific processing techniques are required.

Spherical HA particles can be obtained by different techniques [29–34] in a diverse range of particle sizes. However, process scalability remains a challenge and not all techniques are capable of producing particles in the size range of 15 to 25 μm to be used as filler in a polymeric matrix.

Spray drying (SD) consists of the transformation of a fluid material into dried particles. SD had shown remarkable development in the last decades, being used by different industries [35]. SD commercial equipment may differ in terms of configuration. Rotary, hydraulic and pneumatic nozzle atomizers are commonly used [15]. The variables that affect how the spray is mixed with the hot gas depend upon the type of gas flow: co-current, countercurrent, or mixed flow [36]. Spray-dried HA (SDHA) powder has been successfully employed for distinct biomedical applications, using different manufacturing techniques [37–42]. Moreover, SD enables advantageous powder characteristics that are desirable for 3D printing use [35]. Although SDHA powder morphology indicates suitability for SLS processing, publications concerning this subject are scarce [43].

Regarding the considerable use of HA and UHMWPE materials for implantable devices, along with the benefits of spray drying into particle's morphological features and the

combination of UHMWPE/HA properties, the present work investigated the addition of SDHA particles into the UHMWPE matrix for SLS processing. First, the spray drying process was assessed for the feasibility to obtain narrow particle size distribution and mean diameter within the range of 15 to 25 μm. The produced SDHA powder was further added to UHMWPE, varying the SLS processing parameters to produce rectangular samples for mechanical and dimensional properties assessment. Finally, based on the sample's properties, the chosen SLS parameters were used to produce cylindrical samples for biological analysis.

1.1 General objective

The general objective of this work is to produce and characterize UHMWPE/SDHA samples using the SLS technique, aiming at bone tissue applications.

1.2 Specific objectives

For achieving general objectives, the specific objectives were established:

- Synthesis and characterization of stoichiometric nano-sized HA powder.
- Investigate the suitability of the spray drying process to produce spherical HA particles within the range of 15 to 25 μm.
- Select SLS processing parameters for fabricating UHMWPE/SDHA samples and evaluate if mechanical properties are appropriate for bone tissue applications.
- Preliminary biological essays to evaluate SLS fabricated samples biocompatibility.

1.3 References

[1] F. Akter, J. Ibanez, Bone and Cartilage Tissue Engineering, in: Tissue Eng. Made Easy, Elsevier, 2016: pp. 77–97. https://doi.org/10.1016/B978-0-12-805361-4.00008-4.

[2] S. Ramakrishna, Z.-M. Huang, G. V Kumar, J. Mayer, A.W. Batchelor, An introduction to biocomposites, World Scientific, 2004.

[3] L. Piaia, G.V. Salmoria, D. Hotza, Additive manufacturing of nanostructured bone scaffolds, Elsevier Inc., 2018. https://doi.org/10.1016/B978-0-12-814621-7.00010-X.

[4] M. Sadat-Shojai, M.T. Khorasani, E. Dinpanah-Khoshdargi, A. Jamshidi, Synthesis methods for nanosized hydroxyapatite with diverse structures, Acta Biomater. 9 (2013) 7591–7621. https://doi.org/10.1016/j.actbio.2013.04.012.

[5] K. SATO, Mechanism of Hydroxyapatite Mineralization in Biological Systems(Review), J. Ceram. Soc. Japan. 115 (2007) 124–130. https://doi.org/10.2109/jcersj.115.124.

[6] L. Piaia, G.V. Salmoria, D. Hotza, Additive Manufactured Nanocomposites for Bone Tissue Engineering Applications: an Overview, Mater. Res. 23 (2020) 1–10. https://doi.org/10.1590/1980-5373-mr-2019-0487.

[7] S. Mondal, U. Pal, 3D hydroxyapatite scaffold for bone regeneration and local drug delivery applications, J. Drug Deliv. Sci. Technol. 53 (2019) 101131. https://doi.org/10.1016/j.jddst.2019.101131.

[8] J. D'Alessio, A. Christensen, 3D Printing for Commercial Orthopedic Applications: Advances and Challenges, in: 3D Print. Orthop. Surg., Elsevier, 2019: pp. 65–83. https://doi.org/10.1016/B978-0-323-58118-9.00007-5.

[9] C. Shuai, L. Yu, W. Yang, S. Peng, Y. Zhong, P. Feng, Phosphonic acid coupling agent modification of HAP nanoparticles: Interfacial effects in PLLA/HAP bone scaffold, Polymers (Basel). 12 (2020). https://doi.org/10.3390/polym12010199.

[10] ISO/ASTM 52900: 2015 Additive manufacturing-General principles-terminology, ASTM F2792-10e1. (2012).

[11] X. Wang, S. Shujaat, E. Shaheen, R. Jacobs, Accuracy of desktop versus professional 3D printers for maxillofacial model production. A systematic review and meta-analysis, J. Dent. (2021) 103741. https://doi.org/10.1016/j.jdent.2021.103741.

[12] G.-H. Wu, S. Hsu, Review: polymeric-based 3D printing for tissue engineering, J. Med. Biol. Eng. 35 (2015) 285–292.

[13] K.C.R. Kolan, M.C. Leu, G.E. Hilmas, M. Velez, Effect of material, process parameters, and simulated body fluids on mechanical properties of 13-93 bioactive glass porous constructs made by selective laser sintering, J. Mech. Behav. Biomed. Mater. 13 (2012) 14–24.

[14] S. Singh, S. Ramakrishna, R. Singh, Material issues in additive manufacturing: A review, J. Manuf. Process. 25 (2017) 185–200. https://doi.org/10.1016/j.jmapro.2016.11.006.

[15] C. Shuai, W. Yang, P. Feng, S. Peng, H. Pan, Accelerated degradation of HAP/PLLA bone scaffold by PGA blending facilitates bioactivity and osteoconductivity, Bioact. Mater. 6 (2021) 490–502. https://doi.org/10.1016/j.bioactmat.2020.09.001.

[16] P. Feng, S. Peng, C. Shuai, C. Gao, W. Yang, S. Bin, A. Min, In Situ Generation of Hydroxyapatite on Biopolymer Particles for Fabrication of Bone Scaffolds Owning Bioactivity, ACS Appl. Mater. Interfaces. 12 (2020) 46743–46755. https://doi.org/10.1021/acsami.0c13768.

[17] M. Schmid, A. Amado, K. Wegener, Materials perspective of polymers for additive manufacturing with selective laser sintering, J. Mater. Res. 29 (2014) 1824–1832. https://doi.org/10.1557/jmr.2014.138.

[18] D. Sofia, D. Barletta, M. Poletto, Laser sintering process of ceramic powders: The effect of particle size on the mechanical properties of sintered layers, Addit. Manuf. 23 (2018) 215–224. https://doi.org/10.1016/j.addma.2018.08.012.

[19] R.D. Goodridge, C.J. Tuck, R.J.M. Hague, Laser sintering of polyamides and other polymers, Prog. Mater. Sci. 57 (2012) 229–267. https://doi.org/10.1016/j.pmatsci.2011.04.001.

[20] S.M. Kurtz, The UHMWPE Handbook Principles and Clinical Applications in Total Joint Replacement, Elsevier, 2004.

[21] J.T. Rimell, P.M. Marquis, Selective laser sintering of ultra high molecular weight polyethylene for clinical applications, J. Biomed. Mater. Res. 53 (2000) 414–420. https://doi.org/10.1002/1097-4636(2000)53:4<414::AID-JBM16>3.0.CO;2-M.

[22] R.D. Goodridge, R.J.M. Hague, C.J. Tuck, An empirical study into laser sintering of ultra-high molecular weight polyethylene (UHMWPE), J. Mater. Process. Technol. 210 (2010) 72–80. https://doi.org/10.1016/j.jmatprotec.2009.08.016.

[23] C. Song, A. Huang, Y. Yang, Z. Xiao, J.K. Yu, Effect of energy input on the UHMWPE fabricating process by selective laser sintering, Rapid Prototyp. J. 23 (2017) 1069–1078. https://doi.org/10.1108/RPJ-09-2015-0119.

[24] J.C. Elliott, Structure and chemistry of the apatites and other calcium orthophosphates, Elsevier, 2013.

[25] L.L. Hench, Bioceramics, J. Am. Ceram. Soc. 81 (1998) 1705–1728. https://doi.org/10.1111/j.1151-2916.1998.tb02540.x.

[26] P. Gao, H. Zhang, Y. Liu, B. Fan, X. Li, X. Xiao, P. Lan, M. Li, L. Geng, D. Liu, Y. Yuan, Q. Lian, J. Lu, Z. Guo, Z. Wang, Beta-tricalcium phosphate granules improve osteogenesis in vitro and establish innovative osteo-regenerators for bone tissue engineering *in vivo*, Sci. Rep. 6 (2016) 1–14. https://doi.org/10.1038/srep23367.

[27] Q. Wei, Y. Wang, W. Chai, Y. Zhang, X. Chen, Molecular dynamics simulation and experimental study of the bonding properties of polymer binders in 3D powder printed hydroxyapatite bioceramic bone scaffolds, Ceram. Int. 43 (2017) 13702–13709. https://doi.org/10.1016/j.ceramint.2017.07.082.

[28] A. Szcześ, L. Hołysz, E. Chibowski, Synthesis of hydroxyapatite for biomedical applications, Adv. Colloid Interface Sci. 249 (2017) 321–330. https://doi.org/10.1016/j.cis.2017.04.007.

[29] C. Li, G. Li, S. Liu, J. bai, A. zhang, Spherical hydroxyapatite with colloidal stability prepared in aqueous solutions containing polymer/surfactant pair, Colloids Surfaces A Physicochem. Eng. Asp. 366 (2010) 27–33. https://doi.org/10.1016/j.colsurfa.2010.05.018.

[30] K. Ioku, G. Kawachi, S. Sasaki, H. Fujimori, S. Goto, Hydrothermal preparation of tailored hydroxyapatite, J. Mater. Sci. 41 (2006) 1341–1344. https://doi.org/10.1007/s10853-006-7338-5.

[31] C. Qiu, X. Xiao, R. Liu, Biomimetic synthesis of spherical nano-hydroxyapatite in the presence of polyethylene glycol, Ceram. Int. 34 (2008) 1747–1751. https://doi.org/10.1016/j.ceramint.2007.06.001.

[32] M.H. Hong, J.S. Son, K.M. Kim, M. Han, D.S. Oh, Y.K. Lee, Drug-loaded porous spherical hydroxyapatite granules for bone regeneration, J. Mater. Sci. Mater. Med. 22 (2011) 349–355. https://doi.org/10.1007/s10856-010-4197-z.

[33] X. Ma, Y. Chen, J. Qian, Y. Yuan, C. Liu, Controllable synthesis of spherical hydroxyapatite nanoparticles using inverse microemulsion method, Mater. Chem. Phys. 183 (2016) 220–229. https://doi.org/10.1016/j.matchemphys.2016.08.021.

[34] M. Kamitakahara, S. Takahashi, T. Yokoi, C. Inoue, K. Ioku, Preparation of spherical porous hydroxyapatite granules as support materials for microorganisms, J. Ceram. Soc. Japan. 126 (2018) 732–735. https://doi.org/10.2109/jcersj2.18089.

[35] D. Santos, A.C. Maurício, V. Sencadas, J.D. Santos, M.H. Fernandes, P.S. Gomes, Spray Drying: An Overview, in: Biomater. - Phys. Chem. - New Ed., InTech, 2018. https://doi.org/10.5772/intechopen.72247.

[36] K. Cal, K. Sollohub, Spray Drying Technique. I: Hardware and Process Parameters, J. Pharm. Sci. 99 (2010) 575–586. https://doi.org/10.1002/jps.21886.

[37] Y.J. Fu, S.S. Shyu, F.H. Su, P.C. Yu, Development of biodegradable co-poly(D, L-lactic/glycolic acid) microspheres for the controlled release of 5-FU by the spray drying method, Colloids Surfaces B Biointerfaces. 25 (2002) 269–279. https://doi.org/10.1016/S0927-7765(01)00205-3.

[38] P. López-Gasco, I. Iglesias, J. Benedí, R. Lozano, J.M. Teijón, M.D. Blanco, Paclitaxel-loaded polyester nanoparticles prepared by spray-drying technology: In vitro bioactivity evaluation, J. Microencapsul. 28 (2011) 417–429. https://doi.org/10.3109/02652048.2011.576785.

[39] E. Quinlan, A. López-Noriega, E.M. Thompson, A. Hibbitts, S.A. Cryan, F.J. O'Brien, Controlled release of vascular endothelial growth factor from spray-dried alginate microparticles in collagen–hydroxyapatite scaffolds for promoting vascularization and bone repair, J. Tissue Eng. Regen. Med. 11 (2017) 1097–1109. https://doi.org/10.1002/term.2013.

[40] S. Sequeira, M.H. Fernandes, N. Neves, M.M. Almeida, Development and characterization of zirconia–alumina composites for orthopedic implants, Ceram. Int. 43 (2017) 693–703. https://doi.org/10.1016/j.ceramint.2016.09.216.

[41] Y. Ben, L. Zhang, S. Wei, T. Zhou, Z. Li, H. Yang, Y. Wang, F.A. Selim, C. Wong, H. Chen, PVB modified spherical granules of β-TCP by spray drying for 3D ceramic printing, J. Alloys Compd. 721 (2017) 312–319. https://doi.org/10.1016/j.jallcom.2017.06.022.

[42] R. Cholas, S. Kunjalukkal Padmanabhan, F. Gervaso, G. Udayan, G. Monaco, A. Sannino, A. Licciulli, Scaffolds for bone regeneration made of hydroxyapatite microspheres in a collagen matrix, Mater. Sci. Eng. C. 63 (2016) 499–505. https://doi.org/10.1016/j.msec.2016.03.022.

[43] C.K. Chua, K.F. Leong, K.H. Tan, F.E. Wiria, C.M. Cheah, Development of tissue scaffolds using selective laser sintering of polyvinyl alcohol/hydroxyapatite biocomposite for craniofacial and joint defects, J. Mater. Sci. Mater. Med. 15 (2004) 1113–1121. https://doi.org/10.1023/B:JMSM.0000046393.81449.a5.

CHAPTER 2
Manuscript 1

Introduction to Chapter 2

This chapter contains information found in the related bibliography concerning SLS processing of polymers/calcium phosphate biocomposites. Bone tissue is composed of a mineralized structure with a flexible matrix. The combination of polymer and calcium phosphates are a suitable match in terms of desirable properties. Implantable devices for bone tissue engineering can be obtained by different fabrication processes. However, AM facilitates custom-made implants, enables multi-material usage and is capable of producing complex geometries that mimic bone structure.

Among the available AM techniques, SLS was chosen because of its capability of processing different categories of powder materials, further, it allows the fabrication of complex geometries with interconnecting pores, it is industry scalable and concurrently fabricating tailored pieces.

Nevertheless, material selection and its particle's characteristics must meet some requirements for achieving proper SLS processability. Either, SLS processing parameters are broadly variable and affect the proprieties of the fabricated pieces. A literature review allows acquiring relevant information concerning the target topic, endorsing choices of possible research paths.

Polymer/calcium phosphate biocomposites manufactured by selective laser sintering: an overview

Henrique Schappo[1,2], Karine Giry[2], Gean Salmoria[1], Chantal Damia[2], Dachamir Hotza[3]

[1]Innovation Laboratory for Molding and Additive Manufacturing (NIMMA), Federal University of Santa Catarina (UFSC), 88040-900 Florianópolis, SC, Brazil
[2]University of Limoges, CNRS, IRCER, UMR 7315, F-87000 Limoges, France
[3]Interdisciplinary Laboratory for the Development of Nanostructures (LINDEN), Federal University of Santa Catarina (UFSC), 88040-900 Florianópolis, SC, Brazil

Manuscript under review in the Journal **Progress in Additive Manufacturing**.

Abstract

Additive manufacturing (AM) drove important advancements for implantable devices for tissues regeneration. Selective laser sintering (SLS), also known as powder bed fusion (PBF) is a laser-assisted AM method, capable of producing well-defined pieces using different types of material targeting diverse applications. Regarding bone tissue engineering, calcium phosphates are considered as reference materials for their biocompatibility and bone regeneration capability. Likewise, certain polymers are also widely used for implantable devices due to their processability, adequate properties and bioabsorption. This review article assessed original research articles available between the years 2000 and 2020, that have been processed by SLS polymer/Ca-P composites mixtures. Considering the reviewed articles, it was possible to elaborate an overview of the state of the art and future trends. Important aspects of processing are discussed, indicating powder mixture approaches, employed materials and processing parameters details, as well as biological assessment. Facts and information are provided along with this review article for a comprehensive understanding of the involved proceedings for polymer/Ca-P implantable devices.

Keywords: polymer; calcium phosphate; selective laser sintering; bone tissue engineering.

1. Introduction

Personalized parts are preferred in different applications, being greatly helpful in medicine. It is recognized that custom-made medical devices have improved quality of life and welfare, also favouring faster recovering. In terms of implantable devices, there are many advantages in using patient-match components for bone-related pathologies, particularly oncologic reconstruction [1]. Further, clinical essays have shown that bone-related injuries have considerable benefits when treated using osteoconductive customized implants [2], [3]. These achievements can rely upon the use of additive manufacturing (AM), a breakthrough technology wherein characteristics, still arise opportunities for significant progress in the field of bone tissue engineering.

Bone tissue consists of 30% organic collagen fibrils and 70% inorganic calcium phosphate crystals [4]. Its structure is composed of overall 80% cortical bone and 20% trabecular bone, having respectively, less than 10 vol% and 50-90 vol% porosity [5], [6]. Since bone is a complex mineralized structure with a flexible matrix, the combination of biopolymers and bioceramics is particularly interesting for bone replacing applications. Moreover, these materials have characteristics like biocompatibility and osteoconductivity that are highly desirable [7], [8]. Towards ceramic materials capable of favouring bone tissue formation, calcium phosphates (Ca-P) are considered an overcome and have been used for many years [9], [10]. This group of material was successfully mixed with biopolymers and processed by SLS, however, different mixture methods and performance outcomes can be found in the bibliography. The use of a polymeric matrix together with Ca-P materials, provide benefits in terms of mechanical properties and favours processability. Further, bioabsorbable polymers ensure mechanical stability and can be degraded along with bone tissue recovering.

Selective laser sintering, also know as powder bed fusion by ISO/ASTM 52900 [11] is among the commercially available AM techniques. This process fuses particulate materials

layer by layer, via heat supplied by an infrared laser source, allowing the creation of complex 3D parts. SLS is considered one of the most versatile in terms of material usage, structural stability and, through optimized parameters, it is possible to achieve the desired mechanical properties for tissue engineering scaffolds [12]. The performance of SLS fabricated parts is highly depended on powder materials characteristics and process parameters. Using suitable SLS processing parameters it is possible to enhance cell infiltration, nutrients and metabolites throughout the manufactured scaffold [13]. This fabrication method enables to mimic the bone structure, favouring faster healing of the damaged bone tissue.

This overview presents information from research articles that have processed, through SLS, a combination of polymer and calcium phosphates materials, targeting bone tissue engineering applications. Powder preparation methods, materials selection, processing and final proprieties of the fabricated piece will be outlined and discussed. Finally, future perspectives of polymer/Ca-P biocomposites processed by SLS will be summarized.

2. Methodological approach

The adopted search strategy was to use the Scopus database to find publications associated with the keywords displayed in Table 1. Keywords were selected to compass a vast number of articles indexed by a reputed scientific database. The star keys were used in favour of searching singular and plural forms of the keywords in the database.

The articles found were assorted in lists for checking duplicates and adequacy. The selection criteria were original research articles that fabricated samples by SLS, using polymer and calcium phosphates composite mixture and having publication year between 2000 and 2020. Among a total of 650 articles, 63 were selected and analyzed; review articles, books and conference releases were not considered.

Table 1: Details of search strategy for each database.

Database	Keywords	Search on
Scopus	"selective laser sintering" AND biomaterial* = 158 results "selective laser sintering" AND scaffold* = 425 results "powder bed fusion" AND biomaterial*= 33 results "powder bed fusion" AND scaffold* = 34 results	Article title, abstract, keywords

3. Materials

3.1 Polymer matrix

Aliphatic polyesters are among the most used biopolymers for medical use, thanks to characteristics such as non-toxicity, biocompatibility and biodegradability [14]. Not surprisingly, this category of polymers was the most used among analyzed articles as shown in Figure 1. The majority of reviewed articles have used a polymer as the predominant material of the polymer/Ca-P mixture, whereas around 10% (6 articles) have used less than 20% of polymer content.

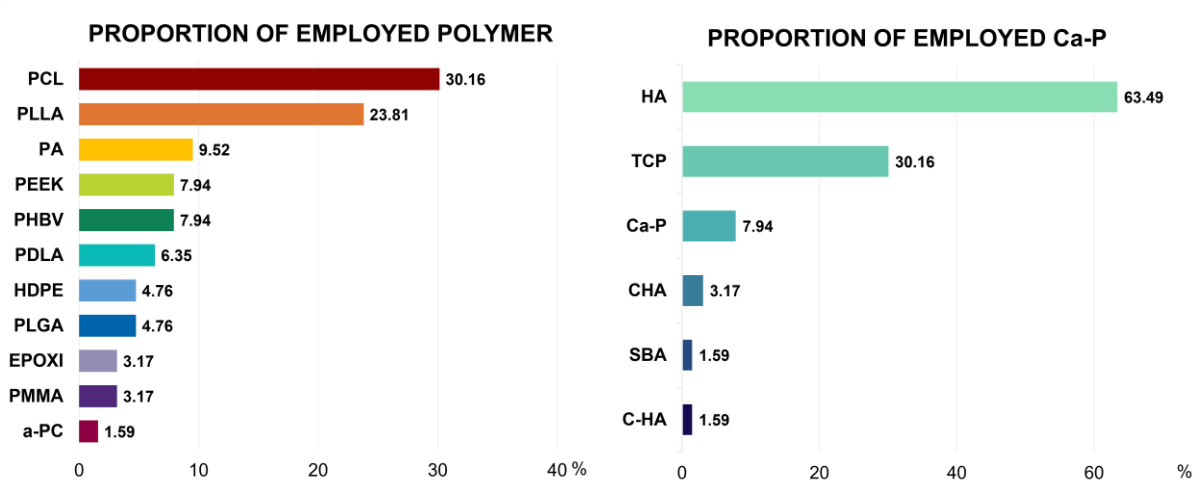

Figure 1: Proportion of each polymer and Ca-P employed.

Medical devices fabricated by SLS requires two main material's characteristics, one related to application demands and the other concerning its processability. Only a few polymers have suitable processing for the SLS technique, limiting the range of commercially available powders options and industrial-scale production of implantable devices [15], [16]. Polyamide (PA) is commercially available and is already well known in the SLS industry. However, in our research, we have found only 3 articles using it. This might be attributed to its low poor cell seeding behaviour [17] and author's greater interest in using bioabsorbable polymers.

The most used polymers were polycaprolactone (PCL) and poly(lactic acid) (PLA) with ~30% of usage each. The largest use of these polymers are probably due to their easy access and proven track record as tissue compatible. Owning a slow degradability (2 to 4 years), PCL is preferable for long-term implantable devices, nonetheless, its degradation rate, bioactivity and mechanical properties can be modified with the incorporation of Ca-P materials [18].

Poly(lactic acid) (PLA) is also approved by Food and Drug Administration (FDA) for human body applications. Its body degradation rate depends on the polymer's characteristics and the implant location. According to the literature, its absorption time may vary from 40 weeks to 6 years [19]. As a consequence of the polymeric chain optical activity, PLA is available in three different variations: D,D-lactide (not employed in the reviewed articles); L,L-lactide (accounting for ~24% of usage) and D,L-lactide (~6% of usage) [20].

Figure 2 displays SEM images of widely used polymer materials, particle's morphology distinction is a result of the applied preparing method. Figure 2a shows pure PCL spherical particles that were produced using a modified S/O/W emulsification solvent evaporation method [21]. This method also allows obtaining the microspheres with HA in the particle's surface (up to 20 wt% content). In Figure 2b, PLLA particles were obtained using cryogenic milling, this method forms irregular morphologies, and in this case, the ceramic particles are added after the milling process.

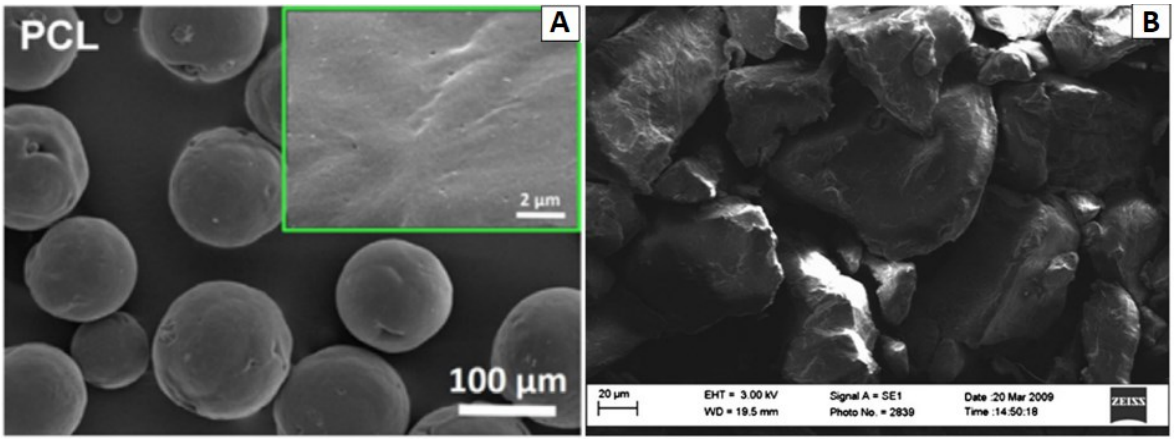

Figure 2: SEM images of polymer powders **a)** PCL microspheres [21] and **b)** PLLA irregular particles [22].

3.2 Ca-P powders

Ca-P materials have substantial chemical similarity with bones, consequently, their biocompatibility, biodegradability and osteoconductivity are suitable for bone tissue applications [23]. Specific chemical formulations differ in each type of Ca-P material.

Concerning the most used Ca-P materials, we can rank hydroxyapatite (HA) followed by tricalcium phosphate (TCP); other Ca-P materials accounted for almost 8% of the total. Only 3 articles have used modified versions of HA, also, 3 articles have used a combination of bioceramics.

The major use of pure HA is probably related to significant benefits and performance advantages, when using HA as a bone repair and bone replacement material [24]. TCP degradation in the human body is faster than HA so that its benefits were explored by a few authors. The combination of HA + β-TCP is useful for certain types of implants by gathering properties of each material [25], [26].

Figure 3 illustrates Ca-P powders used in the reviewed articles, it can be seen that individual nano-HA needle-like particles tend to agglomerate into irregular clusters. Particle geometry influences powder spreading and the best results are achieved with spherical particles

[27]. In this sense, it is preferable to use polymeric/Ca-P particles with spherical morphology for SLS processing such as those shown in Figure 3b.

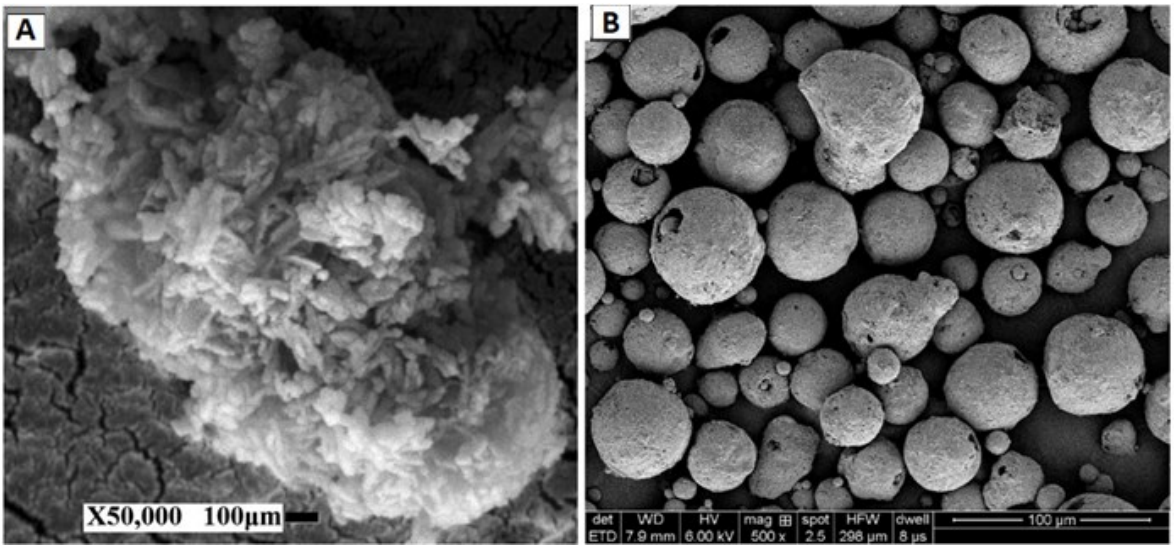

Figure 3: SEM of calcium phosphates used in SLS of biocomposites: **a)** nanostructured HA [28] and **b)** spherical HA powder [29].

3.3 Additives

Biocomposites that are employed for medical applications must have high stability, therefore, surface properties might be improved to enhance material's compatibility [30]. Our findings revealed that additives among polymer/Ca-P composites are mainly used to allow SLS processability, interfacial bonding and to bring supplementary properties for the fabricated device. Carbon/gold nanoparticles can be used as a sensitizing agent to absorb the laser radiation energy, making possible the processability of polymer/Ca-P composites by single-mode fibre laser [31]–[34].

When composites are processed by SLS, employed materials should possess interfacial bonding to achieve better mechanical properties. Shuai *et al.* [35] have evaluated the addition of 2-Carboxyethylphosphonic acid (CEPA), a phosphonic acid coupling agent, when

processing hydroxyapatite (HAP) and poly-l-lactic acid (PLLA). Results have shown an increase of scaffold's tensile strength and modulus up to 2.79 times when using surface-modified HA particles with CEPA.

An example of adding supplementary properties to the fabricated device was seen in the work of Tan *et al.* [36] where they have successfully used PLLA/HA/metformin scaffolds for bone repair and tumour cells inhibition. Liu *et al.* [37] have modified PCL/HA scaffolds with vascular endothelial growth factor (VEGF) and results have shown excellent cytocompatibility and greater blood vessel formation. The addition of mesoporous silica Santa Barbara Amorphous-15 (SBA15) into PLLA/HA scaffolds have improved hydrophilicity, cell proliferation and enhanced mechanical properties [38].

Although SLS can be applied to fabricated devices for drug delivery [39], our research did not find polymer/Ca-P composites with incorporated drugs. However, this possibility is cited by Duan et Wang [40] who have successfully fabricated scaffolds using Ca-P/PHBV nanocomposite microspheres loaded with bovine serum albumin (BSA), demonstrating the viability of incorporating biomolecules on the SLS powder. Nonetheless, SLS technology is already successfully used for processing drugs agents for pharmaceutical purposes [41].

The use of additives has shown great potential to provide benefits and supplementary properties for the fabricated scaffolds. Still, many aspects that should be deeply investigated such as the interaction between materials, properties preservation after laser irradiation and biological response.

4. Manufacturing process

4.1 SLS equipment and powder processability

Around 30% (18 articles) have stated that the SLS equipment was developed in-house, this small amount is probably due to the relative complexity level of hardware assembly and software communication. At the same time, SLS equipment construction requires time and expertise. Not all authors provided enough information related to SLS equipment (20%), while more than a half (32 articles) have informed to use a commercially available machine. Some authors have described modifications on commercial machines, these modifications were mainly to reduce the quantity of powder consumption.

Most available commercial SLS are capable of using inert gas during SLS processing, likewise, in-house SLS equipment might also be constructed to provide this feature. This feature avoids unwanted chemical reactions and degradation. Despite its benefits, we have found only one manuscript [42] that claimed to use nitrogen during processing. The lack of use of inert gas during Ca-P/polymer SLS processing is probably due to the high cost and minor benefits. Notwithstanding, inert gas during SLS processing is desirable while fabricating metal devices [43].

The laser source has great importance for the type of material to be processed. The main laser source in the reviewed articles was CO_2 with a wavelength of 10.6 μm, representing 73% of the total. This observation can be related to the greater efficiency of CO_2 lasers when processing oxide ceramics and polymers [41]. Representing 8% of usage, fibre laser (λ = 1.06 μm) were used for surface selective laser sintering (SSLS), whereas a small amount (0.1 wt%) of carbon/gold nanoparticles is added in the powder mixture. It will absorb laser radiation energy, avoiding internal overheating of polymer particles and minimize degradation. Surprisingly, not all authors have provided information related to which laser type was used, these articles represented 19% of the total.

According to the laser type and material's characteristics, there are key aspects that directly influences powder's processability by SLS, as shown in Figure 4. Although Schmid et *al.* [44] have elaborated this diagram examining polymers, many properties can also be considered when processing Ca-P by SLS. Intrinsic characteristics (optical, thermal and rheological) are related to the molecular structure, being more difficult to change. On the other hand, extrinsic properties (related to powder and particles) are versatile to modify [44].

Employment of adequate SLS processing parameters preserves material's characteristics, also enabling the achievement of expected biological response. Further, the scaffold's surface characteristics, microporosity and mechanical properties are affected by the processing parameters [45]. The absence of sufficient laser energy will lead to poor structural stability (lack of neck formation between particles), in contrast, excessive energy will cause heating that might deteriorate polymers and cause geometric distortion. The importance of suitable processing parameters is reinterred by many authors' in-depth analysis of its consequences on the sample's final properties. Subsequently, most of the reviewed articles applied the design of experiments (DOE) and/or other statistical tools for selecting the optimal processing parameters. Supplementary analysis using scanning electron microscopy (SEM) images, Fourier-transform infrared spectroscopy (FTIR) and X-ray diffraction (XRD) are often used to verify variations on morphological and chemical features as a consequence of different processing parameters.

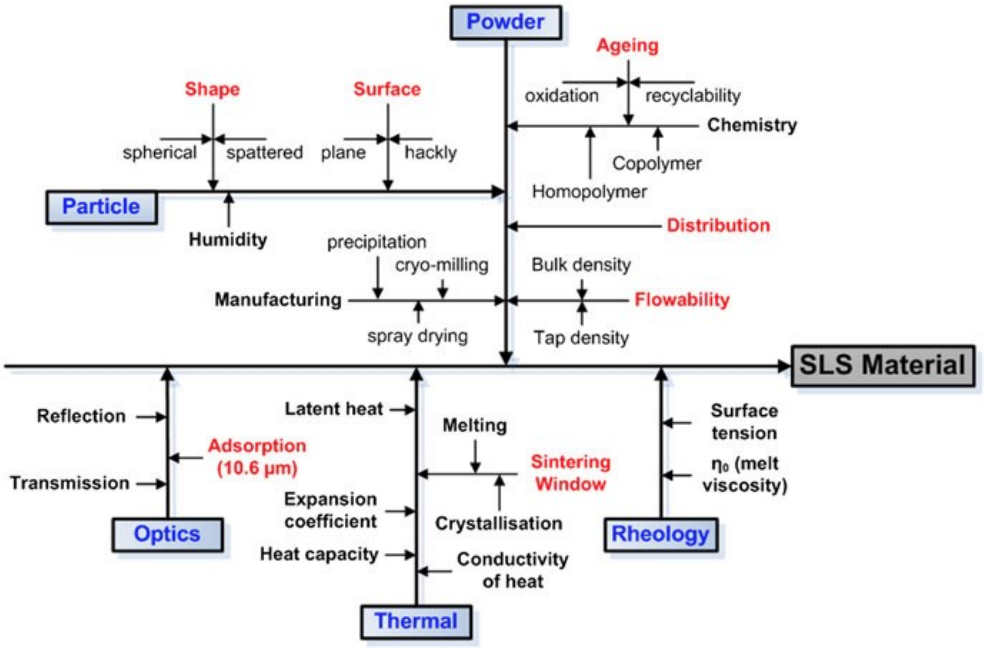

Figure 4: Interconnection between polymer's properties for SLS processing [44].

4.2 Polymer/Ca-P powder mixture and preparation methods

In terms of desirable powder characteristics for proper SLS processing, it is preferable to have a wide sintering window (difference between melting and crystallization onset temperatures), good flowability and relatively narrow particle size distribution (preferably with high sphericity). For polymer particles, the thermal stability, melting and solidification behaviours are particularly important during the SLS process.

Concerning Ca-P materials, particle's morphology and size distribution can be adjusted using distinct powder preparation methods, however, crystal growth formation is highly dependent on which synthesis method is applied. Consequently, it is preferable to use a synthesis method that will approach the most to the desired particle's characteristics, possibly, eliminating a further additional process.

Sadat-Shojai *et al.* [46] have reviewed HA synthesis methods, relating the different synthesis methods with obtained powder characteristics. Among diverse approaches to synthesize HA nanoparticles, wet methods (*e.g.*, chemical precipitation and hydrothermal) have

the advantage of more precise control over the morphology and size of particles [46]. From our study, we observed that the majority of authors have used commercially available Ca-P powders and only a few have synthesized it themselves, this disparity might be justified by the high cost of synthesis related apparatus.

Alternately, no information about self-synthesis was identified for polymers, all authors stated to use commercially obtained materials. Polymers were delivered in pellets or powders, normally requiring an additional process (*e.g.*, milling, sieving) before mixing with Ca-P powder. According to which method, substantial differences in morphological features can be observed. Figure 2a shows SEM images from PCL microspheres prepared by the solid-in-oil-in-water (S/O/W) emulsification solvent evaporation method [21]. Figure 2b shows PLLA cryogenic milled particles [22]. All articles that have used poly(hydroxybutyrate-co-hydroxyvalerate) (PHBV), employed the oil-in-water (O/W) method to obtain polymeric spherical particles. However, other articles in the literature have used SLS to solely process PHBV without further particle modification [47], [48].

Attrition forces present during the milling process can significantly increase powder's temperature, therefore, polymers with a low melting point may benefit from cryogenic milling such as PCL [22], [49]–[55]. As well as to prevent temperature increasing, liquid nitrogen was used during the milling of PA12/HA pellets compounded by a twin-screw extruder [56].

Although the milling process may not provide homogenous spherical particles (Figure 2b), it remains the most convenient and fast method for particle size reduction. As a result, we have observed that the most common process used to achieve polymer desirable particle size was milling followed by sieving.

Towards polymer and Ca-P powder mixture procedure, two principal methods were identified: physical blending and solvent evaporation. Table 2 contains information related to

employed materials, mixture methods and their sub-types. Concerning physical blending, several authors did not provide enough details while describing the method, for these cases, we have considered the sub-type as “general”.

Among physical blending, general mixing is predominant, probably due to its simplicity, equipment accessibility and efficacy, representing around 49% of all preparation methods. Secondly, the solid-in-oil-in-water (S/O/W) emulsion solvent evaporation process represented 14% of the utilized methods. Wet methods (around 12%) consist in diluting and mixing the particles using a liquid carrier, the most used liquid was ethanol. The remaining methods used physical blending and were categorized as detailed by authors (*i.e.,* use of extrusion compound, rotatory tumbler, V or Y type mixer).

Shuai *et al.* have combined PEEK/PGA to unify the advantages of each polymer and adding different amounts of HA content, which were able to improve elastic modulus, bioactivity, cell attachment and proliferation of the fabricated scaffolds. Also using PEEK, Feng *et al.* [83] have fabricated scaffolds containing PEEK/β-TCP/PLLA, *in vivo* bone defect repair results have proven the efficiency of bone formation and regeneration. Targeting to reduce the low degradability time of HA, Gao *et al.* [26] have fabricated specimens containing HA/β-TCP (50/50 w/w). The addition of 1 wt% of PLLA or PLGA introduced a liquid phase during SLS processing, this favours HA/β-TCP grain boundary sliding and rearrangement, leading to better densification and mechanical properties.

Table 2: Polymer/Ca-P composite mixtures, type of blending and number of publications.

Composite mixture	Type of blending	Sub-type	Sources
PMMA + TCP	Physical blending	General	[57], [58]
PCL + TCP	Physical blending	General	[49], [52], [54], [59], [60]
		Rotary tumbler	[61], [62]
PCL + HA	Solvent evaporation	S/O/W	[21], [37], [63]
	Physical blending	General	[51], [55], [64]–[66]
		V-type mixer	[22], [53]
		Rotary tumbler	[67]
PDLA + TCP	Physical blending	Wet method	[68]
PDLA + HA	Solvent evaporation	S/O/W	[69]
	Physical blending	General	[31], [33]
PLLA + TCP	Physical blending	General	[34], [70]–[73]
PLLA + HA	Physical blending	Wet method	[35], [36]
		General	[74], [75]
	Physical blending	Supercritical CO_2	[76]
PLLA + HA + MET	Physical blending	Wet method	[36]
PLLA + CHA	Solvent evaporation	S/O/W	[77]
	Physical blending	Rotary tumbler	[78]
SBA + HA + PLLA	Physical blending	Wet method	[38]
pDA + HA + PLLA	Physical blending	Wet method	[79]
PLGA + HA	Physical blending	General	[80]
PLGA + HA + TCP	Physical blending	General	[26]
PEEK + HA	Physical blending	General	[32], [81]
		Roller mixer	[82]
PEEK + TCP + PLLA	Physical blending	Wet method	[83]
PEEK + PGA + HA	Physical blending	Wet method	[84]
PA + HA	Physical blending	General	[17], [29], [85]
		Extrusion	[56]
		Y-mixer	[86], [87]
a-PC + HA	Physical blending	Planet ball	[28]
HDPE + HA	Physical blending	Y-mixer	[88]
		Extrusion	[42], [89]
PHBV + Ca-P	Solvent evaporation	S/O/W	[40], [77], [90]–[92]
EP + HA + TCP	Physical blending	General	[25]
EP + PA + TCP	Physical blending	General	[93]
EAM + HA	Physical blending	Wet method	[94]

Our findings have also revealed other articles that have used a small amount of polymer in a ceramic matrix. In one of these articles, the effect on scaffold's mechanical properties when adding 0.5 to 3 wt% of PLLA on a β-TCP matrix was investigated by Liu *et al.* [70]. Their findings revealed that the addition of 1 wt% has improved values of compressive strength and fracture toughness, as a consequence of β to α-TCP phase transformation inhibition. The occurrence of this phenomenon, using 1 wt% PLLA, was further studied by Shuai *et al.* [73]. In contrast, unsuccessful processing of TCP particles coated with a thin film of PLA polymer was reported by Antonov *et al.* [34].

The majority of authors have used pure polymer for comparison purposes and to outline SLS processing parameters. Properties contrasts between pure polymer and Ca-P filled scaffolds are often used for benchmark and performance correlation. Although the use of pure polymer can provide valuable information for processing parameters window, Ca-P filler addition might influence the optimal SLS parameters which have a great influence on the scaffold's final properties.

4.3 Processing parameters and characteristics of fabricated specimens

Each powder material has its intrinsic characteristics, requiring fine adjustment of SLS processing parameters for adequate properties. Changes such as type of SLS machine, type of composite powder, particle size and morphology, might imply better tuning of processing parameters. This should be considered for processing parameters selection and comparison with the related bibliography.

A summary of the reviewed articles is displayed in Table 3, which gathers information on polymer/Ca-P combination, type of mixture, SLS equipment and processing parameters.

Some authors did not provide enough data in their manuscripts to allow the completion all the related information.

Table 3 contains all the polymer/Ca-P compositions and proportions that were tested by the authors, although not all proportions were satisfactorily processed and had favourable properties. Likewise, not all processing parameters values indicated by authors were suitable, occurrence of polymer degradation or low sintering degree was often reported by authors until optimal values were found. When a wide range of parameters was tested, authors were able to better investigate its influence on scaffold's densification, mechanical properties and bioactivity. Our findings also revealed a few publications have used directly optimal processing parameters that were established in previous works.

The energy density (ED) indicates the amount of energy provided that reaches the bulk material and it can be represented by Energy density = Laser power/(Scan speed x Scan spacing) [95]. Although ED information can be helpful while comparing processing parameters, only 14% of the authors have explicit values in the manuscript. On the other hand, 17% of the reviewed articles have provided less than 2 parameters information displayed in Table 3. Omitting processing parameters information might be due to secure sensitive information, however, it imposes restrictions for a benchmark with other articles.

In terms of equipment, not every SLS machine was equipped with a powder bed heater (which allows controlling the powder bed temperature), this feature is highly recommended to minimize gradient temperature and avoid curling and shrinkage on the fabricated pieces. Another important feature, but hardly used due to high costs, is a sealed chamber with an inert atmosphere that minimize polymer degradation during processing.

One important factor, that not every author has provided, is the layer thickness used for the sample's fabrication. The layer thickness must be in accordance with powder's particle size,

for example, when using an average particle size of 150 μm, the minimal value for layer thickness must be 150 μm. Thereby, each layer is filled with at least 1 particle in height, this will guarantee proper particle's cohesion, better densification and more homogeneous fabricated layers.

Customized implant devices may have several geometry variations for an appropriate anatomical fit, whereas the type of material, pore size and scaffold design must be selected accordingly with implant location and the type of tissue to be restored [96]. According to Yang *et al.* [97] cell's diameter dictates the minimum pore size to promote bone regeneration, scaffold's suitable pore size is in the range of 100-350 μm. Moreover, it is known that geometries with a controlled interconnected porous structure have great importance and are desirable for bone tissue engineering applications, in this sense, authors generally fabricate porous samples, but varying their architecture.

The fabricated specimens were generally cylindric or rectangular, probably due to enable mechanical properties measurement. A few authors have used ASTM D695 and D638 standards for compressive and ensile testing. For biological analysis, it was common to produce porous/solid cylindrical disks within the range of 5 mm to 15 mm diameter and 0.6 mm to 5 mm height. From our research, it was possible to observe that articles published by the same group/authors mostly have fabricated the same geometry, possibly for results comparison. Fabrication of personalized implants (*i.e.*, Figure 5 left) is one of the purposes of using AM techniques, allowing to better treat large bone defects as reported by Zhang *et al.* [94]. A wide range of fabricated geometries was observed between the reviewed articles, demonstrating the versatility of SLS processing.

Certain authors have reported the occurrence of contraction/distortion on the fabricated pieces during the SLS process, affecting the overall quality of the scaffolds. To address that, a solid base was incorporated for the scaffold (see Figure 5) [40], [77], [78], [98]. This

phenomenon was not mentioned by Du *et al.* [21] while fabricating PCL and HA scaffolds with similar dimensions.

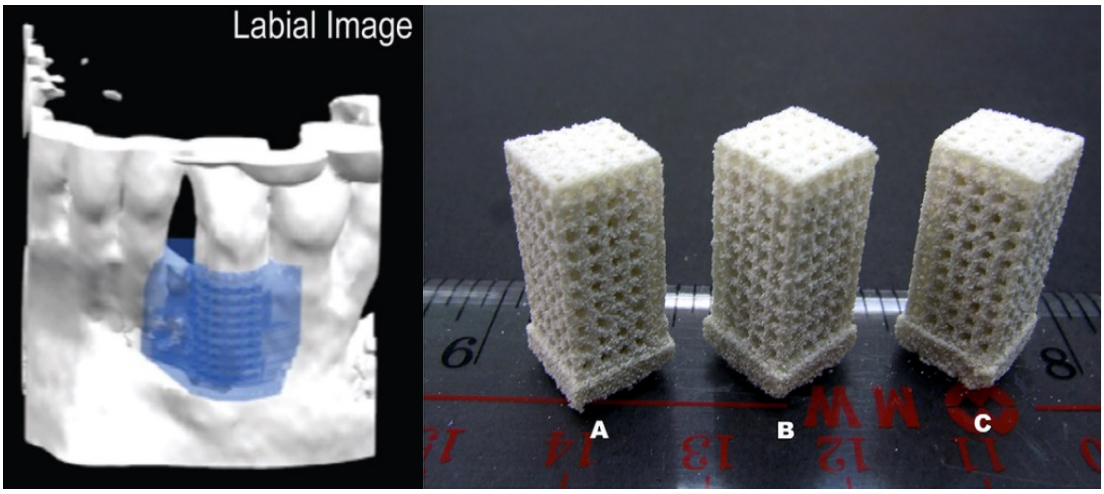

Figure 5: Customized bioresorbable scaffold for periodontal repair (left) [64]. Tetragonal porous scaffold (L x W x H = 8 x 8 x 15.5 mm³ and pores size 1 x 1 x 1 mm³) with solid base (L x W x H = 9 x 9 x 3 mm³) with different processing parameters (right) [40].

Biocompatibility is essential for implantable devices, however, essays related to this aspect were only performed in a small majority (51%) of analyzed articles. Bioactivity analysis is often costly and needs expertise for obtaining reliable results, this might be one of the reasons for only almost half of the reviewed articles to employ these analyses. Among them, only 5 articles (8%) have performed *in vivo* implantation, in which, two have implanted scaffolds in rabbits [63], [79], one in sheep [54] and one in humans [64].

Animal *in vivo* study is an important phase for data assessment for further human trials. Animal implantation studies must be conducted following up-to-date legal provisions, guarantee animal welfare and also have approval of the Animal Experimental Ethics Committee. Within the reviewed articles, two types of animals were used: rabbits and sheep Du *et al.* [63] had successful subchondral bone regeneration with osteochondral repair in rabbits, while Feng *et al.* [79] stated that the implanted scaffold (pDA/HA/PLLA) have

significantly promoted new bone tissue formation, repairing the created bone defect on rabbit's radial bone. Lohfeld *et al.* [54] have conducted *in vivo* study using mountain sheep, a critical size 20 mm cylindrical defect was created in the middle of the diaphysis of the right tibia. PCL/TCP scaffold was placed in the created bone defect, findings revealed promotion of bone regeneration, scaffold degradation and also undesired inflammatory reaction.

Human scaffold implantation and experiments must follow legal and regulatory requirements, therefore most published articles did not conduct them. In the case of Rasperini *et al.* [64] a large periodontal osseous defect was treated using 96% PCL + 4% HA scaffolds, although authors stated that this case was unsuccessful in the long term, they foresee advancements related to this field of interest. Zhang *et al.* [94] have appointed postsurgical infection when implanting 78% HA + 22% EAM scaffolds for treating various complex irregular craniomaxillofacial defects. Results showed that HA/EAM scaffold adhered to the defect area, not showing migration and no foreign body rejection was noticed.

In vitro experiments do not require Ethics Committee approval and provides valuable information to asset the biological response of the fabricated devices. From the reviewed articles, most authors have used commercially available kits to analyze cell culture, viability, proliferation, seeding and attachment. As expected, a greater content of Ca-P material resulted in greater bioactivity. An augmented carbonate apatite layer in the sample's surface was generally cited by authors moreover, the presence of PO_4^{3-} and CO_3^{2-} functional groups were also identified. When samples' weight loss was measured, near-linear weight loss behaviour along time was observed. Finally, the use of additives has demonstrated better results in terms of biocompatibility and osteogenic differentiation.

Table 3: Polymer/Ca-P mixtures and processing parameters.

Materials (wt/wt)	Type of mixing	SLS equipment	Laser source	Range of processing parameters						Reference
				Energy density [J/mm²]	Laser spot size [µm]	Scanning Speed [mm/s]	Laser power [W]	Bed temperature [°C]	Layer thickness [µm]	
100% PMMA 5% β-TCP + 95% PMMA 10% β-TCP + 90% PMMA 15% β-TCP + 85% PMMA 20% β-TCP + 80% PMMA	General	Built in-house	CO_2	0.15	540	450-480	34-38	-	-	[57]
100% PCL 10% HA + 90% PCL 20% HA + 80% PCL	S/O/W	HRPS-IV	CO_2	-	200	1200-2000	6-10	45	200	[21]
100% PCL 10% β-TCP + 90% PCL 50% β-TCP + 50% PCL	General	Sinterstation 2500plus	CO_2	-	410	-	7	49	110	[49]
100% PMMA 5% β-TCP + 95% PMMA 10% β-TCP + 90% PMMA 15% β-TCP + 85% PMMA 20% β-TCP + 80% PMMA	General	Built in-house	CO_2	0.10-0.16	540	250-812	13-42	100	500	[58]
99% β-TCP + 1% PLLA	General	Built in-house	CO_2	0.20-0.60	500	250	20	-	100	[73]

20% HA + 80% β-TCP (20% HA + 80% β-TCP) + 0.5% PLGA (20% HA + 80% β-TCP) + 1% PLGA (20% HA + 80% β-TCP) + 1.5% PLGA (20% HA + 80% β-TCP) + 2% PLGA (50% HA +50% β-TCP) + 0.5% PLGA (50% HA +50% β-TCP) + 1% PLGA (50% HA +50% β-TCP) + 1.5% PLGA (50% HA +50% β-TCP) + 2% PLGA	General	Built in-house	CO_2	-	2000	1.66	6-10	-	200	[26]
58% HA + 42% PA 78% HA + 22% PA	Compounded by extrusion	Built in-house	CO_2	-	-	3400-8350	3.2-10	166	100-200	[56]
100% PHBV 12.9% Ca-P + 87.1% PHBV	S/O/W	Sinterstation 2000	CO_2	-	457	1257	10-15	35	100-200	[92]
20% micro-HA + 80% PLA 20% nano-HA + 80% PLA	Supercritical CO2	Built in-house	-	-	500-1000	-	0.5-4.5	-	-	[76]
100% PEEK 10% HA + 90% PEEK	General	Built in-house	Fibre	-	-	-	-	150	-	[32]
100% PCL 5% HA + 95% PCL up to 30% HA + 70% PCL	S/O/W	HRPS-IV	CO_2	-	-	-	-	-	400	[63]
5% HA + 95% PA 10% HA + 90% PA 15% HA + 85% PA	Manual	Sinterstation 2500 Plus	CO_2	-	-	-	-	132	-	[17]

100% PCL 10% β-TCP + 90% PCL 20% β-TCP + 80% PCL 30% β-TCP + 70% PCL 40% β-TCP + 60% PCL	General	Built in-house	CO_2	-	-	500	1 and 2	40	200	[59]
100% PDLA 20% HA + 80% PDLA	General	SLS-100	Fibre	-	125	-	-	-	-	[33]
100% PEEK/PGA (80/20) 5% HA + 95% PEEK/PGA 7.5% HA + 92.5% PEEK/PGA 10% HA + 90% PEEK/PGA 12.5% HA + 87.5% PEEK/PGA 15% HA + 85% PEEK/PGA	Ethanol solution	Built in-house	CO_2	-	800	6.66	3	-	100-200	[84]
100% PCL 10% β-TCP + 90% PCL	General	Sinterstation 2500 Plus	CO_2	-	-	-	-	-	-	[60]
100% a-PC 5% HA + 95% a-PC 10% HA + 90% a-PC 15% HA + 85% a-PC	Planet ball	HRPS-IV	CO_2	0.16-0.33	200	1800-2200	10-12	135	130-170	[28]
10% β-TCP + 90% PCL 50% β-TCP + 50% PCL	Manual	Sinterstation 2500 Plus	CO_2	-	410	1778	7	49	110	[50]
70% TCP + 30% PLA 75% TCP + 25% PLA 80% TCP + 20% PLA	General	SLS-100	Fibre	-	125	20	-	-	250	[34]
4% HA + 96% PCL	General	Formiga P100	CO_2	-	-	-	-	-	-	[64]
4% HA + 96% PCL	General	Formiga P100	CO_2	-	-	1500	4	52-55	80	[51]
50% β-TCP + 50% PCL	Manual	Sinterstation 2500Plus	CO_2	-	-	-	7	49	110	[52]

100% PCL 5% HA + 95% PCL 10% HA + 90% PCL 15% HA + 85% PCL	V-type mixer	-	-	-	150	550-1330	3-4.5	-	150	[53]
99.50% β-TCP + 0.50% PLLA 99% β-TCP + 1% PLLA 97% β-TCP + 3% PLLA	General	Built in-house	CO_2	-	500	250	10-30	-	100	[70]
100% PLGA 10% HA + 90% PLGA 20% HA + 80% PLGA 30% HA + 70% PLGA 40% HA + 60% PLGA	General	Built in-house	CO_2	0.06-0.12	-	-	-	-	-	[80]
99% β-TCP + 1% PLLA	General	Built in-house	CO_2	-	500	200	10	-	100	[71]
5% HA + 95% HDPE 10% HA + 90% HDPE 20% HA + 80% HDPE	Y-mixer	Built in-house	CO_2	-	250	57	5	80	125	[88]
100% PCL 15% HA + 85% PCL 20% HA + 80% PCL 30% HA + 70% PCL	V-type mixer	Sinterstation 2500Plus	CO_2	-	400	1778-5080	5-10	38	150	[22]
99% HA + 1% PLLA	General	Built in-house	CO_2	-	50	16.66	5-20	150	200	[72]
100% PCL 10% β-TCP + 90% PCL 20% β-TCP + 80% PCL 30% β-TCP + 70% PCL 40% β-TCP + 60% PCL 50% β-TCP + 50% PCL	General	Sinterstation 2500Plus	CO_2	-	410	-	5-9	-	500	[54]

100% PCL 10% HA + 90% PCL 20% HA + 80% PCL 30% HA + 70% PCL	Rotary tumbler	Sinterstation 2000	CO_2	-	450	914	1-1.2	50	-	[67]
8.2% Ca-P + 91.8% PHBV	S/O/W	Sinterstation 2000	CO_2	-	-	1257	15	35	100	[90]
15% Ca-P + 85% PHBV 10% CHA + 90% PLLA	S/O/W	Sinterstation 2000	CO_2	-	457	1257	13-15	35 and 45	100 and 150	[77]
12.9% Ca-P + 87.1% PHBV	S/O/W	-	CO_2	-	-	1257	15	35	100	[91]
15% Ca-P + 85% PHBV	S/O/W	Sinterstation 2000	CO_2	-	-	1257	12.5-15	35	100-150	[40]
100% PCL 30% HA + 70% PCL	General	Sinterstation 2500Plus	CO_2	-	410	1778 and 5080	3.32-11.68	38	150	[55]
70% PEEK + 20% β-TCP + 10% PLLA 60% PEEK + 20% β-TCP + 20% PLLA 50% PEEK + 20% β-TCP + 30% PLLA 40% PEEK + 20% β-TCP + 40% PLLA 30% PEEK + 20% β-TCP + 50% PLLA 80% PEEK + 20% β-TCP	Ethanol solution	-	CO_2	-	500	120	-	-	100-200	[83]
30% HA + 70% PDLA	General	SLS-100	Fibre	-	-	-	≤ 10	-	-	[31]
10% TCP + 90% PCL 20% TCP + 80% PCL 30% TCP + 70% PCL	Rotary tumbler	Sinterstation 2000	CO_2	-	-	863.6 and 1079.5	1 and 2.25	46 and 50	-	[61]
50% β-TCP + 50% PDLA	Ethanol solution	-	-	-	290-360	-	0.30-0.45	-	-	[68]
10% CHA + 90% PLLA	Rotary tumbler	Sinterstation 2000	CO_2	-	457	1257	0.15-0.21	30-40	100	[78]

1.5% SBA + 98.5% PLLA 1.5% SBA + 5% HA + 93.5% PLLA 1.5% SBA + 10% HA + 88.5% PLLA 1.5% SBA + 15% HA + 83.5% PLLA	Ethanol solution	-	-	-	-	-	-	-	-	[38]
100% PA 5% HA + 95% PA 10% HA + 90% PA 20% HA + 80% PA	Y-mixer	-	CO_2	0.281 and 0.351	250	57	-	140	150	[86]
78% HA + 22% EAM	General	AFS320	-	-	-	-	-	-	-	[94]
20% HA + 80% PLA 30% HA + 70% PLA	General	-	-	-	-	2200	9.22	-	500	[74]
100% PA 5% HA + 95% PA 10% HA + 90% PA 15% HA + 85% PA 20% HA + 80% PA	General	Sinterstation 2500 Plus	-	-	-	-	-	-	-	[85]
75% BP (70% HA + 30% TCP) + 25% EP 70% BP (70% HA + 30% TCP) + 30% EP 65% BP (70% HA + 30% TCP) + 35% EP 60% BP (70% HA + 30% TCP) + 40% EP 55% BP (70% HA + 30% TCP) + 45% EP 50% BP (70% HA + 30% TCP) + 50% EP 45% BP (70% HA + 30% TCP) + 55% EP 40% BP (70% HA + 30% TCP) + 60% EP	General	HK S320	CO_2	-	-	200	1.8	-	100	[25]

HA + PCL	General	-	-	-	-	-	-	-	-	[65]
100% PCL 15% HA + 85% PCL 30% HA + 70% PCL	General	Sinterstation 2500Plus	CO_2	-	-	-	5-10	35	150	[66]
40% HA + 60% HDPE	Compounded by extrusion	Built in-house	CO_2	-	193	300-4800	1.2-9.6	-	400	[89]
100% PLA 33.34% HA + 66.66% PLA 25% HA + 75% PLA	General	-	Fibre	-	-	100	3-25	-	-	[75]
100% PA 5% HA + 95% PA 10% HA + 90% PA 20% HA + 80% PA	Y-mixer	-	CO_2	0.281 and 0.351	250	57	4 and 5	140	150	[87]
100% PCL 20% HA + 80% PCL	HRPS-IV	-	CO_2	-	-	-	-	-	-	[37]
5% HA + 95% PA	HW-S4040	-	-	-	-	3500	17	176	100	[29]
pDA + PLLA + HA	Wet route	Built in-house	-	1.3	580	2	2.3	80	100-200	[79]
100% PDLA 10% HA + 90% PDLA	S/O/W	HK P320	CO_2	0.021-0.032	-	1400-2000	3.5-4.5	40-60	80-120	[69]
100% PLLA 5% HA + 95% PLLA 10% HA + 90% PLLA 15% HA + 85% PLLA 20% HA + 80% PLLA 25% HA + 75% PLLA 5% C-HA + 95% PLLA 10% C-HA + 90% PLLA 15% C-HA + 85% PLLA 20% C-HA + 80% PLLA 25% C-HA + 75% PLLA	Ethanol solution	-	-	-	-	-	-	-	-	[35]

PLLA/HA 9:1 PLLA/HA/MET 9:1:2; 9:1:4; 9:1:8	Ethanol solution	Built in-house	CO_2	-	300	2	2.1	175	100-200	[36]
β-TCP + Epoxy resin/nylon	General	HRPS-IIIA	-	-	-	2500	12	50	100	[93]
30% HA + 70% HDPE 40% HA + 60% HDPE	Compounded by extrusion	Built in-house	CO_2	-	193	300-4800	3.6-7.2	110	400	[42]
100% PCL 10% β-TCP + 90% PCL	Rotary tumbler	Sinterstation 2000	CO_2	-	450	1079.5 and 1231.9	4.1 and 5.4	46 and 48	-	[62]
10% HA + 90% PEEK 20% HA + 80% PEEK 30% HA + 70% PEEK 40% HA + 60% PEEK	General	Sinterstation 2500	CO_2	-	-	5080	9-28	140	100	[81]
100% PEEK 10% HA + 90% PEEK 20% HA + 80% PEEK 30% HA + 70% PEEK 40% HA + 60% PEEK	Roller mixer	Sinterstation 2500	CO_2	-	-	5080	9-28	110 and 140	100	[82]

5. Conclusion

Polymer-CaP scaffolds produced by SLS have shown to be a viable solution for bone tissue regeneration applications. SLS processing allows producing complex and functionalized scaffolds, addressing new possibilities for customized implants. However, taking into consideration that only 63 articles were selected to be reviewed from the 650 articles found in the database, it demonstrates how incipient is the combination of polymer/Ca-P for scaffolds fabrication.

Among the materials used, PCL and PLLA, HA and TCP were the major selection. A few articles have used more than 3 materials in the composite mixture, mainly to add beneficial properties such as increase processability or functionalization. The use of certain additives can improve material's sinterability as well as bring supplementary properties for scaffolds, for example, to promote bioactivity.

Selection of mixing technique is important to maintain powder's homogeneity and also must take into account material's properties to avoid degradation. SLS processing parameters have shown great influence on scaffold's properties, therefore, the use of DOE and statistical tools are recommended. Home-made and commercial SLS equipment may have significant differences in performance, but both can achieve complex geometries in the fabricated devices. Biocompatibility essays are fundamental for achieving better bone regeneration, however, these essays were not applied in many of the reviewed articles.

Advancements in bulk material preparation, use of additives, scaffold's geometry, as well as processing parameters optimization, may bring important advancements for polymer/Ca-P implantable devices.

References

[1] J. D'Alessio and A. Christensen, "3D Printing for Commercial Orthopedic Applications: Advances and Challenges," in 3D Printing in Orthopaedic Surgery, Elsevier, 2019, pp. 65–83.

[2] M. Fricia, M. Passanisi, F. Salamanna, A. Parrilli, G. Giavaresi, and M. Fini, "Case Report Osteointegration in Custom-made Porous Hydroxyapatite Cranial Implants : From Reconstructive Surgery to Regenerative Medicine," World Neurosurg., vol. 84, no. 2, pp. 591.e11-591.e16, 2015.

[3] M.-P. Boncoeur et al., "A new custom made bioceramic implant for the repair of large and complex craniofacial bone defects," J. Cranio-Maxillofacial Surg., vol. 41, no. 5, pp. 403–407, 2012.

[4] L. Piaia, G. V. Salmoria, and D. Hotza, Additive manufacturing of nanostructured bone scaffolds. Elsevier Inc., 2018.

[5] E. F. Eriksen, D. W. Axelrod, and F. Melsen, Bone histomorphometry. Raven Press, 1994.

[6] S. Bose, S. Vahabzadeh, and A. Bandyopadhyay, "Bone tissue engineering using 3D printing," Mater. Today, vol. 16, no. 12, pp. 496–504, Dec. 2013.

[7] A. Yahamed, P. Ikonomov, P. D. Fleming, A. Pekarovicova, P. Gustafson, and A. Q. Alden, "Mechanical properties of 3D printed polymers," vol. 5, pp. 273–289, 2016.

[8] F. H. Liu, "Fabrication of Bioceramic Bone Scaffolds for Tissue Engineering," J. Mater. Eng. Perform., vol. 23, no. 10, pp. 3762–3769, 2014.

[9] D. Marchat and E. Champion, Ceramic devices for bone regeneration: Mechanical and clinical issues and new perspectives. Elsevier Ltd, 2017.

[10] M. Parent, H. Baradari, E. Champion, C. Damia, and M. Viana-Trecant, "Design of calcium phosphate ceramics for drug delivery applications in bone diseases: A review of the parameters affecting the loading and release of the therapeutic substance," J. Control. Release, vol. 252, pp. 1–17, 2017.

[11] "ISO/ASTM 52900: 2015 Additive manufacturing-General principles-terminology," ASTM F2792-10e1, 2012.

[12] F. E. Wiria, K. F. Leong, C. K. Chua, and Y. Liu, "Poly-ε-caprolactone/hydroxyapatite for tissue engineering scaffold fabrication via selective laser sintering," Acta Biomater., vol. 3, no. 1, pp. 1–12, 2007.

[13] G. V. Salmoria, R. V. Pereira, M. C. Fredel, and A. P. M. Casadei, "Properties of PLDLA/bioglass scaffolds produced by selective laser sintering," Polym. Bull., vol. 75, no. 3, pp. 1299–1309, 2018.

[14] D. M. Panaitescu, A. N. Frone, and I. Chiulan, "Nanostructured biocomposites from aliphatic polyesters and bacterial cellulose," Ind. Crops Prod., vol. 93, pp. 251–266, 2016.

[15] M. Schmid, A. Amado, and K. Wegener, "Polymer powders for selective laser sintering (SLS)," vol. 160009, no. 2015, p. 160009, 2015.

[16] J. Schmidt, M. Dechet, J. G. Bonilla, S. Kloos, K. E. Wirth, and W. Peukert, "Novel process routes towards the production of spherical polymer powders for selective laser sintering," AIP Conf. Proc., vol. 2139, no. August, pp. 1–6, 2019.

[17] T. Kumaresan, R. Gandhinathan, M. Ramu, M. Ananthasubramanian, and K. B. Pradheepa, "Design, analysis and fabrication of polyamide/hydroxyapatite porous structured scaffold using selective laser sintering method for bio-medical applications," J. Mech. Sci. Technol., vol. 30,

no. 11, pp. 5305–5312, 2016.

[18] R. Dwivedi et al., “Polycaprolactone as biomaterial for bone scaffolds: Review of literature,” J. Oral Biol. Craniofacial Res., vol. 10, no. 1, pp. 381–388, 2020.

[19] D. da Silva et al., “Biocompatibility, biodegradation and excretion of polylactic acid (PLA) in medical implants and theranostic systems,” Chem. Eng. J., vol. 340, no. January, pp. 9–14, 2018.

[20] R. M. Rasal, A. V. Janorkar, and D. E. Hirt, “Poly(lactic acid) modifications,” Prog. Polym. Sci., vol. 35, no. 3, pp. 338–356, 2010.

[21] Y. Du, H. Liu, J. Shuang, J. Wang, J. Ma, and S. Zhang, “Microsphere-based selective laser sintering for building macroporous bone scaffolds with controlled microstructure and excellent biocompatibility,” Colloids Surfaces B Biointerfaces, vol. 135, pp. 81–89, 2015.

[22] S. Eosoly, N. E. Vrana, S. Lohfeld, M. Hindie, and L. Looney, “Interaction of cell culture with composition effects on the mechanical properties of polycaprolactone-hydroxyapatite scaffolds fabricated via selective laser sintering (SLS),” Mater. Sci. Eng. C, vol. 32, no. 8, pp. 2250–2257, 2012.

[23] T. J. Blokhuis, M. F. Termaat, F. C. Den Boer, P. Patka, F. C. Bakker, and H. J. T. M. Haarman, “Properties of calcium phosphate ceramics in relation to their in vivo behavior,” J. Trauma - Inj. Infect. Crit. Care, vol. 48, no. 1, pp. 179–186, 2000.

[24] G. Ma, “Three common preparation methods of hydroxyapatite,” IOP Conf. Ser. Mater. Sci. Eng., vol. 688, no. 3, 2019.

[25] H. Zeng et al., “Indirect selective laser sintering-printed microporous biphasic calcium phosphate scaffold promotes endogenous bone regeneration via activation of ERK1/2 signaling,” Biofabrication, vol. 12, no. 2, p. 025032, Mar. 2020.

[26] C. Gao, B. Yang, H. Hu, J. Liu, C. Shuai, and S. Peng, “Enhanced sintering ability of biphasic calcium phosphate by polymers used for bone scaffold fabrication,” Mater. Sci. Eng. C, vol. 33, no. 7, pp. 3802–3810, Oct. 2013.

[27] P. Bertrand, F. Bayle, C. Combe, P. Goeuriot, and I. Smurov, “Ceramic components manufacturing by selective laser sintering,” Appl. Surf. Sci., vol. 254, no. 4, pp. 989–992, 2007.

[28] S. XiaoHui et al., “Selective laser sintering of aliphatic-polycarbonate/hydroxyapatite composite scaffolds for medical applications,” Int. J. Adv. Manuf. Technol., vol. 81, no. 1–4, pp. 15–25, 2015.

[29] J. Li, Z. Zhao, R. Yan, and Y. Yang, “Mechanical properties of graded scaffolds developed by curve interference coupled with selective laser sintering,” Mater. Sci. Eng. C, vol. 116, no. March, p. 111181, 2020.

[30] S. Ramakrishna and Z.-M. Huang, Biocomposites, no. April 2015. 2016.

[31] D. Kuznetsova et al., “Study of the involvement of allogeneic MSCs in bone formation using the model of transgenic mice,” Cell Adh. Migr., vol. 11, no. 3, pp. 233–244, 2017.

[32] I. Shishkovsky, V. Sherbakov, I. Ibatullin, V. Volchkov, and L. Volova, “Nano-size ceramic reinforced 3D biopolymer scaffolds: Tribomechanical testing and stem cell activity,” Compos. Struct., no. January, pp. 0–1, 2018.

[33] D. S. Kuznetsova et al., “Comparative Analysis of Proliferation and Viability of Multipotent Mesenchymal Stromal Cells in 3D Scaffolds with Different Architectonics,” Bull. Exp. Biol. Med., vol. 160, no. 4, pp. 535–541, 2016.

[34] E. N. Antonov et al., “Selective laser sintering of bioactive composite matrices for bone tissue engineering,” Inorg. Mater. Appl. Res., vol. 6, no. 2, pp. 171–178, 2015.

[35] C. Shuai, L. Yu, W. Yang, S. Peng, Y. Zhong, and P. Feng, "Phosphonic acid coupling agent modification of HAP nanoparticles: Interfacial effects in PLLA/HAP bone scaffold," Polymers (Basel)., vol. 12, no. 1, 2020.

[36] W. Tan et al., "Dual-functional scaffolds of poly(L-lactic acid)/nanohydroxyapatite encapsulated with metformin: Simultaneous enhancement of bone repair and bone tumor inhibition," Mater. Sci. Eng. C, vol. 120, no. November 2020, p. 111592, 2021.

[37] H. Liu et al., "Delivering Proangiogenic Factors from 3D-Printed Polycaprolactone Scaffolds for Vascularized Bone Regeneration," Adv. Healthc. Mater., vol. 9, no. 23, p. 2000727, Dec. 2020.

[38] C. Shuai, Y. Xu, P. Feng, L. Xu, S. Peng, and Y. Deng, "Co-enhance bioactive of polymer scaffold with mesoporous silica and nano-hydroxyapatite," J. Biomater. Sci. Polym. Ed., vol. 30, no. 12, pp. 1097–1113, 2019.

[39] A. Mohammed, A. Elshaer, P. Sareh, M. Elsayed, and H. Hassanin, "Additive Manufacturing Technologies for Drug Delivery Applications," Int. J. Pharm., vol. 580, no. January, p. 119245, 2020.

[40] B. Duan and M. Wang, "Encapsulation and release of biomolecules from Ca-P/PHBV nanocomposite microspheres and three-dimensional scaffolds fabricated by selective laser sintering," Polym. Degrad. Stab., vol. 95, no. 9, pp. 1655–1664, 2010.

[41] F. Fina, S. Gaisford, and A. W. Basit, "Powder Bed Fusion: The Working Process, Current Applications and Opportunities," in 3D Printing of Pharmaceuticals, 2018, pp. 81–105.

[42] L. Hao, M. M. Savalani, Y. Zhang, K. E. Tanner, and R. A. Harris, "Selective laser sintering of hydroxyapatite reinforced polyethylene composites for bioactive implants and tissue scaffold development," Proc. Inst. Mech. Eng. Part H J. Eng. Med., vol. 220, no. 4, pp. 521–531, 2006.

[43] V. Bhavar, P. Kattire, V. Patil, S. Khot, K. Gujar, and R. Singh, "A review on powder bed fusion technology of metal additive manufacturing," Addit. Manuf. Handb., pp. 251–253, 2017.

[44] M. Schmid, A. Amado, and K. Wegener, "Materials perspective of polymers for additive manufacturing with selective laser sintering," J. Mater. Res., vol. 29, no. 17, pp. 1824–1832, 2014.

[45] V. E. Beal, R. A. Paggi, G. V. Salmoria, and A. Lago, "Statistical evaluation of laser energy density effect on mechanical properties of polyamide parts manufactured by selective laser sintering," J. Appl. Polym. Sci., vol. 113, no. 5, pp. 2910–2919, Sep. 2009.

[46] M. Sadat-Shojai, M. T. Khorasani, E. Dinpanah-Khoshdargi, and A. Jamshidi, "Synthesis methods for nanosized hydroxyapatite with diverse structures," Acta Biomater., vol. 9, no. 8, pp. 7591–7621, 2013.

[47] R. Patel, M. Lu, S. H. Diermann, A. Wu, A. Pettit, and H. Huang, "Deformation behavior of porous PHBV scaffold in compression: A finite element analysis study," J. Mech. Behav. Biomed. Mater., vol. 96, no. November 2018, pp. 1–8, 2019.

[48] S. H. Diermann, M. Lu, Y. Zhao, L. J. Vandi, M. Dargusch, and H. Huang, "Synthesis, microstructure, and mechanical behaviour of a unique porous PHBV scaffold manufactured using selective laser sintering," J. Mech. Behav. Biomed. Mater., vol. 84, no. March, pp. 151–160, 2018.

[49] H. Doyle, S. Lohfeld, and P. McHugh, "Evaluating the effect of increasing ceramic content on the mechanical properties, material microstructure and degradation of selective laser sintered polycaprolactone/β-tricalcium phosphate materials," Med. Eng. Phys., vol. 37, no. 8, pp. 767–776, Aug. 2015.

[50] H. Doyle, S. Lohfeld, P. McDonnell, and P. McHugh, "Evaluation of a Multiscale Modelling

Methodology to Predict the Mechanical Properties of PCL/β-TCP Sintered Scaffold Materials," Ann. Biomed. Eng., vol. 43, no. 8, pp. 1989–1998, 2015.

[51] M. R. Dias, J. M. Guedes, C. L. Flanagan, S. J. Hollister, and P. R. Fernandes, "Optimization of scaffold design for bone tissue engineering: A computational and experimental study," Med. Eng. Phys., vol. 36, no. 4, pp. 448–457, 2014.

[52] H. Doyle, S. Lohfeld, and P. McHugh, "Predicting the elastic properties of selective laser sintered PCL/β-TCP bone scaffold materials using computational modelling," Ann. Biomed. Eng., vol. 42, no. 3, pp. 661–677, 2014.

[53] Y. Xia et al., "Selective laser sintering fabrication of nano-hydroxyapatite/poly-ε-caprolactone scaffolds for bone tissue engineering applications," Int. J. Nanomedicine, vol. 8, pp. 4197–213, 2013.

[54] S. Lohfeld et al., "Fabrication, mechanical and in vivo performance of polycaprolactone/tricalcium phosphate composite scaffolds," Acta Biomater., vol. 8, no. 9, pp. 3446–3456, 2012.

[55] S. Eosoly, D. Brabazon, S. Lohfeld, and L. Looney, "Selective laser sintering of hydroxyapatite/poly-ε-caprolactone scaffolds," Acta Biomater., vol. 6, no. 7, pp. 2511–2517, 2010.

[56] M. M. Savalani, L. Hao, P. M. Dickens, Y. Zhang, K. E. Tanner, and R. A. Harris, "The effects and interactions of fabrication parameters on the properties of selective laser sintered hydroxyapatite polyamide composite biomaterials," Rapid Prototyp. J., vol. 18, no. 1, pp. 16–27, 2012.

[57] R. Velu, B. P. Kamarajan, M. Ananthasubramanian, T. Ngo, and S. Singamneni, "Post-process composition and biological responses of laser sintered PMMA and β-TCP composites," J. Mater. Res., pp. 1–12, 2018.

[58] R. Velu and S. Singamneni, "Selective laser sintering of polymer biocomposites based on polymethyl methacrylate," J. Mater. Res., vol. 29, no. 17, pp. 1883–1892, 2014.

[59] H. Liao, M. Lee, W. Tsai, H. Wang, and W. Lu, "Osteogenesis of adipose-derived stem cells on polycaprolactone–β-tricalcium phosphate scaffold fabricated via selective laser sintering and surface coating with collagen type I," J. Tissue Eng. Regen. Med., no. 10, pp. 337–353, 2016.

[60] S. Lohfeld, S. Cahill, H. Doyle, and P. E. McHugh, "Improving the finite element model accuracy of tissue engineering scaffolds produced by selective laser sintering," J. Mater. Sci. Mater. Med., vol. 26, no. 1, pp. 1–12, 2015.

[61] H. Chung, H. Jee, and S. Das, "Selective laser sintering of PCL/TCP composites for tissue engineering scaffolds †," J. Mech. Sci. Technol., vol. 24, pp. 241–244, 2010.

[62] B. Partee, S. J. Hollister, and S. Das, "Selective Laser Sintering of Polycaprolactone Bone Tissue Engineering Scaffolds," MRS Proc., vol. 845, pp. 340–346, Feb. 2004.

[63] Y. Du et al., "Selective laser sintering scaffold with hierarchical architecture and gradient composition for osteochondral repair in rabbits," Biomaterials, vol. 137, pp. 37–48, 2017.

[64] G. Rasperini et al., "3D-printed Bioresorbable Scaffold for Periodontal Repair," J. Dent. Res., vol. 94, no. 9, pp. 153S-157S, 2015.

[65] H. Kang, S. J. Hollister, F. La Marca, P. Park, and C. Y. Lin, "Porous biodegradable lumbar interbody fusion cage design and fabrication using integrated global-local topology optimization with laser sintering," J. Biomech. Eng., vol. 135, no. 10, 2013.

[66] S. Eosoly, S. Lohfeld, and D. Brabazon, "Effect of hydroxyapatite on biodegradable scaffolds fabricated by SLS," Key Eng. Mater., vol. 396–398, pp. 659–662, 2009.

[67] S. Eshraghi and S. Das, "Micromechanical finite-element modeling and experimental characterization of the compressive mechanical properties of polycaprolactone-hydroxyapatite composite scaffolds prepared by selective laser sintering for bone tissue engineering," Acta Biomater., vol. 8, no. 8, pp. 3138–3143, 2012.

[68] C. Gayer et al., "Influence of the material properties of a poly(D,L-lactide)/β-tricalcium phosphate composite on the processability by selective laser sintering," J. Mech. Behav. Biomed. Mater., vol. 87, no. July, pp. 267–278, Nov. 2018.

[69] K. Lin et al., "Selective laser sintered nano-HA/PDLLA composite microspheres for bone scaffolds applications," Rapid Prototyp. J., vol. 26, no. 6, pp. 1131–1143, May 2020.

[70] D. Liu, J. Zhuang, C. Shuai, and S. Peng, "Mechanical properties' improvement of a tricalcium phosphate scaffold with poly-L-lactic acid in selective laser sintering," Biofabrication, vol. 5, no. 2, 2013.

[71] C. Shuai, J. Zhuang, H. Hu, S. Peng, D. Liu, and J. Liu, "In vitro bioactivity and degradability of β-tricalcium phosphate porous scaffold fabricated via selective laser sintering," Biotechnol. Appl. Biochem., vol. 60, no. 2, pp. 266–273, 2013.

[72] C. Shuai et al., "Poly (l-lactide acid) improves complete nano-hydroxyapatite bone scaffolds through the microstructure rearrangement," Electron. J. Biotechnol., vol. 15, no. 6, 2012.

[73] C. Shuai, J. Zhuang, S. Peng, and X. Wen, "Inhibition of phase transformation from β- to α-tricalcium phosphate with addition of poly (L-lactic acid) in selective laser sintering," Rapid Prototyp. J., vol. 20, no. 5, pp. 369–376, Aug. 2014.

[74] A. E. Woźna, A. F. Junka, and P. E. Szymczyk, "The influence of different composite mixtures (PLA/HA) manufactured with additive laser technology on the ability of S. aureus and P. aeruginosa to form biofilms," Acta Bioeng. Biomech., vol. 20, no. 3, pp. 101–106, 2018.

[75] Q. Zhang, F. Liu, and J. Chen, "Development of porous scaffolds using selective laser sintering of polylactic acid/ hydroxyapatite for bone tissur engineering," Adv. Mater. Res., vol. 291–294, pp. 1399–1404, 2011.

[76] E. N. Antonov, S. A. Bochkova, and A. V. Popova, "Formation of a bioactive material for selective laser sintering from a mixture of powdered polylactide and nano-hydroxyapatite in supercritical carbon dioxide," Russ. J. Phys. Chem. B, vol. 5, no. 8, pp. 1253–1257, 2011.

[77] B. Duan, M. Wang, W. Y. Zhou, W. L. Cheung, Z. Y. Li, and W. W. Lu, "Three-dimensional nanocomposite scaffolds fabricated via selective laser sintering for bone tissue engineering," Acta Biomater., vol. 6, no. 12, pp. 4495–4505, 2010.

[78] W. You, M. Wang, W. Lam, and W. Yuk, "Selective Laser Sintering of Poly(L-Lactide)/Carbonated Hydroxyapatite Nanocomposite Porous Scaffolds for Bone Tissue Engineering," Tissue Eng., 2010.

[79] P. Feng et al., "In Situ Generation of Hydroxyapatite on Biopolymer Particles for Fabrication of Bone Scaffolds Owning Bioactivity," ACS Appl. Mater. Interfaces, vol. 12, no. 41, pp. 46743–46755, 2020.

[80] C. Shuai, B. Yang, S. Peng, and Z. Li, "Development of composite porous scaffolds based on poly(lactide-co-glycolide)/nano-hydroxyapatite via selective laser sintering," Int. J. Adv. Manuf. Technol., vol. 69, no. 1–4, pp. 51–57, 2013.

[81] K. H. Tan, C. K. Chua, K. F. Leong, M. W. Naing, and C. M. Cheah, "Fabrication and characterization of three-dimensional poly(ether-ether-ketone)/-hydroxyapatite biocomposite scaffolds using laser sintering," Proc. Inst. Mech. Eng. Part H J. Eng. Med., vol. 219, no. 3, pp. 183–194, Mar. 2005.

[82] K. H. Tan et al., "Scaffold development using selective laser sintering of polyetheretherketone-hydroxyapatite biocomposite blends," Biomaterials, vol. 24, no. 18, pp. 3115–3123, 2003.

[83] P. Feng, P. Wu, C. Gao, Y. Yang, W. Guo, and W. Yang, "A Multimaterial Scaffold With Tunable Properties: Toward Bone Tissue Repair," vol. 1700817, pp. 1–15, 2018.

[84] C. Shuai et al., "Characterization and bioactivity evaluation of (polyetheretherketone/polyglycolicacid)-hydroyapatite scaffolds for tissue regeneration," Materials (Basel)., vol. 9, no. 11, 2016.

[85] M. Ramu, M. Ananthasubramanian, T. Kumaresan, R. Gandhinathan, and S. Jothi, "Optimization of the configuration of porous bone scaffolds made of Polyamide/Hydroxyapatite composites using Selective Laser Sintering for tissue engineering applications," Biomed. Mater. Eng., vol. 29, no. 6, pp. 739–755, 2018.

[86] F. Dabbas, S. L. Stares, H. Schappo, D. Hotza, and G. V. Salmoria, "Viscoelastic Properties and Creep-Fatigue Behavior of PA2200/HA Composites Manufactured by Selective Laser Sintering," J. Mater. Sci. Eng. B, vol. 9, no. 1, pp. 25–31, 2019.

[87] F. Dabbas, S. L. Stares, J. M. Mascheroni, D. Hotza, and G. V. Salmoria, "Selective Laser Sintering of Polyamide/Hydroxyapatite Scaffolds," in Proceedings of the 3rd Pan American Materials Congress, 2017, pp. 95–103.

[88] G. V. Salmoria, E. A. Fancello, C. R. M. Roesler, and F. Dabbas, "Functional graded scaffold of HDPE/HA prepared by selective laser sintering: Microstructure and mechanical properties," Int. J. Adv. Manuf. Technol., vol. 65, no. 9–12, pp. 1529–1534, 2013.

[89] L. Hao, M. M. Savalani, R. a. Harris, Y. Zhang, and K. E. Tanner, "Rapid manufacturing of bioceramic/polymer composite implants by selective laser sintering," Int. J. Comput. Appl. Technol., vol. 36, no. 1, p. 25, 2009.

[90] B. Duan, M. Wang, Z. Y. Li, W. C. Chan, and W. W. Lu, "Surface modification of three-dimensional Ca-P/PHBV nanocomposite scaffolds by physical entrapment of gelatin and its in vitro biological evaluation," Front. Mater. Sci. China, vol. 5, no. 1, pp. 57–68, 2011.

[91] M. Wang and B. Duan, "Customized Ca–P/PHBV nanocomposite Scaffolds for Bone Tissue Engineering: Design, Fabrication, Surface Modification and Sustained Release of Growth Factor," MRS Proc., vol. 1301, 2011.

[92] B. Duan, W. L. Cheung, and M. Wang, "Optimized fabrication of Ca-P/PHBV nanocomposite scaffolds via selective laser sintering for bone tissue engineering," Biofabrication, vol. 3, no. 1, p. 015001, 2011.

[93] L. Liulan, H. Qingxi, H. Xianxu, and X. Gaochun, "Design and Fabrication of Bone Tissue Engineering Scaffolds via Rapid Prototyping and CAD," J. Rare Earths, vol. 25, no. SUPPL. 2, pp. 379–383, 2007.

[94] L. Zhang, S. Shen, H. Yu, S. G. Shen, and X. Wang, "Computer-aided design and computer-aided manufacturing hydroxyapatite/epoxide acrylate maleic compound construction for craniomaxillofacial bone defects," J. Craniofac. Surg., vol. 26, no. 5, pp. 1477–1481, 2015.

[95] J. D. Williams and C. R. Deckard, "Advances in modeling the effects of selected parameters on the SLS process," Rapid Prototyp. J., vol. 4, no. 2, pp. 90–100, 1998.

[96] H. Qu, H. Fu, Z. Han, and Y. Sun, "Biomaterials for bone tissue engineering scaffolds: A review," RSC Adv., vol. 9, no. 45, pp. 26252–26262, 2019.

[97] S. Yang, K. F. Leong, Z. Du, and C. K. Chua, "The design of scaffolds for use in tissue engineering. Part I. Traditional factors," Tissue Eng., vol. 7, no. 6, pp. 679–689, 2001.

[98] W. Y. Zhou, S. H. Lee, M. Wang, W. L. Cheung, and W. Y. Ip, "Selective laser sintering of

porous tissue engineering scaffolds from poly(L-lactide)/carbonated hydroxyapatite nanocomposite microspheres," J. Mater. Sci. Mater. Med., vol. 19, no. 7, pp. 2535–2540, 2008.

Conclusions of Chapter 2

The preceding review article has provided substantial information in terms of SLS processing of polymer/Ca-P. Therefore, the outcomes and observations from the authors were considered for the further steps of the present work.

Physical powder mixture has shown to be effective and propitious for homogeneous mixing of the composite powders, thus, it was chosen as a method for mixing UHMWPE/SDHA powders. No concense was found regarding the geometry of fabricated samples, most authors have used rectangular and cubic forms. The selected geometries for the present work considered former dimensions already employed in our research group. Cylindrical forms were selected due to the better fitting inside cell-culture dishes.

CO_2 laser source was proven to be suitable for polymer/Ca-P composites processing accounting for the majority of users. The use of commercially available SLS machines have the advantage of not requiring hardware/software expertise for building it, however, the self-made machines are more cost-effective. This work was conducted using an experimental self-developed SLS machine, available at NIMMA (UFSC) laboratory facilities.

Finally, the choice of HA from the available calcium phosphate materials is well endorsed by the available publications. TCP was also widely employed in the reviewed articles, but its faster degradability and absorption within the body, its use should be in accordance with new bone growth and formation to avoid poor local stability. The lack of UHMWPE employment as a polymer of choice might be justified because of the challenges towards SLS processing.

The combination of UHMWPE and HA particles were not revealed among the selected keywords and database. Therefore, with the purpose to investigate the state of the art and related

bibliography of SLS processing of UHMWPE and HA, the following keyworks were searched using Google Scholar: UHMWPE, hydroxyapatite, “selective laser sintering”.

Among the 339 results revealed, only 10 met the following selection criteria: original research articles that were processed by SLS, using UHMWPE (with or without HA) powder as feedstock for fabricating implantable devices. Among the selected 10 articles, none of them has used the combination of UHMWPE and HA or SDHA, revealing a research opportunity of these widely used biomaterials.

CHAPTER 3
Manuscript 2

Introduction to Chapter 3

The following chapter contains experiments conducted at IRCER (*Institut de Recherche sur les Céramiques*), being the first experimental published article. It describes the method employed for investigating the adequacy of the spray drying method for producing HA particles suitable for SLS processing. Synthesized HA particles have a needle-like morphology and tend to agglomerate, deleterious characteristics for the SLS processing. Ideally, the HA particles added into the UHMWPE matrix would be spherical and with a size compatible to occupy voids among polymeric particles. The spray drying technique showed the potential to produce HA spherical particles with a mean diameter in the range of 15 to 25 μm. Further, this technique is scalable and can be used by industry.

A large number of experiments were conducted to achieve the summarized results shown in the article. This methodology allowed a better understanding of the spray drying machine and its particularities. Understanding machine limitations and performance have great importance for larger powder production.

Screening Method for Producing Suitable Spray-dried HA powder for SLS application

Henrique Schappo[1,2], Karine Giry[2], Chantal Damia[2], Dachamir Hotza[3]

[1]Innovation Laboratory for Molding and Additive Manufacturing (NIMMA), Federal University of Santa Catarina (UFSC), 88040-900 Florianópolis, SC, Brazil
[2]University of Limoges, CNRS, IRCER, UMR 7315, F-87000 Limoges, France
[3]Interdisciplinary Laboratory for the Development of Nanostructures (LINDEN), Federal University of Santa Catarina (UFSC), 88040-900 Florianópolis, SC, Brazil

Manuscript was published in the Journal **Powder Technology** (Impact Factor: 4.142).

Schappo, H., Giry, K., Damia, C., & Hotza, D. (2021). Screening method for producing suitable spray-dried HA powder for SLS application. *Powder Technology*, 384, 62-69.
https://doi.org/10.1016/j.powtec.2021.02.004

Abstract

Screen methods are time-saving tools, assisting the establishment of a new process or technique for laboratory and industrial scale. This paper presents a step-by-step approach to use spray drying (SD) for obtaining hydroxyapatite (HA) powder, with suitable characteristics to be used as a filler in a polymer matrix, for selective laser sintering (SLS) processing. The proposed method consists of adjusting the departing HA suspension and SD processing parameters, briefly discussing relevant elements that must be considered. Suspension's rheological behaviour and spray-dried powder morphological features were investigated, serving as selection criteria for the favourable set-up. Variations on slurry feed and atomization pressure of SD processing parameters have allowed obtaining different powder characteristics. A major influence of atomization pressure variation was identified, a greater pressure value resulted in smaller particle size. Desirability function was employed to determine the optimal SD processing parameters, in other words, conditions that made it possible to obtain spherical particles with the proposed mean diameter in the range of 15 to 25 μm, with narrow particle size distribution.

Keywords: spray drying; hydroxyapatite; selective laser sintering; tissue engineering.

1. Introduction

Customized fabricated parts are required in a wide range of applications, being particularly important in medicine. The feasibility of manufacturing complex geometries, combining different materials, matches the requirements of implantable devices used for human tissue recovery. Tissue engineering (TE) seeks to restore, maintain, or improve damaged tissues through the combination of scaffolds, cells, and biologically active molecules into functional tissues [1].

Human bone is a complex vascularized structure, composed of organic collagen fibrils and inorganic calcium phosphate (CaP) crystals [2]. CaP materials [3,4] such as hydroxyapatite (HA) and beta-tricalcium phosphate (β-TCP) are widely used as bone substitutes and are commercially found in a few different geometries (*e.g.*, granules and sticks). Great interest is found on synthetic HA due to its strong affinity to hard tissues, also, HA is the most stable Ca-P compound in physiological conditions [5]. However, the fabrication of customized scaffolds from these materials remains a challenge, especially in terms of patient's implant fitting. Additive manufacturing (AM) is a breakthrough technology that allowed significant progress for tissue engineering applications, and still reveals promising solutions for custom-made bone scaffolds [6–9].

Powder bed fusion, frequently referred to as selective laser sintering (SLS) is one of the commercially available AM processes [10]. In this process, particulate materials are fused layer by layer via heat supplied by an infrared laser source, creating 3D parts that were originally designed using computer-assisted design (CAD) tools. SLS does not need any support during manufacturing and presents high resolution and fast processing. On the other hand, SLS is carried out at high processing temperatures and the manufactured parts are characterized by a rough surface finish [11]. Nevertheless, SLS can be considered one of the most versatile AM

techniques in terms of material usage and structural stability. Moreover, through optimized parameters, it is possible to achieve the desired mechanical properties for TE scaffolds [12]. SLS processing with proper materials selection can contribute to enhancing the scaffold's final properties, particularly bioactivity [13,14]. When processing composite materials (*i.e.*, bioceramic fillers in a polymeric matrix) a substantial difference between material's particle size is beneficial, allowing the filler to occupy voids in the interstices of matrix particles. Concerning polymer SLS feedstock, there are preferable powder characteristics that improve the sinterability and final properties of the fabricated piece [15,16]. Related literature has indicated better processing and geometry accuracy when using spherical particles and narrow particle size distribution with an average size below 150 μm or equivalent to the laser beam diameter [15,17]. Spherical HA particles can be obtained by different techniques [18–24] in a diverse range of particle sizes. However, process scalability remains a challenge and not all techniques are capable of producing particles in the range of 15 to 25 μm.

Spray drying (SD) consists of the transformation of a fluid material into dried particles. SD had shown remarkable development in the last decades, being used by different industries [25]. SD commercial equipment may differ in terms of configuration. Rotary, hydraulic and pneumatic nozzle atomizers are commonly used [15]. The variables that affect how the spray is mixed with the hot gas depend upon the type of gas flow: co-current, countercurrent, or mixed flow [26]. Spray-dried HA (SDHA) powder has been successfully employed for distinct biomedical applications, using different manufacturing techniques [27–32]. Moreover, SD enables advantageous powder characteristics that are desirable for 3D printing use [25]. Although SDHA powder morphology indicates suitability for SLS processing, publications concerning this subject are scarce [33]. Similarly, comprehensive information about how to produce SDHA powders for SLS processing is rarely reported in the literature. This paper proposes a screening method for producing suitable HA powders for SLS processing.

2. Materials and methods

2.1. Materials and compositions

Suspensions to be spray-dried were prepared with nano-sized HA synthesized in-house by hydrothermal route. Synthesis further details can be found elsewhere [34]. Methylcellulose (Methocel A15 Premium LV, Dow Chemical) was added as a binder to form an aqueous suspension using deionized water, according to the compositions in Table 1.

Table 1: Compositions of spray-drying HA aqueous suspensions.

Sample	Hydroxyapatite (wt%)	Methylcellulose (wt%)	Deionized water (wt%)
SD01	20.00	3.20	76.80
SD02	20.16	2.42	77.42
SD03	20.32	1.63	78.05
SD04	20.49	0.82	78.69

2.2. Spray drying parameters

A mini spray drying machine (Buchi B-290) was used. As displayed in Figure 1, the slurry mixture is pumped through a pneumatic external mixing nozzle (2) and sprayed by the spray gas (1) into the drying chamber (4). The drying gas (3) is heated and serves as a carrier for the spray-dried particles that will be deposited in the recipient (5) under the cyclone (6). Larger particles that were not carried by the drying gas can be recuperated under the drying chamber. Smaller particles will be retained in the filter (7).

Some spray drying parameters were kept constant in all experiments: inlet temperature of hot air 170 °C, volume flow of hot air aspiration 39 m^3 h^{-1}, slurry feed 21 $mL.min^{-1}$, and atomization flow 45 mmHg.

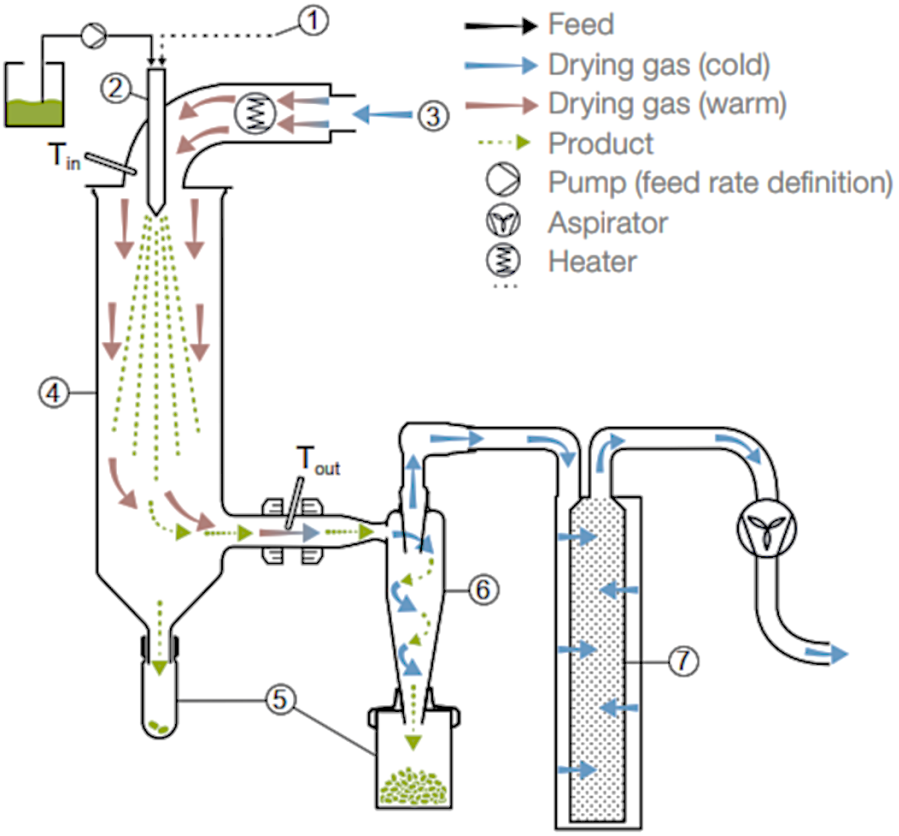

Figure 1: Scheme of BUCHI B-290 mini spray drying [35].

A pneumatic nozzle with a 2.00 mm diameter was used. It is possible to rotate the nozzle cap to get different widths of the spraying cone. Nozzle circumference of 8.5 mm was divided into 5 positions: 0, I, II, III, IV, whereas position 0 was only used as a point of reference (nozzle cap tightest position). Each position represents a different width of the cone spray produced by the nozzle, being position I the widest cone spray.

The intention is to use spray dried HA particles as a filler in a polymeric matrix. In this sense, better homogeneity and cohesion within materials can be achieved when HA particles are smaller and can be located in the voids of polymeric particles. Therefore, to obtain spherical HA particles, possessing an average diameter of 15 to 25 μm and narrow particle size distribution, two SD parameters were varied slurry feed and atomization pressure. A factorial design experiment with two factors and two levels was carried out (Table 2). The optimal point

among the experimental results originated from factorial design was determined using a desirability function. Results were ranked by preferable attributes taking into consideration the D50 value, (D90-D10)/D50 and particle morphology.

2.3. Characterization of powder and suspension

Morphological analysis was performed using a scanning electron microscope (SEM, JEOL IT300LV), after coating the samples with platinum (Agar Scientific). Departure HA powder was analyzed, without coating, using a field emission gun microscope (FEI, Quanta 450). Particle size and distribution (PSD) were determined by a laser scattering (Partica LA-950V2, Horiba). The specific surface area was measured by nitrogen adsorption (ASAP 2020, Micromeritics) and calculated according to the Brunauer–Emmet–Teller equation. X-ray diffraction (XRD, D8 Advance, Bruker) was carried out with a scan range from 27° to 40°, 2θ of 0.02° and acquisition time of 5 s. For XRD phase identification, EVA software was employed using HA's diffraction pattern (Powder Diffraction Files – PDF: 00-09-0432) from International Center for Diffraction Data (ICDD). The rheological behaviour of HA slurries was assessed with a concentric rheometer (AR1500 TA Instruments, US) using a 40 mm parallel plate. Rheology flow sweep measurements were performed on suspensions 20 °C, namely 10 points over stress rates from 0.1 to 40 Pa. The Herschel–Bulkley model was fitted to experimental data. After spray drying, the sprayed powder was submitted to thermal treatment using ramps of 3 °C/min up to 500 °C, for binder removal, and 10 °C/min up to 1000 °C, with a hold at this temperature for 1 h, for densification (LHT 04/17, Nabertherm GmbH).

3. Results and discussion

3.1. Raw powder characteristics

The synthesized HA powder had a specific surface area of around 80 m² g-1. As a means to reduce its reactivity, the powder was heat-treated at 650 °C for 30 min resulting in a surface area of 34 m² g-1. This heat treatment allows eliminating synthesis residues (*i.e.*, nitrate and ammonium ions), providing a homogeneous specific surface and reproducible characteristics of the departing powder. Further, it contributes to a more stable suspension and minimizing agglomeration between HA particles. Heat treatment and SD processing did not affect the phase compositions, being the same as pure HA according to diffraction pattern (Figure 2). As revealed on SEM images (Figure 3) and PSD curve (Figure 4) the nano-sized HA particles (D50 value 0.13 µm) tend to agglomerate; therefore, the suspension for SD processing must be carefully prepared.

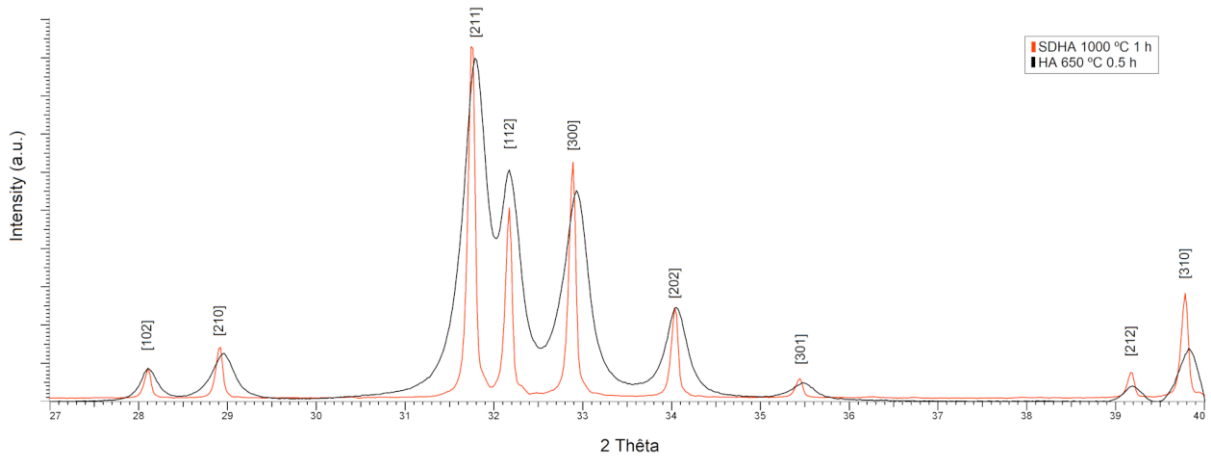

Figure 2: XRD curves of pure HA treated at 650 °C for 0.5 h and SDHA treated at 1000 °C for 1 h.

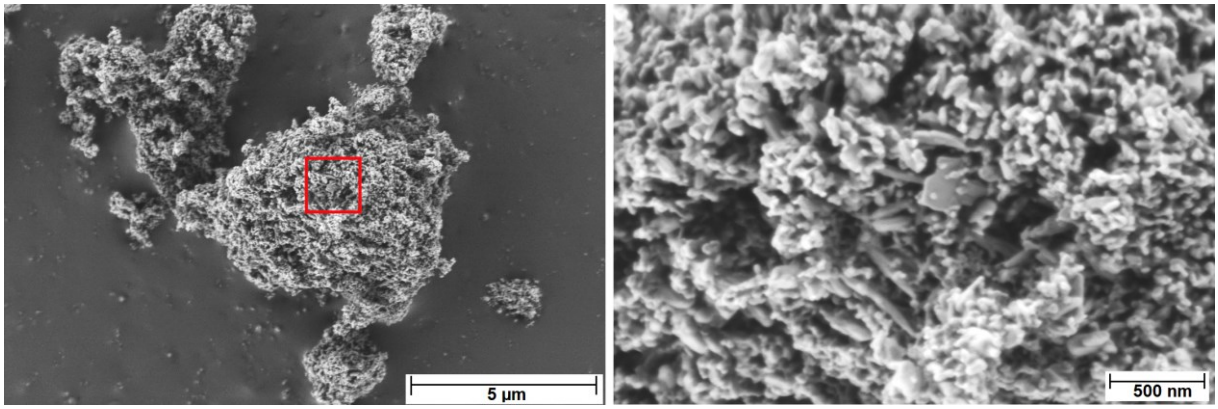

Figure 3: SEM-FEG images of heat-treated departing HA powder, indicating the tendency of the agglomeration (left). Close-up of agglomerated nano-sized particles (right).

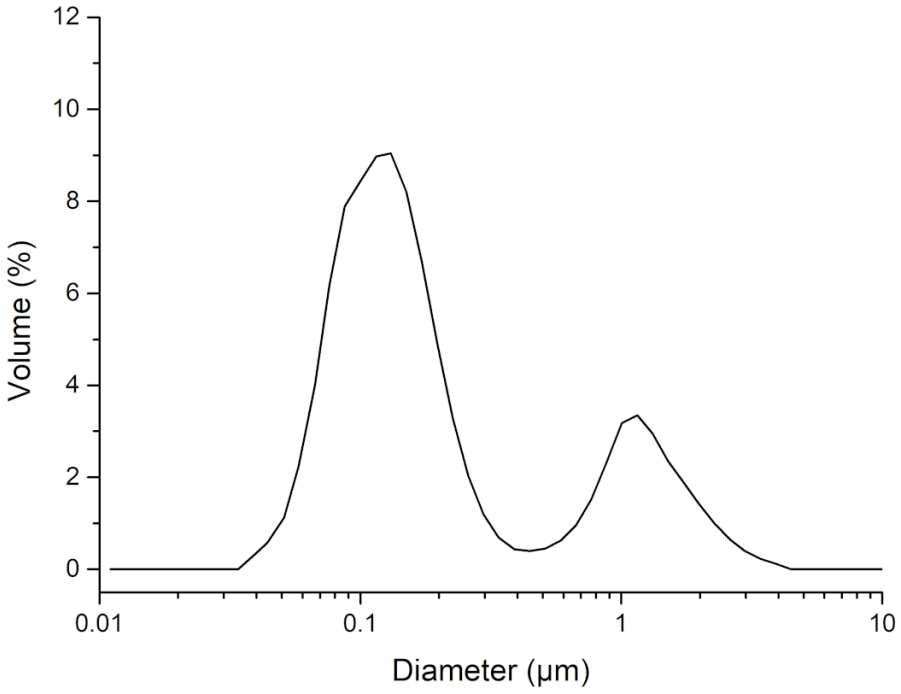

Figure 4: PSD curve of heat-treated departing HA powder.

3.2. Effect of suspension formulation

Suspension composition has major importance because its characteristics will influence the spray drying process as a whole. For this step, the trial and error experimentation method is applicable when no information is found in the literature. However, there are aspects of

fundamental importance to be considered (*e.g.*, maximal solid content, slurry viscosity) that can be easily found in the related bibliography. Moreover, machine manufacturers can provide elementary information about recommended processing characteristics. Early trial and error experiments, together with literature information, have provided a point of departure in terms of mixture preparation, solid content, binder selection, and processing parameter values.

First, the binder selection must consider the powder's final application (in this case, bone tissue applications). Therefore, after processing, it must maintain the original HA chemical composition. In previous essays, the performance of different binders: corn starch (Roquette, ref: 764071), polyvinylpyrrolidone (grade 30 and 90 from BASF), and methylcellulose (Methocel A15-LV Premium) were analyzed. Methylcellulose demonstrated a larger average particle size, better process efficiency, and requiring lower concentrations. Spray-dried HA (SDHA) powder, after heat treatment at 1000 °C for 1 h, has matching phase compositions to heat-treated HA as shown in Figure 2, confirming the suitability of methylcellulose in terms of not modifying powder composition.

Once the type of binder is selected, the amount of HA must be defined. Adding too much HA in the suspension will prevent good homogeneity and induce solid deposition. Moreover, it will increase viscosity and difficult spray drying processing (*i.e.*, nozzle blocking). On the other hand, a low solid concentration will result in smaller particle size [36]. Previous essays indicated the use of around 20 wt% HA content for the proposed screening method and particle size objectives. To guarantee suspension homogeneity, it is recommended to agitate with a magnetic stirrer for at least 10 h before starting the spray drying process. While processing, continuously stirring is required to maintain the mixture uniform and with constant viscosity [37].

SD process is highly dependent on the suspension's characteristics and its viscosity has a great influence on the obtained powder. As detailed in Figure 5, the amount of methylcellulose

has a large effect on the suspension's rheology. Table 2 provides the values obtained from the slurry rheological analysis, Herschel–Bulkley model was used given its fitting with experimental results. Yield stress values were similar between SD01-SD02 and SD03-SD04, indicating two types of behaviour according to binder amount. All the suspensions showed pseudoplastic shears thinning behaviour, implicating in a viscosity decrease with increasing shear rate. This is an important characteristic that guarantees suspension uniform viscosity along with all the SD processing, under constant agitation. Large viscous forces will need more energy for breaking the droplets, resulting in larger droplets [38]. This phenomenon was observed when processing SD01, where occurred slurry droplets deposition in the drying chamber.

PSD analyses were performed for all suspensions (Figure 6). Although the suspensions have similar dispersion curves, SD01 and SD02 indicate a larger volume of particles around 50 μm area, suggesting that the suspension is not well homogenized. As detailed in Table 2, this bimodal distribution reflects the values of D10, D50, D90, and its ratio. Particle size values of D10 mean that 10% of particles have smaller diameters than the D10 value, in the same way, D50 and D90 represent the 50% and 90% portions. (D90-D10)/D50 ratio provides information related to the particles' distribution width, in which, a wider distribution is observed with high ratio values. The values obtained by the (D90-D10)/D50 ratio enhance the significant distribution behaviour of SD01-SD02 versus SD03-SD04. It is possible that suspensions SD01 and SD02 have not completely dissolved the binder, remaining agglomerates. Individual nano-sized HA particles tend to gather together (Figure 3), accentuating agglomeration effects.

SEM images (Figure 7) suggest that the high amount of methylcellulose binder in suspensions SD01 and SD02 formed binder agglomerates in the particles, causing defects after sintering that can be observed by the empty spaces in the particles (forming doughnut-like particles). Contrastingly, heat-treated SD04 powder presented some particles with an

insufficient amount of binder, preventing proper cohesion between HA departing particles (also evidenced by smaller values on PSD) and restricting the formation of appropriate morphology.

According to rheological analysis and PSD values, SD03 and SD04 have shown the most suitable results. When also considering morphological characteristics of spray-dried granules, SD04 did not have a sufficient amount of binder to guarantee proper cohesion of nano-sized HA particles, therefore, SD03 was chosen to proceed with the following steps.

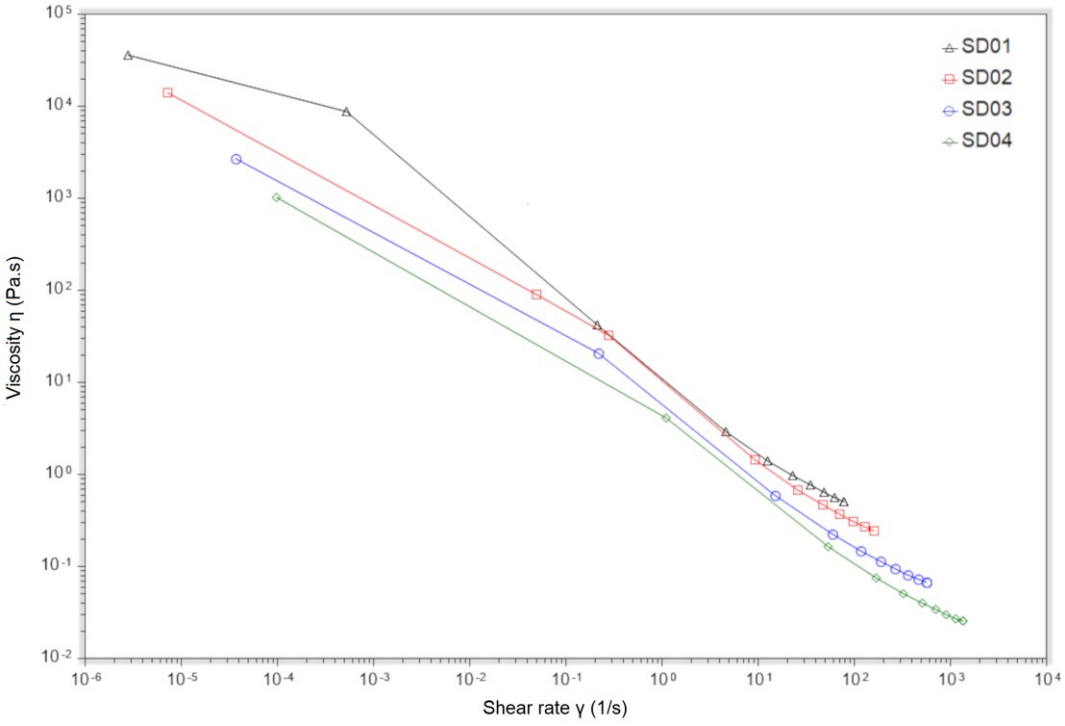

Figure 5: Viscosity measurements of HA suspensions SD01, SD02, SD03, and SD04.

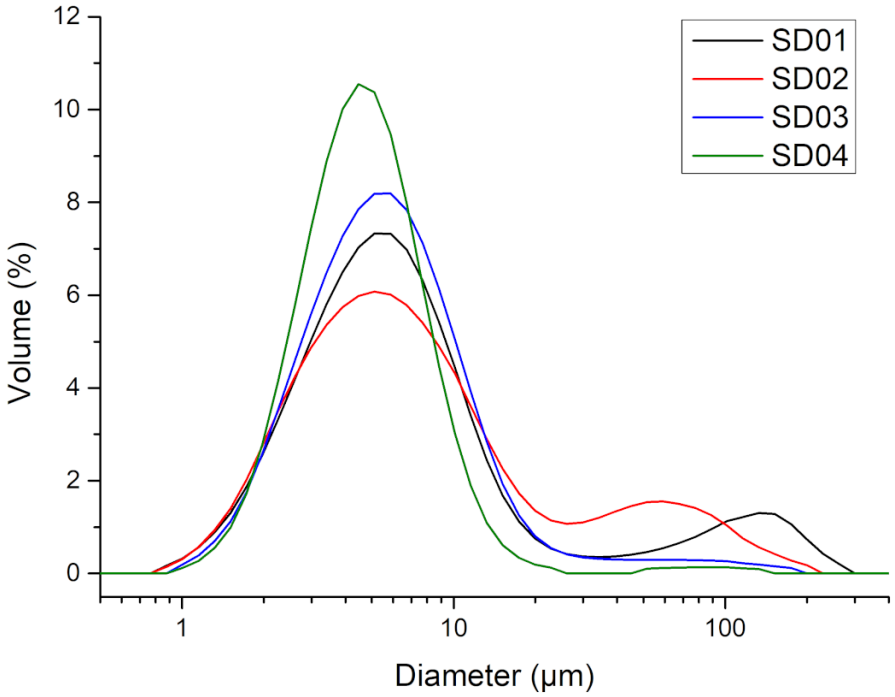

Figure 6: PSD curves of suspensions SD01, SD02, SD03, and SD04.

Table 2: Rheological values obtained from the Herschel–Bulkley model and respective D10, D50, D90, and ratio measures for HA suspensions.

Sample	Yield Stress (Pa)	Viscosity (Pa·s)	Rate index	D10 (µm)	D50 (µm)	D90 (µm)	(D90-D10)/D50 (µm)
SD01	8.47	1.70	0.67	2.18	5.43	55.65	23.08
SD02	8.56	1.07	0.66	2.13	5.88	46.99	19.32
SD03	5.91	0.51	0.65	2.24	5.10	12.42	3.26
SD04	5.92	0.18	0.70	2.22	4.29	8.36	1.83

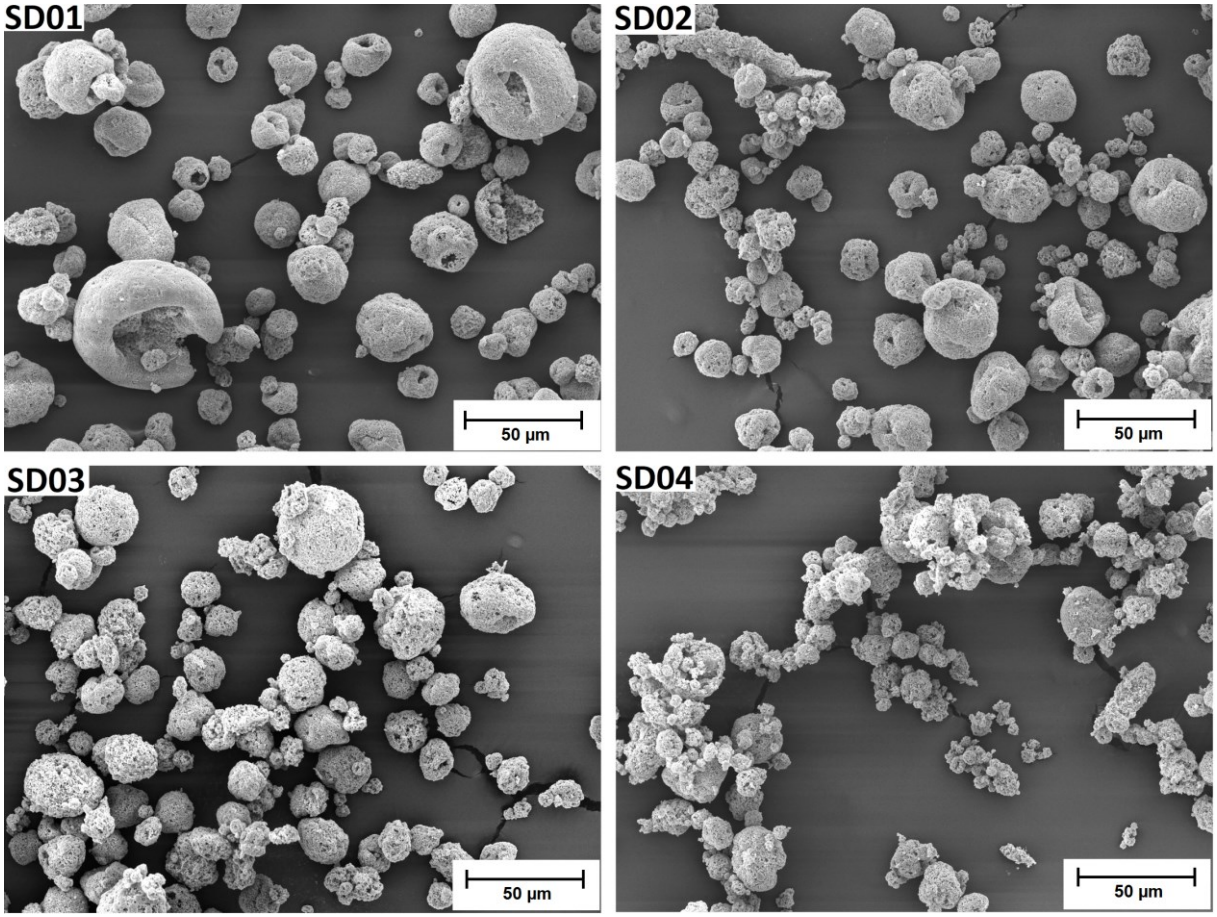

Figure 7: SEM images of HA particles from SD01, SD02, SD03, and SD04, after heat treatment at 1000 °C for 1 h.

3.3. Effect of spray drying parameters

Nozzle cap position is important to avoid excessive droplets deposition on the drying chamber wall, which can result in lower process efficiency. In order to verify any influence of spray width on the particle's morphology, particle measurement and SEM images were conducted. Particle size distribution (Figure 8) and morphology have shown to be similar between the nozzle's four positions (SD05 to SD08), hence, these attributes were not directly affected by the changes in the spray angles, neither they were sufficient to validate an optimal nozzle position.

Considering the similarity in morphology and particle size distribution, position II was chosen because SD06 had around 5% more process yield (powder recover quantity) when compared to the others.

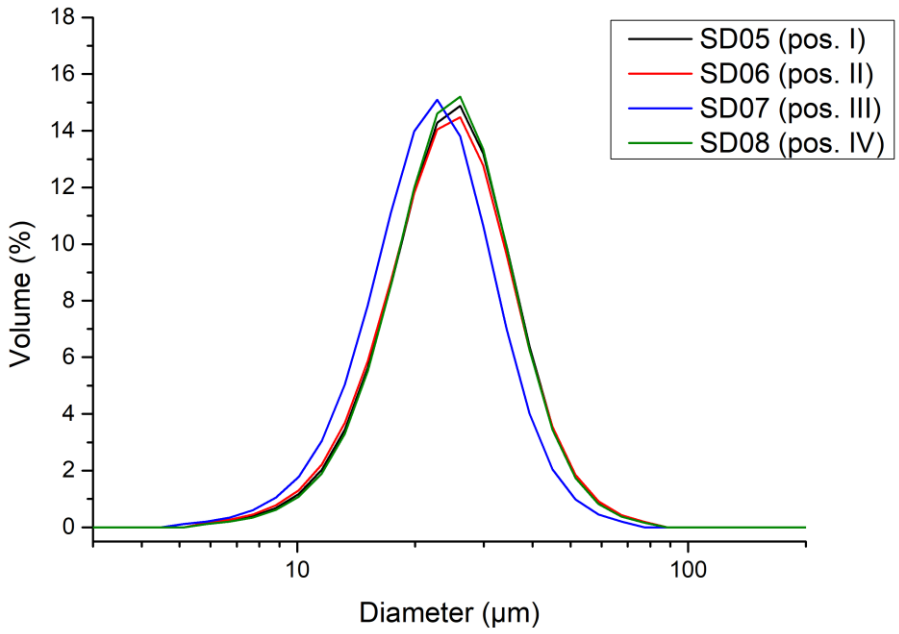

Figure 8: PSD of HA densified particles (after heat treatment at 1000 °C for 1 h): SD05 (pos. I), SD06 (pos. II), SD07 (pos. III), SD08 (pos. IV).

The final properties of spray-dried particles are highly dependent on processing parameters, as well as equipment's features and configurations. Although it is possible to adjust particle characteristics by changing the processing parameters, it is necessary to establish a suitable departing suspension to achieve the targeted goals in terms of particle. Afterwards, the heat treatment process will affect the particle density, crystallinity, and mechanical integrity [39]. Considering that heat treatment is a post-process of spray drying, not directly influencing the particle size distribution and morphology, it will not be investigated here. In terms of particle-size distribution and process yield, key parameters are suspension's solid content, spray drying slurry feed, and atomization pressure; yet, other factors like nozzle diameter, inlet

temperature, aspirator velocity, and drying gas humidity also influence the obtained particles [26,39,40]. As mentioned before, an early trial and error method should be applied to comprehend the basic correlations between all the processing factors. In-depth analysis for investigating the influence of different processing variables should be done using statistical tools and it is recommended to perform at least 3 replicates for establishing any conclusions.

Table 3: Factorial design parameters and values and respective D10, D50, D90 mean size and size ratios, after heat treatment at 1000 °C for 1 h. The (-) signal represents lower and (+) higher values of the two levels factorial design.

Run	Sample	Atomization pressure (mmHg)	Slurry feed (mL min^{-1})	D10 (µm)	D50 (µm)	D90 (µm)	(D90-D10)/D50 (µm)
1	SD09	45 (-)	21.00 (-)	13.92	23.67	38.15	1.04
2	SD10	45(-)	25.50 (+)	13.90	23.12	36.53	0.96
3	SD11	60 (+)	21.00 (-)	9.71	19.02	39.52	2.11
4	SD12	60 (+)	25.50 (+)	9.01	16.85	29.24	1.37

Particle size information is displayed in Figure 8 and Table 3. It has been reported in the related bibliography that a higher atomization pressure decreases the particle size [36,39,41]. This observation is in accordance with our results, when comparing SD09 and SD11 (same slurry feed and SD11 with higher atomization pressure), SD11 possesses lower particle values for D10 and D50. In the same manner, SD12 has D10, D50, and D90 particle sizes lower than SD10 (same slurry feed and SD12 with higher atomization pressure). On the other hand, from our results, it was not possible to observe the association between larger particle sizes with increases in slurry feed rate reported in the literature [39,41]. Analyzing the curves in Figure 9, it can be observed similarities between SD09-SD10 and SD11-SD12, this might indicate a minor influence of slurry feed in our experiences. Probably, a greater difference between slurry feed values would evidence variances in particle size. Nevertheless, it is important to highlight

that these comparisons are only illustrative, for representative conclusions it would be necessary more replicates, experimental error determination, and the use of statistical analysis of variance (ANOVA). SEM images (Figure 10) have shown similar spherical morphology for the respecting spray-dried powder and, as expected, a greater population of bigger particles were observed on SD09 and SD10.

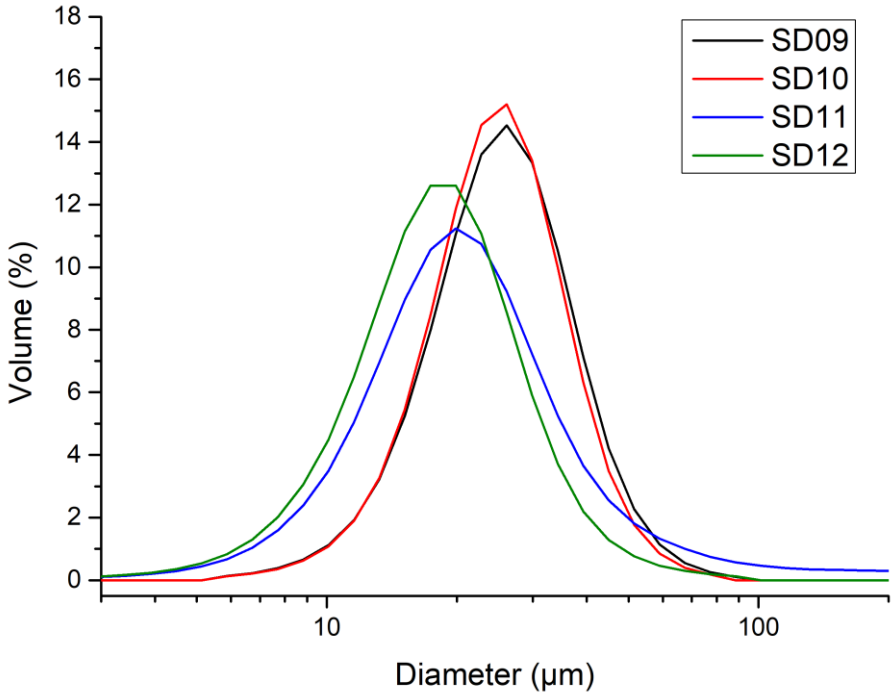

Figure 9: PSD dispersions of HA particles SD09, SD10, SD11, SD12, after heat treatment at 1000 °C for 1 h.

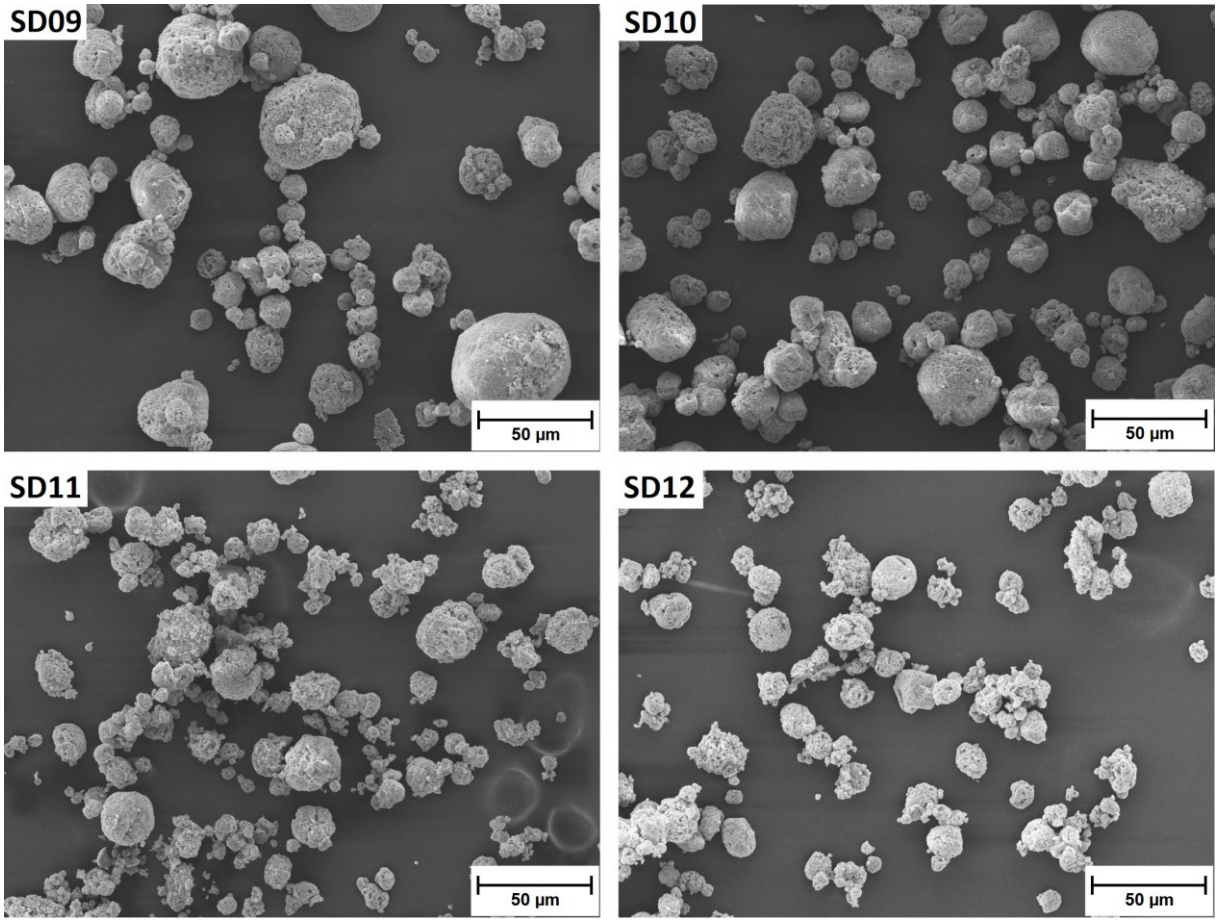

Figure 10: SEM images of HA particles SD09, SD10, SD11, and SD12, heat-treated at 1000 °C for 1 h.

Introducing satisfaction index for the responses D50, (D90-D10)/D50 and particle morphology, desirability values were obtained (Table 4). Individual desirability of D50 and morphology were calculated using $\mathcal{D} = (Yi - L)/(T - L)$ equation, where Yi is the response, L the lower value, and T the target value. Conversely, for (D90-D10)/D50 desirability a minimized result was targeted, therefore, $\mathcal{D} = (U - Yi)/(U - T)$ equation was used (U means upper value). The applied ranges of values were: i) D50: 100% desirability if value greater than 25 and 0% desirability if value less than 15; ii) (D90-D10)/D50: 100% desirability if value less than 1 and 0% desirability if value greater than 3; iii) particle morphology: 100% desirability if value greater than 5, 0% desirability if value less than 1. For particle morphology, SEM images were analyzed and for each sample, it was given a 1 to 5 score (5 is the most suitable

morphology). Higher values of desirability were observed on SD09 and SD10 mainly due to D50 and (D90-D10)/D50.

Although global desirability pointed out SD09 and SD10 as the most suitable powder characteristics, all SD powders achieved the proposed morphology and size objectives. The variation of two processing parameters has shown the capability of adjusting particle size characteristics.

Table 4: Samples and respective desirability responses.

Sample	**Analyzed responses**			**Individual desirability**			**Global desirability**
	D50 (μm)	(D90-D10)/D50 (μm)	Particle morphology	D50	(D90-D10)/D50	Particle morphology	
SD09	23.67	1.04	4	86.70%	97.33%	75.00%	85.86%
SD10	23.12	0.96	4	81.20%	100.00%	75.00%	84.76%
SD11	19.02	2.11	3	40.20%	26.00%	50.00%	37.39%
SD12	16.85	1.37	3	18.50%	75.33%	50.00%	41.15%

4. Conclusions

This screening method contemplates the main steps for powder preparation suitable for SLS. Spray-dried HA particles were successfully produced within the proposed morphology. Binder and HA content of the departing slurry have an important effect on viscosity. Therefore, special attention must be given to preparing the departing suspension. Variations on spray drying processing parameters have shown the possibility of tailoring particle size and distribution. For a proper analysis of the processing parameters variation, statistical tools must be used. PSD and SEM images have indicated suitable particle characteristics for SLS processing, although additional studies must be conducted to confirm SLS processability. The

versatility of the proposed method makes it possible to be applied in other bioceramic materials and types of binders, targeting different particle sizes.

Acknowledgements

This study was financed in part by Coordenação de Aperfeiçoamento de Pessoal de Nível Superior – Brasil (CAPES) - Finance Code 001, and Fundação de Amparo à Pesquisa e Inovação do Estado de Santa Catarina (FAPESC). The authors thank the French Agence Nationale de la Recherche in the scope of the LabExSigmaLim (ANR-10-LABX-0074-01 Sigma-LIM). The authors are grateful to the Service Commun de Caractérisation des Matériaux de Limoges (CARMALIM) and more especially to Yann Launay for SEM acquisitions, Marguerite Bienia and Mickäel Lacroix for rheological measurements. The authors also thank Emeline Renaudie for her assistance in the elaboration of calcium phosphate ceramics, and Geoffroy Rivaud for the support in spray drying.

References

[1] R. Langer, J. Vacanti, Tissue engineering, Science (80-.). 260 (1993) 920–926. https://doi.org/10.1126/science.8493529.

[2] L. Piaia, G.V. Salmoria, D. Hotza, Additive manufacturing of nanostructured bone scaffolds, Elsevier Inc., 2018. https://doi.org/10.1016/B978-0-12-814621-7.00010-X.

[3] J.C. Elliott, Structure and chemistry of the apatites and other calcium orthophosphates, Elsevier, 2013.

[4] L.L. Hench, Bioceramics, J. Am. Ceram. Soc. 81 (1998) 1705–1728. https://doi.org/10.1111/j.1151-2916.1998.tb02540.x.

[5] S.J. Kalita, A. Bhardwaj, H.A. Bhatt, Nanocrystalline calcium phosphate ceramics in biomedical engineering, Mater. Sci. Eng. C. 27 (2007) 441–449. https://doi.org/10.1016/j.msec.2006.05.018.

[6] L. Piaia, G.V. Salmoria, D. Hotza, Additive Manufactured Nanocomposites for Bone Tissue Engineering Applications: an Overview, Mater. Res. 23 (2020) 1–10. https://doi.org/10.1590/1980-5373-mr-2019-0487.

[7] S. Mondal, U. Pal, 3D hydroxyapatite scaffold for bone regeneration and local drug delivery applications, J. Drug Deliv. Sci. Technol. 53 (2019) 101131. https://doi.org/10.1016/j.jddst.2019.101131.

[8] J. D'Alessio, A. Christensen, 3D Printing for Commercial Orthopedic Applications: Advances and Challenges, in: 3D Print. Orthop. Surg., Elsevier, 2019: pp. 65–83. https://doi.org/10.1016/B978-0-323-58118-9.00007-5.

[9] C. Shuai, L. Yu, W. Yang, S. Peng, Y. Zhong, P. Feng, Phosphonic acid coupling agent modification of HAP nanoparticles: Interfacial effects in PLLA/HAP bone scaffold, Polymers (Basel). 12 (2020). https://doi.org/10.3390/polym12010199.

[10] ISO/ASTM 52900: 2015 Additive manufacturing-General principles-terminology, ASTM F2792-10e1. (2012).

[11] G.-H. Wu, S. Hsu, Review: polymeric-based 3D printing for tissue engineering, J. Med. Biol. Eng. 35 (2015) 285–292.

[12] F.E. Wiria, K.F. Leong, C.K. Chua, Y. Liu, Poly-ε-caprolactone/hydroxyapatite for tissue engineering scaffold fabrication via selective laser sintering, Acta Biomater. 3 (2007) 1–12. https://doi.org/10.1016/j.actbio.2006.07.008.

[13] C. Shuai, W. Yang, P. Feng, S. Peng, H. Pan, Accelerated degradation of HAP/PLLA bone scaffold by PGA blending facilitates bioactivity and osteoconductivity, Bioact. Mater. 6 (2021) 490–502. https://doi.org/10.1016/j.bioactmat.2020.09.001.

[14] P. Feng, S. Peng, C. Shuai, C. Gao, W. Yang, S. Bin, A. Min, In Situ Generation of Hydroxyapatite on Biopolymer Particles for Fabrication of Bone Scaffolds Owning Bioactivity, ACS Appl. Mater. Interfaces. 12 (2020) 46743–46755. https://doi.org/10.1021/acsami.0c13768.

[15] M. Schmid, A. Amado, K. Wegener, Materials perspective of polymers for additive manufacturing with selective laser sintering, J. Mater. Res. 29 (2014) 1824–1832. https://doi.org/10.1557/jmr.2014.138.

[16] D. Sofia, D. Barletta, M. Poletto, Laser sintering process of ceramic powders: The effect of particle size on the mechanical properties of sintered layers, Addit. Manuf. 23 (2018) 215–224. https://doi.org/10.1016/j.addma.2018.08.012.

[17] R.D. Goodridge, C.J. Tuck, R.J.M. Hague, Laser sintering of polyamides and other polymers, Prog. Mater. Sci. 57 (2012) 229–267. https://doi.org/10.1016/j.pmatsci.2011.04.001.

[18] C. Li, G. Li, S. Liu, J. bai, A. zhang, Spherical hydroxyapatite with colloidal stability prepared in aqueous solutions containing polymer/surfactant pair, Colloids Surfaces A Physicochem. Eng. Asp. 366 (2010) 27–33. https://doi.org/10.1016/j.colsurfa.2010.05.018.

[19] G.C. Koumoulidis, A.P. Katsoulidis, A.K. Ladavos, P.J. Pomonis, C.C. Trapalis, A.T. Sdoukos, T.C. Vaimakis, Preparation of hydroxyapatite via microemulsion route, J. Colloid Interface Sci. 259 (2003) 254–260. https://doi.org/10.1016/S0021-9797(02)00233-3.

[20] K. Ioku, G. Kawachi, S. Sasaki, H. Fujimori, S. Goto, Hydrothermal preparation of tailored hydroxyapatite, J. Mater. Sci. 41 (2006) 1341–1344. https://doi.org/10.1007/s10853-006-7338-5.

[21] C. Qiu, X. Xiao, R. Liu, Biomimetic synthesis of spherical nano-hydroxyapatite in the presence of polyethylene glycol, Ceram. Int. 34 (2008) 1747–1751. https://doi.org/10.1016/j.ceramint.2007.06.001.

[22] M.H. Hong, J.S. Son, K.M. Kim, M. Han, D.S. Oh, Y.K. Lee, Drug-loaded porous spherical hydroxyapatite granules for bone regeneration, J. Mater. Sci. Mater. Med. 22 (2011) 349–355. https://doi.org/10.1007/s10856-010-4197-z.

[23] X. Ma, Y. Chen, J. Qian, Y. Yuan, C. Liu, Controllable synthesis of spherical hydroxyapatite nanoparticles using inverse microemulsion method, Mater. Chem. Phys. 183 (2016) 220–229. https://doi.org/10.1016/j.matchemphys.2016.08.021.

[24] M. Kamitakahara, S. Takahashi, T. Yokoi, C. Inoue, K. Ioku, Preparation of spherical porous hydroxyapatite granules as support materials for microorganisms, J. Ceram. Soc. Japan. 126 (2018) 732–735. https://doi.org/10.2109/jcersj2.18089.

[25] D. Santos, A.C. Maurício, V. Sencadas, J.D. Santos, M.H. Fernandes, P.S. Gomes, Spray Drying: An Overview, in: Biomater. - Phys. Chem. - New Ed., InTech, 2018. https://doi.org/10.5772/intechopen.72247.

[26] K. Cal, K. Sollohub, Spray Drying Technique. I: Hardware and Process Parameters, J. Pharm. Sci. 99 (2010) 575–586. https://doi.org/10.1002/jps.21886.

[27] Y.J. Fu, S.S. Shyu, F.H. Su, P.C. Yu, Development of biodegradable co-poly(D, L-lactic/glycolic acid) microspheres for the controlled release of 5-FU by the spray drying method, Colloids Surfaces B Biointerfaces. 25 (2002) 269–279. https://doi.org/10.1016/S0927-7765(01)00205-3.

[28] P. López-Gasco, I. Iglesias, J. Benedí, R. Lozano, J.M. Teijón, M.D. Blanco, Paclitaxel-loaded polyester nanoparticles prepared by spray-drying technology: In vitro bioactivity evaluation, J. Microencapsul. 28 (2011) 417–429. https://doi.org/10.3109/02652048.2011.576785.

[29] E. Quinlan, A. López-Noriega, E.M. Thompson, A. Hibbitts, S.A. Cryan, F.J. O'Brien, Controlled release of vascular endothelial growth factor from spray-dried alginate microparticles in collagen–hydroxyapatite scaffolds for promoting vascularization and bone repair, J. Tissue Eng. Regen. Med. 11 (2017) 1097–1109. https://doi.org/10.1002/term.2013.

[30] S. Sequeira, M.H. Fernandes, N. Neves, M.M. Almeida, Development and characterization of zirconia–alumina composites for orthopedic implants, Ceram. Int. 43 (2017) 693–703. https://doi.org/10.1016/j.ceramint.2016.09.216.

[31] Y. Ben, L. Zhang, S. Wei, T. Zhou, Z. Li, H. Yang, Y. Wang, F.A. Selim, C. Wong, H. Chen, PVB modified spherical granules of β-TCP by spray drying for 3D ceramic printing, J. Alloys Compd. 721 (2017) 312–319. https://doi.org/10.1016/j.jallcom.2017.06.022.

[32] R. Cholas, S. Kunjalukkal Padmanabhan, F. Gervaso, G. Udayan, G. Monaco, A. Sannino, A. Licciulli, Scaffolds for bone regeneration made of hydroxyapatite microspheres in a collagen matrix, Mater. Sci. Eng. C. 63 (2016) 499–505. https://doi.org/10.1016/j.msec.2016.03.022.

[33] C.K. Chua, K.F. Leong, K.H. Tan, F.E. Wiria, C.M. Cheah, Development of tissue scaffolds using selective laser sintering of polyvinyl alcohol/hydroxyapatite biocomposite for craniofacial and joint defects, J. Mater. Sci. Mater. Med. 15 (2004) 1113–1121. https://doi.org/10.1023/B:JMSM.0000046393.81449.a5.

[34] S. Raynaud, E. Champion, D. Bernache-Assollant, P. Thomas, Calcium phosphate apatites with variable Ca/P atomic ratio I. Synthesis, characterisation and thermal stability of powders, Biomaterials. 23 (2002) 1065–1072. https://doi.org/10.1016/S0142-9612(01)00218-6.

[35] Büchi Labortechnik AG, Mini Spray Dryer B-290: Product Brochure, (2020).

[36] A.J. Wang, Y.P. Lu, R.F. Zhu, S.T. Li, X.L. Ma, Effect of process parameters on the performance of spray dried hydroxyapatite microspheres, Powder Technol. 191 (2009) 1–6. https://doi.org/10.1016/j.powtec.2008.10.020.

[37] Q. Murtaza, J. Stokes, M. Ardhaoui, Experimental analysis of spray dryer used in hydroxyapatite thermal spray powder, J. Therm. Spray Technol. 21 (2012) 963–974. https://doi.org/10.1007/s11666-012-9791-9.

[38] S.P. Anandharamakrishnan, C.; Ishwarya, Spray Drying Techniques for Food Ingredient

Encapsulation, John Wiley & Sons, 2015.

[39] F.E. Bastan, G. Erdogan, T. Moskalewicz, F. Ustel, Spray drying of hydroxyapatite powders: The effect of spray drying parameters and heat treatment on the particle size and morphology, J. Alloys Compd. 724 (2017) 586–596. https://doi.org/10.1016/j.jallcom.2017.07.116.

[40] Büchi Labortechnik AG, Process parameters Spray drying, 2020. https://www.buchi.com/en/products/spray-drying-and-encapsulation/mini-spray-dryer-b-290.

[41] P. Luo, T.G. Nieh, Preparing hydroxyapatite powders with controlled morphology, Biomaterials. 17 (1996) 1959–1964. https://doi.org/10.1016/0142-9612(96)00019-1.

Conclusions of Chapter 3

Results achieved in the published article were satisfactory in terms of particle size and morphology. However, deficiency in terms of powder production (low process efficiency) has motivated deeper research for improvement. In this sense, different processing parameters values were evaluated to achieve greater spray-dried powder production.

Table 5 displays the employed parameters to attempt higher levels of efficiency, in this occasion 3 replicates were performed, all using the favourable suspension formulation (20.32% of HA, 1.63% of MC and 78.05% of H_2O) and nozzle position. The fixed parameters were airflow temperature of 170 ºC and aspiration at 100%, suspensions were prepared following the same procedure and agitation time.

Table 5: Factorial design rounds and obtained results.

Round	Slurry Feed (mL min^{-1})	Atom. Press. (mmHg)	D50 (µm)	(D90-D10)/D50	Efficiency (%)
1	9.5 (-)	45 (-)	19.92	1.70	10.85
2	15 (+)	45 (-)	18.94	1.24	17.99
3	9.5 (-)	45 (-)	22.76	1.24	11.96
4	15 (+)	45 (-)	23.31	1.12	6.47
5	15 (+)	60 (+)	19.40	1.20	24.35
6	15 (+)	60 (+)	19.23	1.49	17.39
7	9.5 (-)	60 (+)	16.75	1.33	21.60
8	9.5 (-)	60 (+)	17.62	1.44	26.57
9	15 (+)	45 (-)	23.33	1.11	9.45
10	9.5 (-)	45 (-)	22.75	1.22	16.05
11	15 (+)	60 (+)	19.57	1.51	19.38
12	9.5 (-)	60 (+)	17.09	1.44	26.38

Results have shown that two parameters combination with favourable efficiency: i) slurry feed of 50% and an atomization pressure of 60 mmHg and ii) slurry feed of 30% and an atomization pressure of 60 mmHg, the respective rounds are highlighted in the table in light green (i) and darker green (ii). It can be noticed that i) possess greater D50 and (D90-10)/D50

values, along with lower efficiency, therefore, the chosen parameters for producing SDHA for the SLS experiments were ii) slurry feed of 30% and an atomization pressure of 60 mmHg.

Once the parameters were selected, a greater amount of prepared suspension was spray-dried for producing SDHA to use with UHMWPE in the SLS machine. When processing larger amounts of suspension, it was possible to achieve higher amounts (up to 44%) of process efficiency, this can be attributed to inherent process loss that is more evidenced when processing lower amounts of suspension.

The collected SDHA powder was also submitted to thermal treatment, before SLS processing, using ramps of 3 °C/min up to 500 °C, for binder removal, and 10 °C/min up to 1000 °C, holding this temperature for 1 h. This heat treatment was chosen to slowly remove the binder in the first ramp (avoid morphological changes in the particles). The second ramp was intended to enhance particle densification and, at the same time, to prevent HA phase change (that occurs above 1100 °C).

CHAPTER 4
Manuscript 3

Introduction to Chapter 4

The following chapter (to be submitted to publication) consisted in the final part of the doctorate, mainly conducted at NIMMA (*Núcleo de Inovação em Moldagem e Manufatura Aditiva*) but the biological analyses were conducted at IRCER (*Institut de Recherche sur les Céramiques*) with the help of Amandine Magnaudeix, Adeline Dumur and Emeline Renaudie.

Similar to spray drying equipment, a large number of experiments were conducted to comprehend equipment performance and limitations. Initial trials for SLS processing UHMWPE powder have considered values found in the related bibliography. The varied parameters were powder bed temperature, layer thickness, laser power and speed. It was possible to notice that layer thickness greater than 200 μm caused excessive distortion, impeding homogeneous powder spreading of the following layer, causing critical defects in the sample. Limitations on the lens system (galvanometric mirror system) were also observed, whereas laser speed greater than 1,000 mm/s fails to keep pace with the designed piece geometry.

Visual inspection and manual handling were used to assess samples' fabrication while varying the processing parameters. This phase was essential for better knowledge for SLS processing UHMWPE powder, enabling to establish a departure point in terms of processing parameters.

Selective Laser Sintering of UHMWPE/HA composites for bone tissue engineering

Henrique Schappo[1,2], Gean Vitor Salmoria[1], Dachamir Hotza[3], Amandine Magnaudeix[2], Adeline Dumur[2], Emeline Renaudie[2], Karine Giry[2], Chantal Damia[2]

[1]Innovation Laboratory for Molding and Additive Manufacturing (NIMMA), Federal University of Santa Catarina (UFSC), 88040-900 Florianópolis, SC, Brazil
[2]University of Limoges, CNRS, IRCER, UMR 7315, F-87000 Limoges, France
[3]Interdisciplinary Laboratory for the Development of Nanostructures (LINDEN), Federal University of Santa Catarina (UFSC), 88040-900 Florianópolis, SC, Brazil

Manuscript to be submitted.

Abstract

Selective laser sintering (SLS) has been proving to be a valuable manufacturing technique for implantable devices. Polymeric/ceramic biocomposites emerge as favourable materials for fabricating customized implants targeting bone tissue applications. However, improvements in processability and properties are still required. This work has investigated the use of different amounts of spray-dried hydroxyapatite (SDHA) particles in a polymeric matrix of ultra-high-molecular-weight polyethylene (UHMWPE), varying SLS processing parameters. Powder characteristics were assessed, samples' dimensional and mechanical properties were measured, and preliminary *in vitro* assays were conducted. Biological results demonstrated the biocompatibility of the SLS fabricated samples, not inhibiting cell growth and supporting pre-osteoblast attachment. Nevertheless, a greater amount of SDHA has hindered samples' mechanical properties, so a compromise must be found.

Keywords: spray-dried hydroxyapatite, UHMWPE, selective laser sintering, bone tissue engineering.

1. Introduction

Additive manufacturing (AM) techniques introduced significant advancements for tissue engineering applications and it is still revealing favourable solutions for customized bone scaffolds [1–4]. Selective laser sintering (SLS), also called as powder bed fusion, [5] is a power-based AM technique that uses a laser beam as a heating source to fuse particles layer by layer to create 3D parts that were conceived using computed assisted design (CAD) tools. SLS is versatile in terms of structural stability and material usage, but spherical particles and good flowability characteristics are preferable for suitable processing [6]. Besides the wide use of metallic materials, the combination of biomaterials as feedstock for SLS has been intensively researched due to its interest in bone tissue applications [7–9]. Moreover, through optimized parameters, it is possible to achieve the desired mechanical properties for tissue engineering scaffolds [10].

Bone is a complex tissue with intricate hierarchical architectures, composed of organic collagen fibrils and inorganic calcium phosphate (CaP) crystals [11,12]. According to the bone location in the skeleton, functions and mechanical requirements will change; therefore, its characteristics and geometry vary accordingly.

For proper bone tissue treatment and recovery, it is highly desired that the applied materials induce osteoconduction and osteoinduction [13]. Osteoconduction means that the material surface is able to support the adhesion, proliferation and differentiation of bone cells. On the other hand, osteoinduction implies releasing molecular inducers such as growth factors and cytokines for mesenchymal precursors to differentiate into the osteoblastic lineage. Either osseointegration is highly desirable to guarantee bone-to-implant anchorage and it is particularly important for oral applications [14]. The bioceramics, more specifically calcium phosphates (CaPs), have been widely used as bone substitutes due to compositional similarities

and excellent biocompatibility [15]. More recently, these materials also gained attention in view of their versatility and tailored attributes, allowing the employment of growth factors and drug delivery systems [16]. Among the available CaPs, hydroxyapatite (HA) and tricalcium phosphate (TCP) are the most commonly used in bone tissue engineering [13]. HA [$Ca_{10}(PO_4)_6(OH)_2$] has a proven track record associated with bone tissue and dental applications, being commercially available in different shapes such as powder, granules and sticks. Its chemical and structural properties, similar to the natural bone, minimize body rejection of implanted devices and promotes bone formation through osteoconduction. The difficulty of processing and inherent brittleness restrain applications with bioceramics as medical devices [17]. Thus, adding polymers while processing bioceramics by AM techniques is beneficial, especially in terms of providing supplementary characteristics to the fabricated bioproducts [18].

UHMWPE is a biocompatible polymer, widely used for implantable devices and it is being particularly important for bearing replacement in the knee, hip and shoulder joints. Its powder is produced using the Ziegler process [19] and the requirements for medical-grade purity are specified in ASTM F648 [20] and ISO standard 5834 [21]. To consolidate UHMWPE into different forms, elevated temperatures and pressures are necessary due to its high melt viscosity. Therefore, processing techniques like injection moulding and screw extrusion are not practical [22]. Hence, UHMWPE devices are mainly obtained by machining, which implies size and shape limitations. SLS provided advancements related to devices for tissue engineering. Its versatility allows the processing of different kinds of materials and composites, including UHMWPE. Rimell and Marquis [23] reported remarkable shrinking while producing sheetlike UHMWPE structures, and suggested the improvement of starting powders. When optimizing processing parameters, as well as providing accurate preheating to the feedstock powder, Song *et al.* [24] effectively produced UHMWPE sample parts. Kalil *et al.* [25]

manufactured rectangular samples in which length and width shrinking was evident, also mentioning dimensional inaccuracy as a major challenge. Fumed silica particles as an anti-caking agent were applied in UHMWPE in order to reduce sintering difficulties; however, mechanical properties decreased [26]. Thus, research is needed to enhance UHMWPE processability and properties of the fabricated devices.

UHMWPE/HA composites processed by SLS are poorly investigated in the literature, possibly due to the processing complexity. While SLS has the capability of processing powder materials, whereas UHMWPE can provide the strength and structure, HA can provide the osteoconductivity. Finally, the powder preparation for fulfilling SLS feedstock requirements might provide suitable processability. Production of rounded HA particles can be performed through different techniques [27–33]. Essentially, spray drying (SD) is a process that transforms fluid feedstock into dried particles, being employed in different kinds of industry. This process is scalable and capable of producing spherical granules with adaptive size, according to the hardware setup [34]. Further, spray-dried HA (SDHA) has been effectively employed in manufacturing processes for biomedical applications [35–40]. In terms of 3D printing use, SD powder possesses desirable characteristics that allow fabricating precise products with complex geometry [41]. Although SDHA powder morphology indicates suitability for SLS processing, publications concerning this subject are scarce [42]. Nevertheless, the challenge remains to produce polymer/ceramic spray-dried composite granules with a suitable mechanical behaviour [43]. In this work, SDHA was mechanically mixed with UHMWPE powder for further SLS processing. Processing parameters were evaluated to find the most beneficial combination in terms of processability and mechanical strength. Preliminary *in vitro* biological analyses were conducted for assessing cell proliferation and viability.

2. Materials and methods

2.1. Materials and compositions

HA particles, synthesized by hydrothermal route [44], were used in an aqueous suspension (with deionized water) for the spray-drying process. Methylcellulose (Methocel A15 Premium LV, Dow Chemical) was used as a binder. The spray-dried HA powder (SDA) was mixed with a commercially manufactured ultra-high-molecular-weight polyethylene (UHMWPE) powder (Ticona, GUR 1020).

Three different powder mixtures were used for the SLS processing, varying SDHA content and identified as follows: UH (100 wt% UHMWPE); UH5HA (95 wt% UHMWPE + 5 wt% SDHA) and UH10HA (90 wt% UHMWPE + 10 wt% SDHA). Powders were mechanically mixed for 4 h using 3D dry powder mixer equipment.

2.2. Powder characterization

Powder particle size and distribution (PSD) were measured by laser scattering (Partica LA-950V2, Horiba). Scanning electron microscopy (SEM, JSM-6390, JEOL) was employed to analyse pre-SLS powder's morphology and fabricated samples surface, both coated with a thin gold layer. Morphological analysis of spray-dried HA (SDHA) particles was performed by SEM (IT300LV, JEOL), after platinum coating (Agar Scientific). Synthesized HA particles and SLS samples submitted to bioactivity essays were observed using a field emission gun microscope (Quanta 450, FEI). Particle flow and apparent density were determined using a Hall flowmeter. Concerning the particle's flow, a passing time of 50 g of each powder combination was taken 3 times and the average value was considered. For the apparent density calculations, a standard 25 cm^3 cylinder was filled and weighed.

The thermal behaviour of UH, UH5HA and UH10HA powders was analysed by differential scanning calorimetry (DSC, Jade, Perkin Elmer). Samples were sealed in an aluminium capsule and heated from 0 to 220 ºC at 10 ºC/min with isothermal mode and nitrogen gas at 20 ml/min.

Synthesized HA and SDHA particles were analysed by X-ray diffractometry (XRD, D8 Advance, Bruker), with a scan range from 27° to 40°, 2θ of 0.02° and acquisition time of 5 s. Moreover, a wider scan range, from 10° to 40°, 2θ of 0.02° and acquisition time of 1 s was applied for UHMWPE and SDHA powders, as well as for UH, UH5HA and UH10HA. EVA software and Powder Diffraction Files (PDF: 00-09-0432) from the International Center for Diffraction Data (ICDD) were used to identify the XRD phases.

2.3. Spray drying of HA powder

In order to determine the formulation of spray-drying suspension and its processing parameters, a screening method was employed as described in previous work [34]. In the present study, the suspension to be spray-dried contained, in weight, 20.32% HA, 1.63% methylcellulose and 78.05% deionized water. The employed spray-drying equipment was Büchi B-290 and the processing parameters were inlet temperature 170 °C, aspiration 100%, atomization pressure 60 mmHg and slurry feed 8.75 ml min^{-1}. After spray drying, the granules were submitted to thermal treatment using ramps of 3 °C/min up to 500 °C, for binder removal, and 10 °C/min up to 1000 °C with a hold of 1 h for densification in a resistive oven (LHT 04/17, Nabertherm). The obtained SDHA particle characteristics were D10 = 9.05 ± 0.14 μm; D50 = 17.15 ± 0.44 μm and D90 = 29.90 ± 1.15 μm.

2.4. SLS processing

SLS processing was conducted using a SLS equipment (Alkimat) with a CO_2 laser source (λ = 10.6 μm), 100 W maximum power, 200 μm spot diameter and a simple internal heating system.

To establish appropriate SLS processing conditions, the following parameters were varied: laser speed (LS), laser power (LP), hatch spacing (HS), layer thickness (LT) and powder bed temperature (BT). Visual observation and sample integrity were considered for suitable parameters selection. After that, laser power and scan speed were varied according to a factorial plan (Table 1), keeping the following parameters constant: hatch spacing (200 μm), layer thickness (200 μm) and powder bed temperature (100 ºC). Parameters presented in Table 1 were applied to fabricate rectangular prismatic samples with 35 mm × 5 mm × 1.40 mm (length × width × height). To guarantee better homogeneity and powder spreading on each fabricated layer, the rectangular samples were positioned perpendicularly to the powder's roller. The most suitable SLS processing parameters were chosen according to the sample characterization and used to fabricate cylindrical discs of 10 × 5 mm (diameter × height) for biological analysis.

Low cooling rates induce homogeneous shrinking and minimum distortion of components [45]. Therefore, to minimize shrinking by thermal gradients, samples were kept at around 100 ºC for 30 min (machine heating system) after SLS processing. Subsequently, the heating system was switched off and samples were held in the fabrication chamber until samples' temperature achieved 60 ºC (in around 30 min). Finally, the surrounding powder was removed using a brush and the samples were taken from the polyamide base using a razor blade knife (to avoid physical efforts in the samples).

Table 1: Factorial plan for SLS sample fabrication. The (−) signal represents lower, (0) central and (+) higher values.

Run	Laser power (W)	Laser speed (mm/s)
1	25 (+)	450 (+)
2	25 (+)	600 (0)
3	25 (+)	750 (-)
4	20 (0)	450 (+)
5	20 (0)	600 (0)
6	20 (0)	750 (-)
7	15 (-)	450 (+)
8	15 (-)	600 (0)
9	15 (-)	750 (-)

2.5. SLS samples characterization

SLS samples mechanical behaviour was measured through a single cantilever mode on dynamic-mechanical analysis equipment (Q800, TA Instruments). Single cantilever mode essay is suitable for thermoplastic materials and bar shaped samples. The stress-strain curves were obtained at a strain rate of 2 mm/min and a constant temperature of 37 ^{o}C, mechanical properties were measured using 3 different samples for each SLS fabrication parameters. Samples dimensional variation was quantified using a digital Vernier calliper, also using 3 samples. SEM images and EDS analysis (TM3030, Hitachi) were performed to verify particle coalescence/dispersion and chemical composition.

2.6. Biological analysis

For routine cell culture, murine calvaria pre-osteoblast MC3T3-E1 cells subclone 14 (ATCC, United States) were cultured in ascorbic acid-free alpha modified Eagle's medium (α-MEM; Gibco, United States) containing 2 mM L-glutamine and supplemented with 10% fetal calf serum (ThermoFisher, United States) 100 UI/ml penicillin and 100 µg/mL streptomycin (Gibco, United States), incubated at 37°C under 5% humidified CO_2 atmosphere (complete culture medium). For routine cultivation, the cells were seeded in T75 flasks (Sarstedt,

Germany). The complete culture medium was replaced every 2 to 3 days and cells were split when confluence reached 70-80 % of the culture area.

Prior to the cell culture, the different samples were sterilized by exposition to UV light under the culture laminar flow hood (ThermoFisher) for 30 min each side. Because the UH, UH5HA and UH10HA samples were floating in the complete culture medium, they were immobilized at the bottom of the culture wells (24-well culture plate, Sarstedt, Germany) by using a fibrin gel moulded around the UHs samples. Briefly, after having placed the samples in the wells, were added subsequently in the bottom of the well: 100 µl of a bovine fibrinogen solution (MP Biomedicals) in PBS 1X (Gibco) at 6 mg/ml, 100 µl of a complete culture medium and 100 µl of an aqueous solution of bovine thrombin (Merck) 25 U/ml. The solidification of the gel was starting immediately but the fibrin gel polymerization was let to complete for 30 min at 37 °C. Afterwards, the samples were covered by a complete culture medium and equilibrated for 1 h at 37 °C.

For each experiment, cells were rinsed in PBS 1X, detached by incubation in Tryple 1X (Gibco) for 3-5 min at 37 °C and centrifuged at 300 g for 5 min at room temperature. The pellet was resuspended in a complete culture medium, the cells were numbered on a Malassez chamber and seeded at the density of 25,000 cells/cm^2 on the samples in a complete culture medium (1 ml in 24-well culture plates). The cells were cultured at 37 °C under a 5 % humidified CO_2 atmosphere for the desired duration.

The cell metabolic activity was evaluated using an MTT assay. Briefly, after 24 h and 48 h of culture, 1.2 mM of MTT was added to the culture medium of the cells at the surface of the tested materials and let to incorporate during 2 h at 37 °C. The cell medium containing the soluble MTT is then discarded, 100 µl of DMSO (Sigma Aldrich) are added on top of the samples to lyse the cells and dissolve the water-insoluble formazan crystals resulting of the MTT reduction by cell enzymes such as succinate dehydrogenases. The lysis is completed by

15 min of agitation on a rotative plate, in the dark, at room temperature. Afterwards, 25 µl of the supernatant are taken in triplicate and distributed into a 96 well plate (Sarstedt, Germany) for OD reading at 595 nm on a plate reader (FluoSTAR Optima, BMG Labtek, Germany). Cells seeded over glass coverslips (ThermoFisher) in a complete culture medium or complete culture medium containing 100 µM of H_2O_2 were respectively used as control of viable and dead cells.

After 24, h of culture, viable cells were stained with 10 µM Calcein Red-Orange AM (Molecular probes). The dye was added to the culture media and incubated for 30 min at 37 °C. Cells were then rinsed in complete culture medium 3 times, then in PBS 1X and fixed in PFA 4 % for 10 min. They were again rinsed 3 times for 5 min in PBS 1X. Nuclei were stained by incubation in a Hoescht 33342 20µM (ThermoFisher, United States) solution in PBS 1X for 5 min and cells were rinsed again 3 times for 5 min in PBS 1X. Subsequently, samples were observed under AxioImager M2 microscope (Carl Zeiss, Germany), pictures were processed using the Zen blue software (Carl Zeiss, Germany). For each experiment, the analysis was performed at 10 different fields of the sample's surface. Finally, the pictures taken were analysed by ImageJ software (NIH, http://rsb.info.nih.gov/ij/). The cell density was evaluated by counting the number of cells attached to the pellet by surface area unit (cm^2).

For each assay, three independent experiments were performed. Statistical analyses were done using GraphPad Prism 9. Data were assayed for normality using the Shapiro-Wilk test. According to the data set and normality test results, the Kruskal-Wallis test was performed, followed by a Dunn's post hoc test. Differences were considered as significant for $p < 0.05$.

3. Results and discussion

3.1. Feedstock powder characteristics

The synthesized HA powder is composed of nano needle-like structures (Figure 1). These structures tend to agglomerate in the form of irregular clusters that have low flowability, which is unfavourable for SLS processing. SDHA particles have the advantage of being more spherical and show a homogenous particle size dispersion (Figure 2).

SEM images (Figure 3) also revealed that UHMWPE is composed of small particles agglomerations and interconnected by fibrils. This feature has already been documented in the literature, being a consequence of Zeigler Natta catalyst production route, not being the most favourable morphology for laser sintering [46,47]

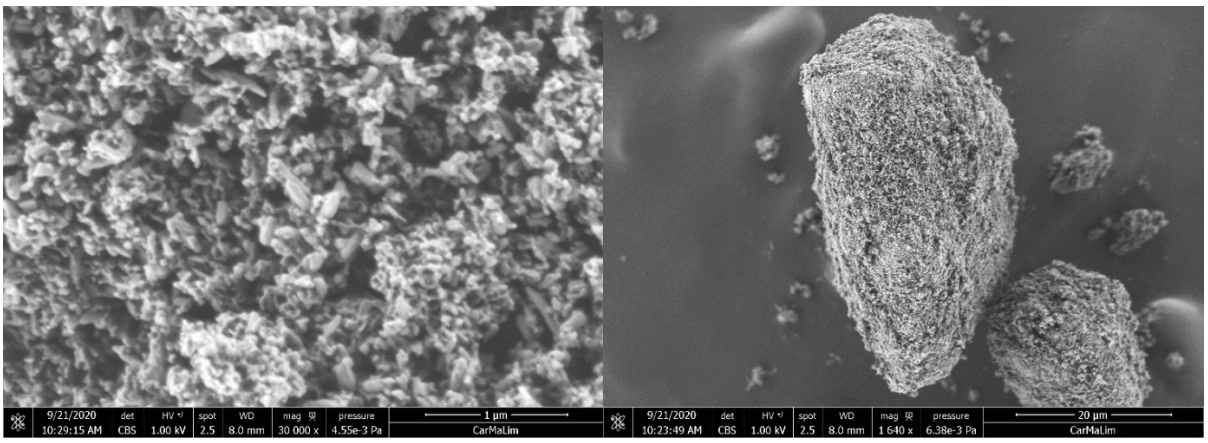

Figure 1: FEI images from departing HA powder: need-like nanostructures, scale bar: 1 µm (left) and irregular cluster agglomerations, scale bar: 20 µm (right).

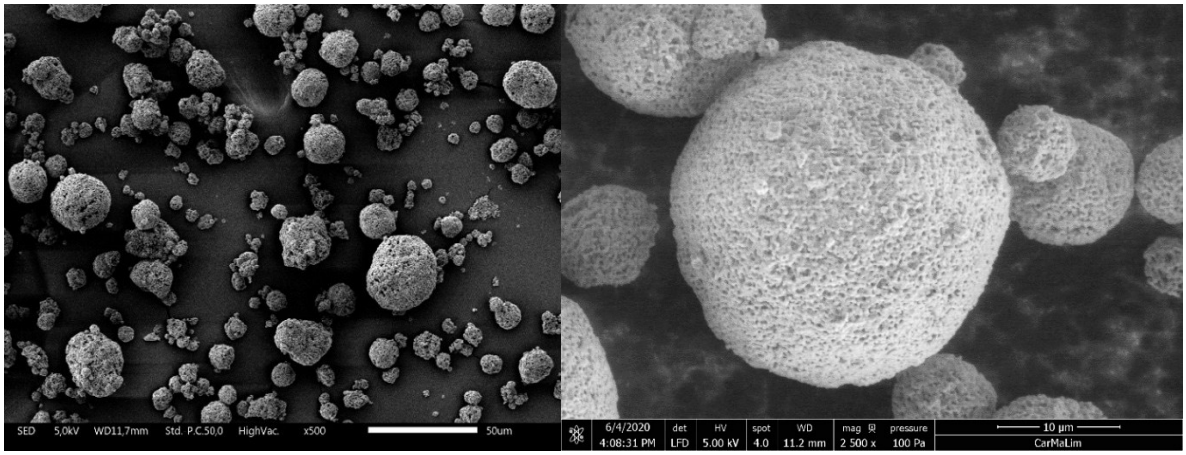

Figure 2: SEM images of SDHA particles, scale bar: 50 µm (left). FEI detailed images of SDHA particles, scale bar: 10 µm (right).

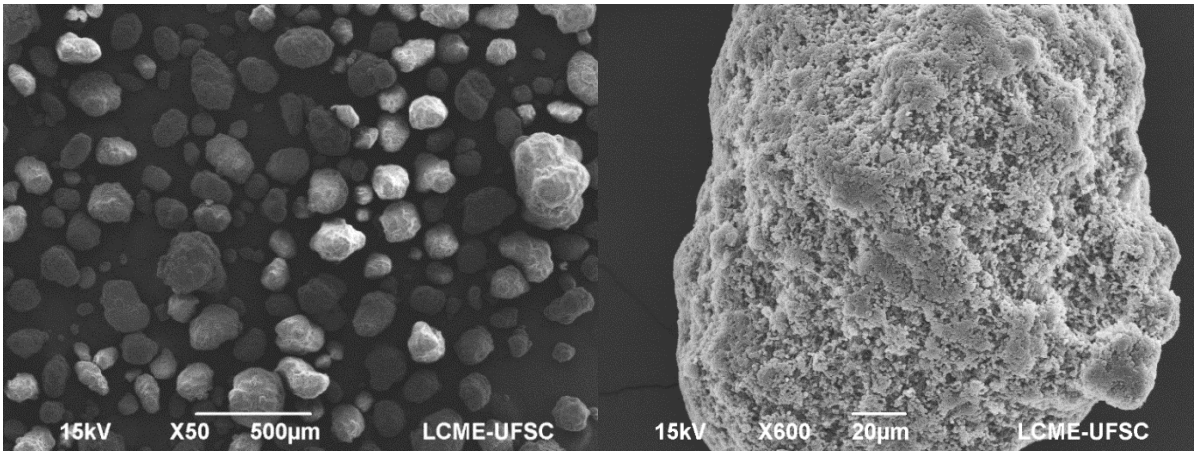

Figure 3: SEM images from Sample A. Various particles, scale bar: 500 µm (left) and individual particle, scale bar: 20 µm (right).

SDHA have a lower particle mean diameter than UHMWPE, so they are capable of filling voids left between UHMWPE particles and increase apparent density (Table 2). The lower flow time of UH5HA and UH10HA can be related to the smaller HA particles, which act as a lubricant and facilitate particles flow. It can be observed a greater value of (D90-D10)/D50 ratio along with great HA content, this is related to the increase of HA small particles in the mixture. In addition, PSD graphs (Figure 4) of UH5HA and UH10HA have shown bimodal behaviour, associated with the considerably different particle sizes from UHMWPE and SDHA.

Table 2: SLS feedstock powder characteristics.

Sample	Flow time (s)	Apparent Density (g/cm^3)	D10 (µm)	D50 (µm)	D90 (µm)	(D90-D10)/D50
UH	49.09	10.20	85.97	138.12	213.30	0.92
UH5HA	44.21	10.46	85.02	146.78	223.44	0.94
UH10HA	40.02	10.63	71.90	140.28	217.66	1.04

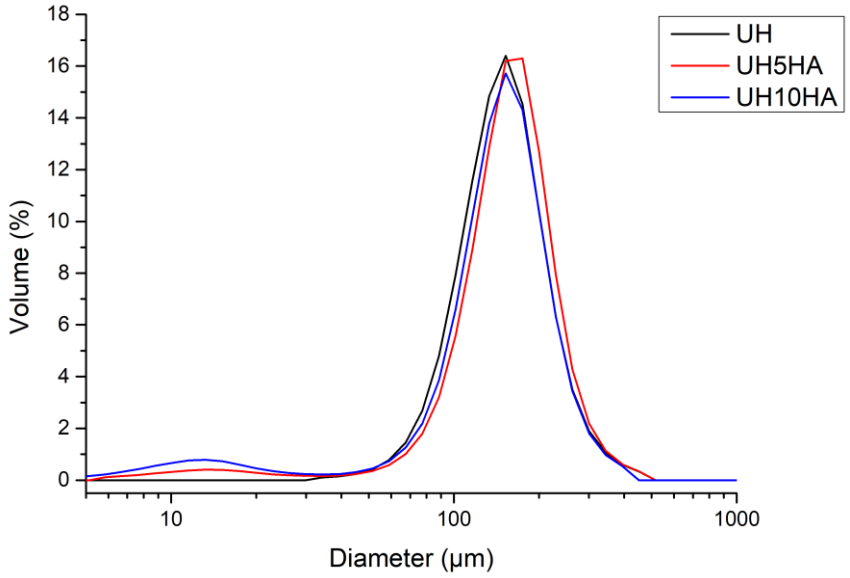

Figure 4: PSD of UH, UH5HA and UH10HA powder mixtures.

In a previous study [34], we did not identify phase modifications from synthesized HA to SDHA, and concerning UH, UH5HA and UH10HA samples there were also no phase divergences. XRD curves (Appendix I) intensities were according to HA's content, whereas UH10HA sample has shown greater intensity at HA's diffraction pattern due to the higher content.

Powder mixtures of UH (100% UHMWPE), UH5HA (5% HA) and UH10HA (10% HA) were also analysed by DSC. As seen in Figure 5, the powder thermal behaviour has changed with the addition of SDHA in the powder mixture as the crystallization temperature has dropped ~7.65 ºC and the melting temperature dropped ~4.70 ºC. These changes, as well as the lower and wider pics observed for UH5HA and UH10HA, can be attributed to different

powder composition. Additionally, HA (ceramic) has a different heat transfer coefficient than UHMWPE (polymer), which alters the heat transfer kinetics.

The SLS sintering window can be defined between onset points of crystallization temperature (T_c) and melting temperature (T_m). However, this sintering window is an idealized representation (considering cooling/heating rates of 10 ºC/min), being a completely different circumstance of the hardly controllable temperature changing rates during the SLS processing [6]. Nevertheless, DSC graphs (Figure 5) show clear diverse thermal behaviour and SLS sintering windows. The calculated values for the sintering window, using data from DSC were ~3.40 ºC for UH; ~14 ºC for UH5HA; and ~13.25 ºC for UH10HA. Khalil *et al.* [47] have confirmed different values for UHMWPE sintering windows, according to distinct heating and cooling rates. Therefore, the disparate thermal behaviour from UH toward UH5HA and UH10HA can affect the SLS processing behaviour.

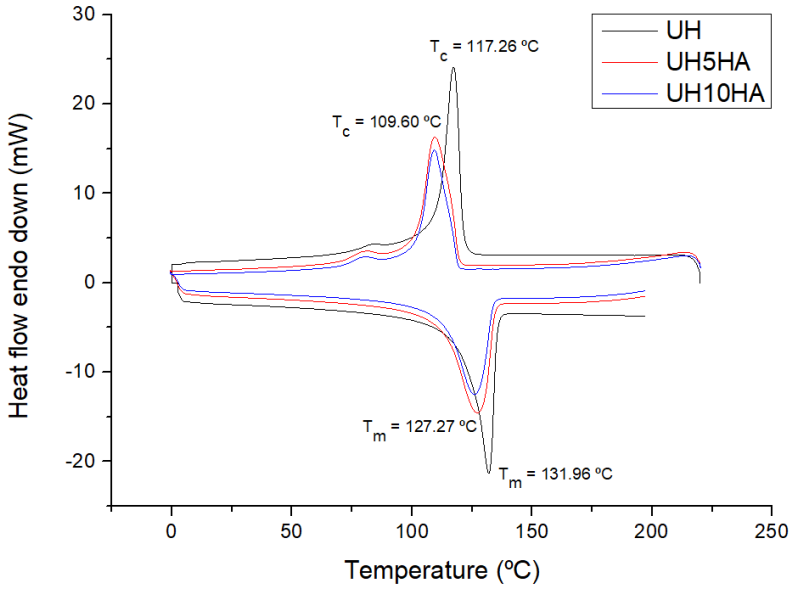

Figure 5: DSC runs from Sample A and B (left). DSC runs for UH, UH5HA and UH10 powder mixtures (right).

3.2. SLS processing and parameters

While fabricating pieces by additive manufacturing techniques, piece design and building orientation must be considered. Component design specifications must be according to the manufacturing capabilities and limitations of the intended AM technique [48]. Further, building orientation has a significant effect on the properties of fabricated pieces by SLS [49–51]. Figure 6 exhibit how samples were disposed of in the fabrication chamber. One of the reasons for this positioning was because rollers for powder feed moves along the x-axis (red line), providing more homogenous powder disposal. Another important reason is the building orientation, whereas the selected placement provides the larger surface perpendicular to the build direction. This means that the laser beam is exposed to a greater surface area, favouring cohesion between subsequent layers.

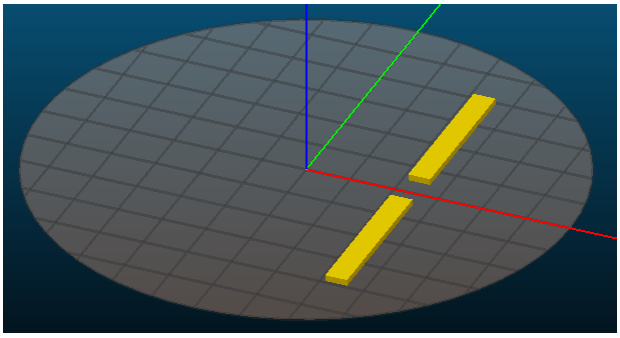

Figure 6: Sample's arrangement in the print bed, lines represent z (blue), y (green) and x (red) axes.

The energy density (ED) can be used to quantify the amount of energy that is placed on the feedstock powder during the SLS processing. It can be calculated using Eq. (1), being expressed in J/mm^3 [52–57], whereas LP is laser powder (W), LT is layer thickness, LS is laser speed (mm/s) and HS is hatch spacing (mm) – also known as scan spacing. Values of LT and HS were fixed in 200 µm during all experiments, Table 3 indicates the respective ED for each

combination of SLS parameters displayed in Table 1, where the lighter colour represents lower ED values.

$$ED = \frac{LP}{LT \times LS \times HS} \quad (1)$$

Table 3: Energy density (ED) for SLS sample fabrication.

ED (J/mm³)		Laser speed (mm/s)		
		750	600	450
Laser power (W)	15	0.500	0.625	0.833
	20	0.667	0.833	1.111
	25	0.833	1.042	1.389

As seen in Figure 5, the UHMWPE polymer possesses a narrow SLS sintering window (~3.40 ºC), therefore, slight changes in processing parameters are preferable. However, considering SLS equipment limitations for small changes in processing parameters, we have chosen to investigate a wider variety of parameters and the possible outcomes of parameters combination.

Some of the employed ED were not suitable for the sample fabrication due to low particle cohesion or, in contrast, excessive energy application leading to polymer degradation (smoke/flame with laser beam passage). Concerning UH samples values of ED of 0.500; 0.625 and 0.667 J/mm^3 did not achieve a proper particle cohesion, therefore, samples were not rigid enough to conduct accurate mechanical and dimensional measurements. Diversely, when processing UH5HA and UH10HA samples with 1.042 and 1.389 J/mm^3 flame was produced with a laser beam passage on the powder bed, therefore, polymer degradation was evident, and the samples were unconsidered. Interestingly, the ED value of 1.111 J/mm^3, which is greater than 1.042 J/mm^3, did not show flames during processing but some smoke was produced. This might be attributed to the longer exposure time (lower laser speed) of the laser

beam in the powder bed. Although smoke is also considered indicative of polymer degradation, it was chosen to go forward with these samples for mechanical and dimensional analysis.

3.3. Fabricated sample's properties

The fabricated samples were submitted to SEM analysis, images revealed homogeneous SDHA powder dispersion in the polymeric matrix. The UH samples that were processed with low ED (*i.e.* 0.500; 0.625 and 0.667 J/mm^3) evidenced poor particle cohesion and sintering neck formation was not observed. The EDS technique has confirmed the presence of SDHA particles along with the UHMWPE matrix as indicated in Figure 7, chemical composition is displayed in Table 4. It can be observed the substantial difference in phosphorous, calcium and carbon content in the measured points. Additionally, SDHA particles kept their morphological features after SLS processing, while UHMWPE particles fused between each other.

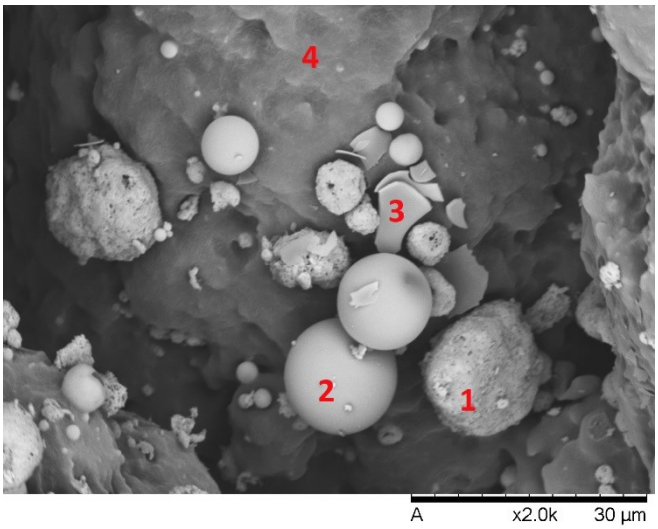

Figure 7: SEM image of UH10HA sample with respective points of EDS analysis.

Table 4: EDS results of each element found on different points of UH10HA sample.

	Carbon (wt%)	Oxygen (wt%)	Phosphorus (wt%)	Calcium (wt%)
Point 1	26.73	28.15	12.00	33.10
Point 2	26.69	25.78	13.75	33.78
Point 3	31.40	23.60	10.90	34.08
Point 4	88.79	8.70	-	2.50

Dimensional variation and warpage effects after processing has been evidenced by diverse studies while processing polymers [58–62]. Further, substantial warpage and dimensional variation are frequently cited by authors that have processed UHMWPE by SLS [23,24,63]. Dimensional variations can be attributed to inhomogeneous shrinkage as a result of inhomogeneous temperature distribution during SLS processing, leading to piece distortion due to stress forces [64]. For customized implantable devices, dimensional accuracy is essential. Eventual piece shrinkage must be considered in the project in the fabrication phases. In our study, pieces were fabricated in the same position of the coordinate plane (Figure 6), whereas axis x refers to piece width, axis y to length and axis z to thickness. The employed SLS equipment had limitations related to layer thickness accuracy and homogeneity. Therefore, sample thickness values were not taken into consideration for discussing dimensional results. Thus, for assessing dimensional variation only the length and width of the fabricated pieces were compared with the nominal values. A total of 3 samples from each powder composition (UH, UH5HA and UH10HA) were measured using vernier callipers; in length, only 1 measure was taken on each sample, and in width, 3 measures were taken (2 in the extremities and 1 in the middle).

Appendix II contains the arithmetic mean values and standard deviation for the measured values of each powder mixture. Regarding length and width measures, it can be observed that a greater ED implied greater mean dimensions. This can be related to the fusion of adjacent particles that originally were not supposed to be fused by the programmed laser

track. When compared to the nominal length dimension (35 mm), it can be observed certain degree of shrinkage in all the ED values, probably due to material shrinkage. Contrastingly, width values have shown greater variation between the different ED values, in some cases, exceeding the nominal value (5 mm). In those instances, a greater ED value was applied to the samples and the increased dimensions can be related to a higher warping effect [65].

Table 5 contains the mean area variation of fabricated pieces, where negative values denote piece shrinkage. For UH samples, lower area variation was observed with ED of 1.389 J/mm^3, followed by ED of 1.042 J/mm^3 and the only positive area variation was the ED of 1.389 J/mm^3. Concerning UH5HA samples, relative uniform area variation values were observed with the different parameters combinations whereas ED is 0.833 J/mm^3 and shown positive area variation with ED of 1.111 J/mm^3. UH10HA samples have shown the greatest area variation among the different ED values employed, this might be related to the more heterogeneous composition due to higher SDHA amount, like UH5HA that had bigger area variation when compared to UH samples.

Table 5: Mean area variation from nominal values of fabricated samples.

Laser speed (mm/s)		UH (%)			UH5HA (%)			UH10HA (%)		
		750	600	450	750	600	450	750	600	450
Laser power (W)	15	-	-	-4,83	-6,36	-4,85	-1,25	-9,90	-4,30	3,99
	20	-	-7,33	-4,15	-6,32	-0,66	5,74	-2,63	2,20	13,34
	25	-7,20	-2,20	1,30	-1,91	-	-	4,14	-	-

Stress versus strain graphs from the fabricated samples are illustrated in Figure 8 and Table 6 indicate the arithmetic mean ultimate strength and deviation values for each parameter combination. All results are presented in Appendix III. A total of 3 samples of each ED were

submitted to mechanical analysis and most samples had homogenous curve behaviour up to around 10% strain. After this point, a different curve pattern was observed suggesting the occurrence of a different deformation mechanism in the polymeric chain. It can be observed that the strain at break value systematically decreases with higher SDHA content. Although SEM images have shown good interparticle bonding of the UHMWPE matrix and homogeneous SDHA dispersion into the matrix, the low chemical affinity between UHMWPE and SDHA phases contributes to lower mechanical properties. Further, a higher weight content of SDHA particles will corroborate to fewer UHMWPE particles' contact area and, ultimately, leading to less particle cohesion and a more heterogeneous microstructure. Facilely evidenced in UH10HA samples, the reduced area under the stress-strain curves denotes that SDHA particles have induced a reduction in toughness.

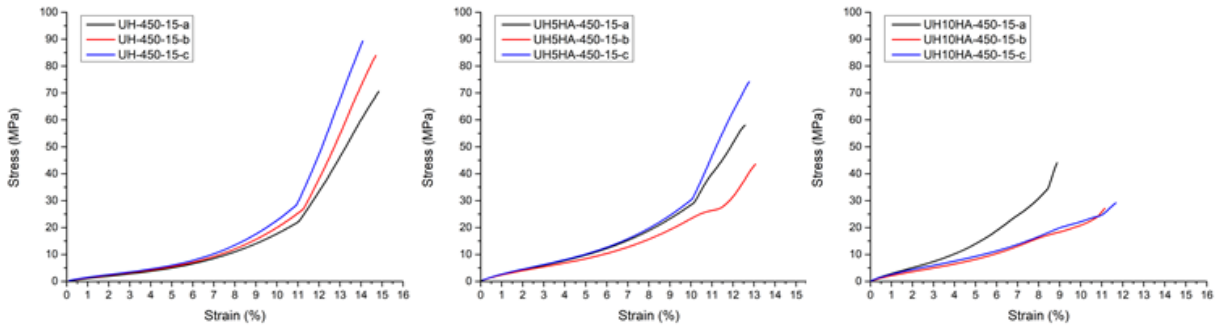

Figure 8: Selected stress-strain graphs with ED of 0.833 J/mm³ for UH, UH5HA and UH10HA.

Stress versus strain graphs have also shown discrepancies in mechanical behaviour for the same group of samples, leading to great deviations in the ultimate strength values. The employed equipment for mechanical analysis considers the cross-section area (width × thickness) for plotting stress versus strain graphs, therefore, considering the low accuracy related to sample's thickness, this might justify disparities between stress-strain curves among the same samples. Other than that, inconsistences in the microstructure (*e.g.*, voids, micro-

fissures, agglomeration of SDHA particles) may also lead to weakening polymeric matrix resulting in atypical mechanical behaviour. Some processing parameters combination of UH and UH5HA samples achieved strength values that are comparable to cortical bone [1]. Better mechanical properties might be achieved using a more precise parameters combination or post-treatment methods, such as heat treatment and hot isostatic pressure [66]. To select suitable processing parameters to fabricate cylindrical samples for biological analysis, the selection criteria were in accordance with mechanical properties. High ultimate strength and stress-strain homogenous curve behaviour were considered essential. Therefore, for UH samples the chosen ED of 0.833 J/mm^3 (LS of 450 mm/s and LP of 15 W), for UH5HA samples the ED of 0.833 J/mm^3 (LS of 600 mm/s and LP of 20 W) and for UH10HA ED of 0.625 J/mm^3 (LS of 600 mm/s and LP of 15 W).

Table 6: Mean values and deviation of ultimate strength for fabricated samples.

Laser speed (mm/s)		UH (MPa)			UH5HA (MPa)			UH10HA (MPa)		
		750	600	450	750	600	450	750	600	450
Laser power (W)	15	-	-	81.27 ± 9.65	51.18 ± 14.22	46.50 ± 7.65	58.57 ± 15.32	16.51 ± 0.55	41.22 ± 5.31	33.40 ± 9.28
	20	-	56.26 ± 16.24	70.00 ± 8.67	53.31 ± 7.22	79.41 ± 3.56	39.24 ± 4.18	34.35 ± 20.88	26.57 ± 4.04	21.61 ± 3.22
	25	83.34 ± 13.59	51.79 ± 24.66	49.00 ± 11.76	75.60 ± 13.85	-	-	26.21 ± 2.51	-	-

3.4. Biological assays

Preliminary biological assays were conducted to evaluate differences in the biological response of the sample with different SDHA content. Pure dense HA disks (HA), produced using uniaxial presage using 0.5 ton and 10 mm matrix and heat treatment at 1200 ºC (30 ºC/min ramps), were used as a standard to compare results with the UH, UH5HA and UH10HA samples.

In a first approach, was evaluated the metabolic activity of the cells seeded at the different material surfaces and cultivated for 24 h and 48 h. The results are presented in Figure 9. Because the HA samples were smaller than UH, UH5HA and UH10HA samples, the values were normalized on the available geometric surface. The results were expressed as a percentage of activity relative to the control, which is HA, as a biocompatible material. At 24 h, considering the variations related to the measurements, all the values were similar except for the cells that have grown at the surface of UH. While not significantly different from HA ($p = 0.01$), the metabolic activity measured for UH is low and may be associated either with a defect in initial cell attachment or potential toxicity.

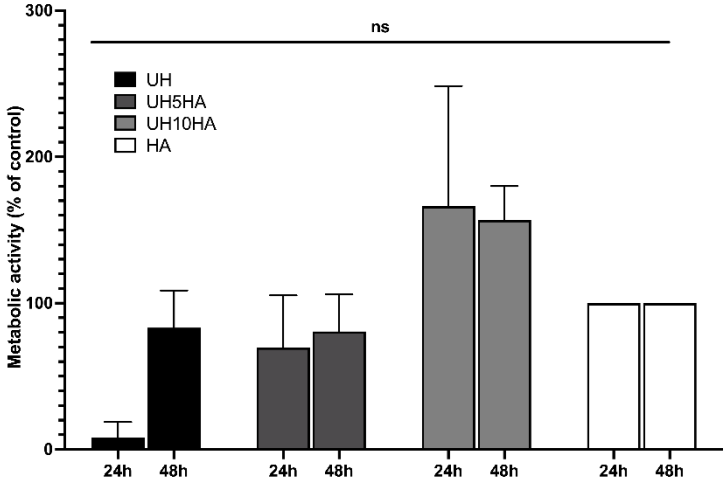

Figure 9: Metabolic activity of cells grown at the surface of UH, UH5HA, UH10HA and HA during 24 h and 48 h. The results were normalized on the geometric available surface and expressed as a % of control (HA). Statistical analysis: Kruskall-Wallis by Dunn's post hoc test. ns: non-significant ($p > 0.05$), *: $p \leq 0.05$.

At 48 h, no significant difference was detected whatever the considered sample even for the UH sample. This would indicate that, on one hand, at 24 h the cell had likely some difficulties to adhere to the material with a possible delay for adhesion explaining at less in part the result obtained at 48 h. On the other hand, cell growth would be not affected in this

condition. Preliminary MTT results performed for 72h of cell culture no exhibit an alteration in cell viability with results comparable to those obtained for HA samples.

To go further and evaluate the initial attachment of the cell an *in situ* observation of the cells at the sample surfaces was performed after 24h of culture (Figure 10) and allowed to estimate the cell density (Figure 11 and Figure 12). The first observation is that most of the cells observed, regardless of the samples nature on which they were growing, were positive for calcein (red staining) so viable cells. The density is apparently higher on HA as confirmed by the quantitative analysis with more than 40,000 cells/cm^2 on HA against fewer than 10,000 cells/cm^2 on UH samples.

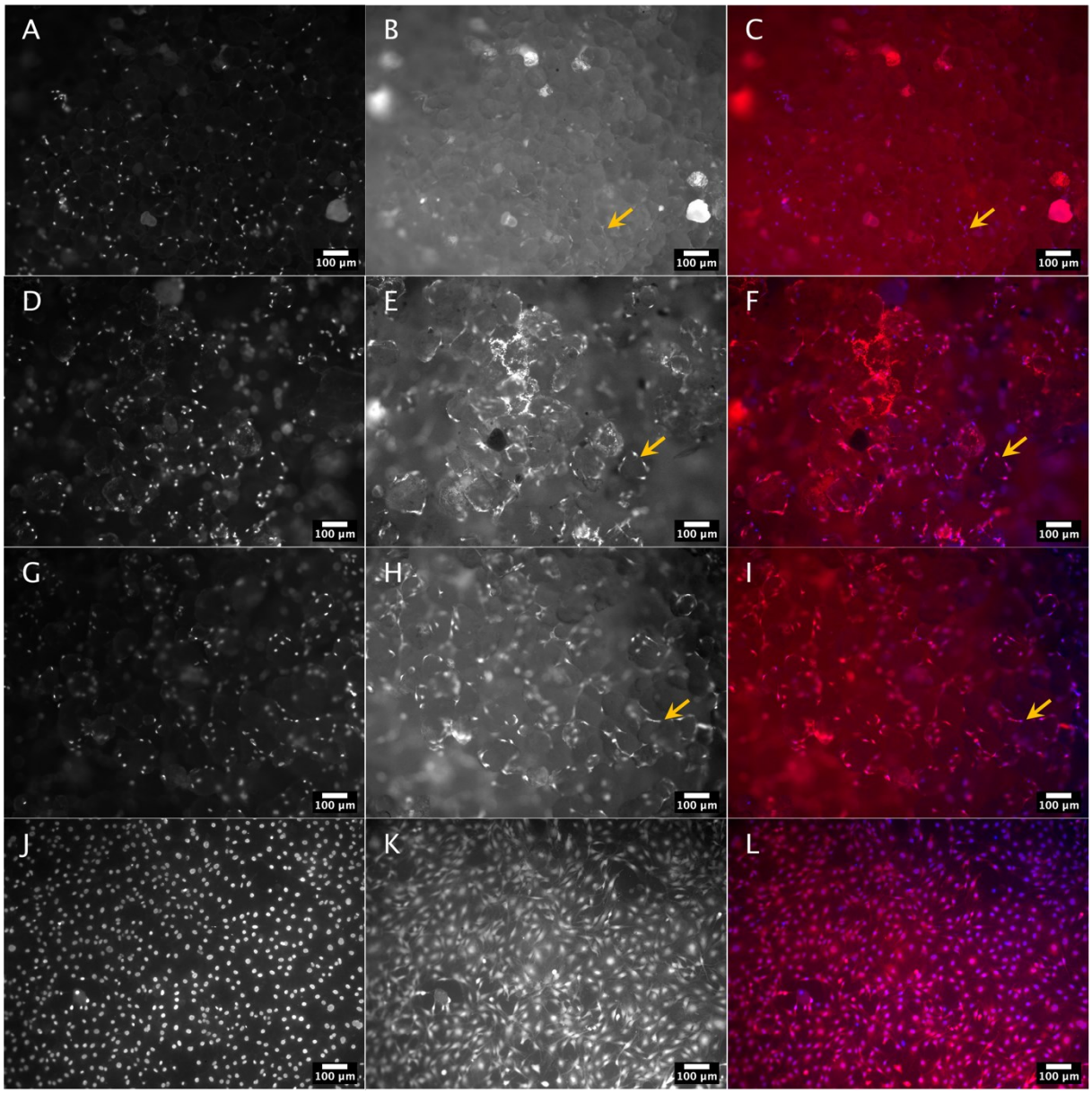

Figure 10: In situ observation of cell growing onto the surface of respectively UH (A to C), UH5HA (D to F), UH10HA (G to I) and HA (J to L). A, D, G and J: nuclei stained by Hoescht33342 (blue); B, E, H and K: viable cells are stained by calcein (red); C, F, I and L: merge. Scale bar: 100 µm. Arrows point to cells growing along asperities.

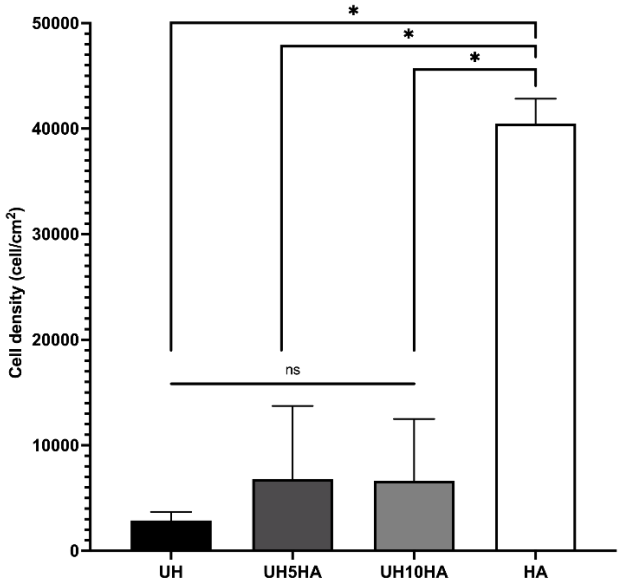

Figure 11: Cell density at the surface of materials after 24 h of cell culture. Statistical analysis: Kruskall-Wallis followed by Dunn's post hoc test; ns: non-significant ($p > 0.05$); *: $p \leq 0.05$.

However, it is important to note that the surface topography on UH samples is more uneven than on HA disks, with peaks and valleys, possibly with cells outside the focal plane of the microscope objective. Hence, the cellular density at the surface of those materials may have been a little underestimated. That would explain the discrepancy with MTT results, in which no difference in terms of cellular metabolic activity was detected when HA was compared with UHs samples. Fluorescence microscope images also revealed the influence of the sample's surface roughness and morphology on cells.

While HA disposed of homogeneous cell dispersion along the sample surface, UH samples have shown low cellular density. To go further, whereas on the relatively flat surface of HA disks when compared to UH samples, cells exhibited rounded nuclei (Hoescht33342 channel, left panel on Figure 12) with a spread morphology and presence of extensions, at the surface of the composite samples, the nuclei were smaller and elongated and it was observed that cells tended to allocate along the asperities (Figure 12). This can be related to the greater energy amount required for cells to allocate in curved surfaces [67]. Due to the important role

of the cytoskeleton in cell behaviour, the topography of the UH samples may certainly impact bone cell biology that needs further experiments to be assessed. Finally, it should be reported that on the border of the UH samples (highest than those of HA), some residues of the fibrin gels used to immobilize the samples in the culture well bottoms were found. Fibrin being a protein of the extracellular matrix, cells can adhere easily to it. On fibrin above the material surface, cells were well spread with numerous extensions that contrasted with the morphology of the cells directly growing on composite disks (Figure 13) and did not follow any asperities.

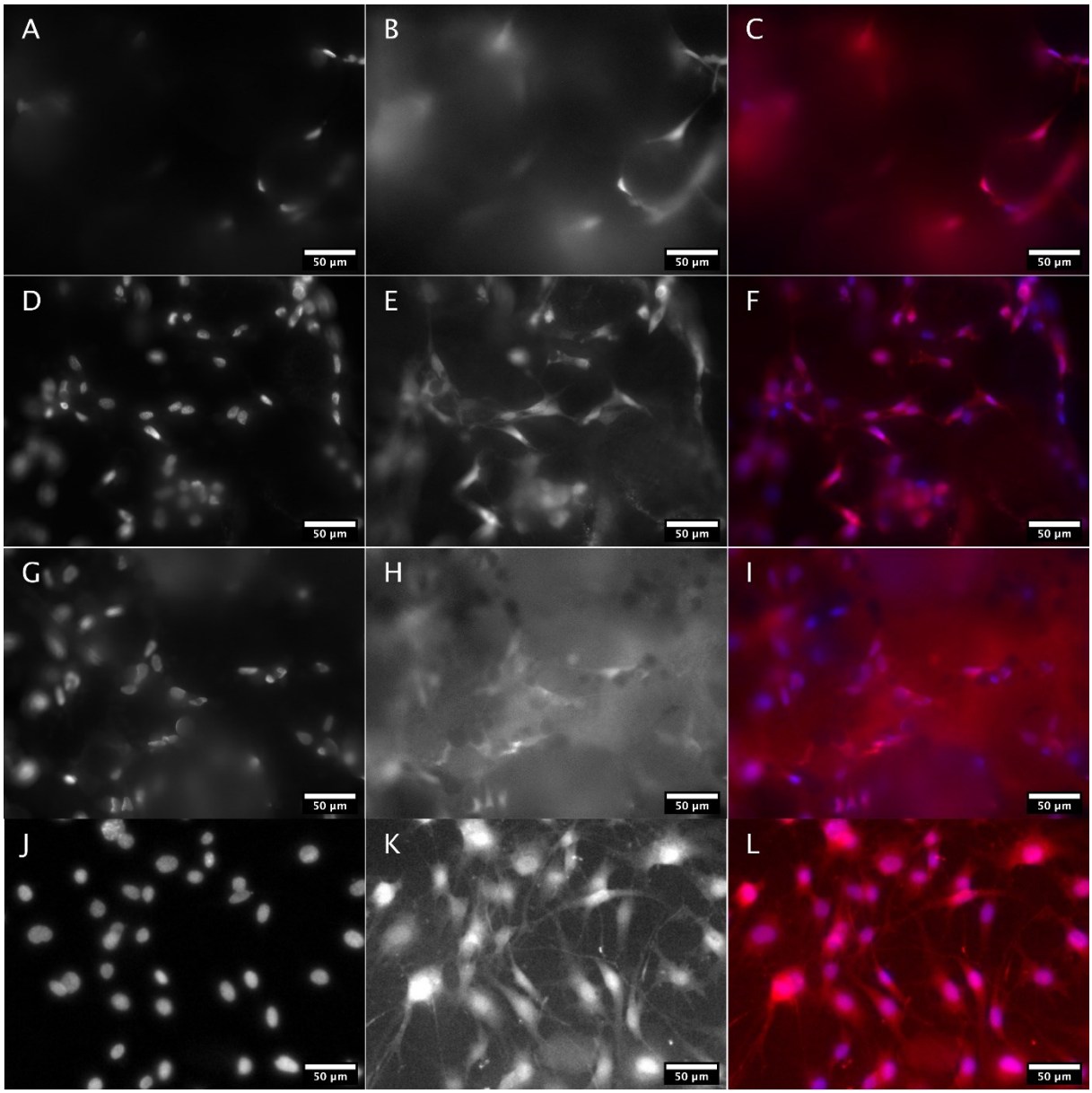

Figure 12: In situ observation of cell growing onto the surface of respectively UH (A to C), UH5HA (D to F), UH10HA (G to I) and HA (J to L). A, D, G and J: nuclei stained by Hoescht33342 (blue); B, E, H and K: viable cells are stained by calcein (red); C, F, I and L: merge. Scale bar: 50 µm.

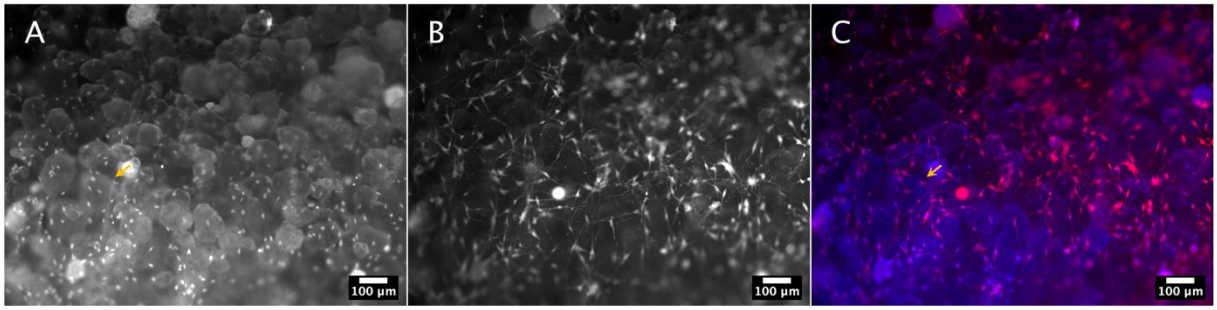

Figure 13: Cells on fibrin on UH sample. Scale bar: 100 µM. Arrows point to visible fibrin fibres.

4. Conclusions

Selective laser sintering of UHMWPE has inherent difficulties related to material properties and powder characteristics; nevertheless, feedstock preparation has shown prominent results. The addition of spray-dried hydroxyapatite (SDHA) particles to UHMWPE increased the powder flowability and apparent density. Further, DSC results showed that the thermal behaviour was affected, but no phase modification was observed by XRD. Biological essays demonstrated the biocompatibility of the employed UHMWPE/HA composite mixture. The SLS fabricated samples showed to be non-toxic, seem to not inhibit cell growth and were able to support pre-osteoblast attachment. It was observed that SDHA content and the selected SLS processing parameters have a great influence on the mechanical properties of the fabricated pieces. The mean ultimate strength values varied from 16.51 to 83.34 MPa and samples revealed greater dimensional measures when using higher energy density values. Further work is necessary to assess and verify correlations between the processing parameters and achieved results. Moreover, due to the small sintering window of UHMWPE/SDHA powders it is necessary to employ SLS machine with high precision of processing parameters. Finally, the UH polymers were not toxic, seem not to inhibit cell growth and were able to support pre-osteoblast attachment. No difference was observed between the rates of HA incorporation into UH samples.

Acknowledgements

This study was financed in part by Coordenação de Aperfeiçoamento de Pessoal de Nível Superior – Brasil (CAPES) - Finance Code 001 and the support of Fundação de Amparo à Pesquisa e Inovação do Estado de Santa Catarina (FAPESC/287/2018). The authors thank the French Agence Nationale de la Recherche in the scope of the LabExSigmaLim (ANR-10-LABX-0074-01 Sigma-LIM). The authors are grateful to the Service Commun de

Caractérisation des Matériaux de Limoges (CARMALIM) and more especially to Yann Launay for SEM acquisitions. The authors would like to thank the LCME-UFSC for technical support during electron microscopy.

References

[1] L. Piaia, G.V. Salmoria, D. Hotza, Additive Manufactured Nanocomposites for Bone Tissue Engineering Applications: an Overview, Mater. Res. 23 (2020) 1–10. https://doi.org/10.1590/1980-5373-mr-2019-0487.

[2] S. Mondal, U. Pal, 3D hydroxyapatite scaffold for bone regeneration and local drug delivery applications, J. Drug Deliv. Sci. Technol. 53 (2019) 101131. https://doi.org/10.1016/j.jddst.2019.101131.

[3] J. D'Alessio, A. Christensen, 3D Printing for Commercial Orthopedic Applications: Advances and Challenges, in: 3D Print. Orthop. Surg., Elsevier, 2019: pp. 65–83. https://doi.org/10.1016/B978-0-323-58118-9.00007-5.

[4] C. Shuai, L. Yu, W. Yang, S. Peng, Y. Zhong, P. Feng, Phosphonic acid coupling agent modification of HAP nanoparticles: Interfacial effects in PLLA/HAP bone scaffold, Polymers (Basel). 12 (2020). https://doi.org/10.3390/polym12010199.

[5] ISO/ASTM 52900: 2015 Additive manufacturing-General principles-terminology, ASTM F2792-10e1. (2012).

[6] M. Schmid, A. Amado, K. Wegener, Materials perspective of polymers for additive manufacturing with selective laser sintering, J. Mater. Res. 29 (2014) 1824–1832. https://doi.org/10.1557/jmr.2014.138.

[7] D. Grossin, A. Montón, P. Navarrete-Segado, E. Özmen, G. Urruth, F. Maury, D. Maury, C. Frances, M. Tourbin, P. Lenormand, G. Bertrand, A review of additive manufacturing of ceramics by powder bed selective laser processing (sintering / melting): Calcium phosphate, silicon carbide, zirconia, alumina, and their composites, Open Ceram. 5 (2021). https://doi.org/10.1016/j.oceram.2021.100073.

[8] H. Shi, Z. Zhou, W. Li, Y. Fan, Z. Li, J. Wei, Hydroxyapatite based materials for bone tissue engineering: A brief and comprehensive introduction, Crystals. 11 (2021) 1–18. https://doi.org/10.3390/cryst11020149.

[9] J. Gunasekaran, P. Sevvel, I.J. Solomon, Metallic materials fabrication by selective laser melting: A review, Mater. Today Proc. 37 (2020) 252–256. https://doi.org/10.1016/j.matpr.2020.05.162.

[10] F.E. Wiria, K.F. Leong, C.K. Chua, Y. Liu, Poly-ε-caprolactone/hydroxyapatite for tissue engineering scaffold fabrication via selective laser sintering, Acta Biomater. 3 (2007) 1–12. https://doi.org/10.1016/j.actbio.2006.07.008.

[11] L. Piaia, G.V. Salmoria, D. Hotza, Additive manufacturing of nanostructured bone scaffolds, Elsevier Inc., 2018. https://doi.org/10.1016/B978-0-12-814621-7.00010-X.

[12] Á.E. Mercado-Pagán, A.M. Stahl, Y. Shanjani, Y. Yang, Vascularization in Bone Tissue

Engineering Constructs, Ann. Biomed. Eng. 43 (2015) 718–729. https://doi.org/10.1007/s10439-015-1253-3.

[13] G. Battafarano, M. Rossi, V. De Martino, F. Marampon, L. Borro, A. Secinaro, A. Del Fattore, Strategies for bone regeneration: From graft to tissue engineering, Int. J. Mol. Sci. 22 (2021) 1–22. https://doi.org/10.3390/ijms22031128.

[14] T. Albrektsson, C. Johansson, Osteoinduction, osteoconduction and osseointegration, Eur. Spine J. 10 (2001) S96–S101. https://doi.org/10.1007/s005860100282.

[15] S. Bose, S. Tarafder, Calcium phosphate ceramic systems in growth factor and drug delivery for bone tissue engineering: A review, Acta Biomater. 8 (2012) 1401–1421. https://doi.org/10.1016/j.actbio.2011.11.017.

[16] É.R. Oliveira, L. Nie, D. Podstawczyk, A. Allahbakhsh, J. Ratnayake, D.L. Brasil, A. Shavandi, Advances in growth factor delivery for bone tissue engineering, Int. J. Mol. Sci. 22 (2021) 1–33. https://doi.org/10.3390/ijms22020903.

[17] F.W. Cooke, Ceramics in orthopedic surgery., Clin. Orthop. Relat. Res. (1992) 135–146.

[18] Y. Han, Q. Wei, P. Chang, K. Hu, O.V. Okoro, A. Shavandi, L. Nie, Three-dimensional printing of hydroxyapatite composites for biomedical application, Crystals. 11 (2021). https://doi.org/10.3390/cryst11040353.

[19] H.-G. Willert, P. Eyerer, G. Buchhorn, Ultra-high molecular weight polyethylene as biomaterial in orthopedic surgery, Hogrefe & Huber Pub, 1991.

[20] ASTM F648-21, Standard Specification for Ultra-High-Molecular-Weight Polyethylene Powder and Fabricated Form for Surgical Implants, ASTM International, West Conshohocken, PA, (2021). www.astm.org.

[21] ISO 5834-1:2019, Implants for surgery — Ultra-high-molecular-weight polyethylene — Part 1: Powder form, (2019).

[22] S.M. Kurtz, The UHMWPE Handbook Principles and Clinical Applications in Total Joint Replacement, Elsevier, 2004.

[23] J.T. Rimell, P.M. Marquis, Selective laser sintering of ultra high molecular weight polyethylene for clinical applications, J. Biomed. Mater. Res. 53 (2000) 414–420. https://doi.org/10.1002/1097-4636(2000)53:4<414::AID-JBM16>3.0.CO;2-M.

[24] C. Song, A. Huang, Y. Yang, Z. Xiao, J.K. Yu, Effect of energy input on the UHMWPE fabricating process by selective laser sintering, Rapid Prototyp. J. 23 (2017) 1069–1078. https://doi.org/10.1108/RPJ-09-2015-0119.

[25] Y. Khalil, A. Kowalski, N. Hopkinson, Influence of energy density on flexural properties of laser-sintered UHMWPE, Addit. Manuf. 10 (2016) 67–75. https://doi.org/10.1016/j.addma.2016.03.002.

[26] X. Zhu, Q. Yang, Sintering the feasibility improvement and mechanical property of UHMWPE via selective laser sintering, Plast. Rubber Compos. 0 (2020) 1–11. https://doi.org/10.1080/14658011.2020.1718321.

[27] C. Li, G. Li, S. Liu, J. bai, A. zhang, Spherical hydroxyapatite with colloidal stability prepared in aqueous solutions containing polymer/surfactant pair, Colloids Surfaces A Physicochem. Eng. Asp. 366 (2010) 27–33. https://doi.org/10.1016/j.colsurfa.2010.05.018.

[28] G.C. Koumoulidis, A.P. Katsoulidis, A.K. Ladavos, P.J. Pomonis, C.C. Trapalis, A.T. Sdoukos, T.C. Vaimakis, Preparation of hydroxyapatite via microemulsion route, J. Colloid Interface Sci. 259 (2003) 254–260. https://doi.org/10.1016/S0021-9797(02)00233-3.

[29] K. Ioku, G. Kawachi, S. Sasaki, H. Fujimori, S. Goto, Hydrothermal preparation of tailored hydroxyapatite, J. Mater. Sci. 41 (2006) 1341–1344. https://doi.org/10.1007/s10853-006-7338-5.

[30] C. Qiu, X. Xiao, R. Liu, Biomimetic synthesis of spherical nano-hydroxyapatite in the presence of polyethylene glycol, Ceram. Int. 34 (2008) 1747–1751. https://doi.org/10.1016/j.ceramint.2007.06.001.

[31] M.H. Hong, J.S. Son, K.M. Kim, M. Han, D.S. Oh, Y.K. Lee, Drug-loaded porous spherical hydroxyapatite granules for bone regeneration, J. Mater. Sci. Mater. Med. 22 (2011) 349–355. https://doi.org/10.1007/s10856-010-4197-z.

[32] X. Ma, Y. Chen, J. Qian, Y. Yuan, C. Liu, Controllable synthesis of spherical hydroxyapatite nanoparticles using inverse microemulsion method, Mater. Chem. Phys. 183 (2016) 220–229. https://doi.org/10.1016/j.matchemphys.2016.08.021.

[33] M. Kamitakahara, S. Takahashi, T. Yokoi, C. Inoue, K. Ioku, Preparation of spherical porous hydroxyapatite granules as support materials for microorganisms, J. Ceram. Soc. Japan. 126 (2018) 732–735. https://doi.org/10.2109/jcersj2.18089.

[34] H. Schappo, K. Giry, C. Damia, D. Hotza, Screening method for producing suitable spray-dried HA powder for SLS application, Powder Technol. 384 (2021) 62–69. https://doi.org/10.1016/j.powtec.2021.02.004.

[35] Y.J. Fu, S.S. Shyu, F.H. Su, P.C. Yu, Development of biodegradable co-poly(D, L-lactic/glycolic acid) microspheres for the controlled release of 5-FU by the spray drying method, Colloids Surfaces B Biointerfaces. 25 (2002) 269–279. https://doi.org/10.1016/S0927-7765(01)00205-3.

[36] P. López-Gasco, I. Iglesias, J. Benedí, R. Lozano, J.M. Teijón, M.D. Blanco, Paclitaxel-loaded polyester nanoparticles prepared by spray-drying technology: In vitro bioactivity evaluation, J. Microencapsul. 28 (2011) 417–429. https://doi.org/10.3109/02652048.2011.576785.

[37] E. Quinlan, A. López-Noriega, E.M. Thompson, A. Hibbitts, S.A. Cryan, F.J. O'Brien, Controlled release of vascular endothelial growth factor from spray-dried alginate microparticles in collagen–hydroxyapatite scaffolds for promoting vascularization and bone repair, J. Tissue Eng. Regen. Med. 11 (2017) 1097–1109. https://doi.org/10.1002/term.2013.

[38] S. Sequeira, M.H. Fernandes, N. Neves, M.M. Almeida, Development and characterization of zirconia–alumina composites for orthopedic implants, Ceram. Int. 43 (2017) 693–703. https://doi.org/10.1016/j.ceramint.2016.09.216.

[39] Y. Ben, L. Zhang, S. Wei, T. Zhou, Z. Li, H. Yang, Y. Wang, F.A. Selim, C. Wong, H. Chen, PVB modified spherical granules of β-TCP by spray drying for 3D ceramic printing, J. Alloys Compd. 721 (2017) 312–319. https://doi.org/10.1016/j.jallcom.2017.06.022.

[40] R. Cholas, S. Kunjalukkal Padmanabhan, F. Gervaso, G. Udayan, G. Monaco, A. Sannino, A. Licciulli, Scaffolds for bone regeneration made of hydroxyapatite microspheres in a collagen matrix, Mater. Sci. Eng. C. 63 (2016) 499–505. https://doi.org/10.1016/j.msec.2016.03.022.

[41] D. Santos, A.C. Maurício, V. Sencadas, J.D. Santos, M.H. Fernandes, P.S. Gomes, Spray Drying: An Overview, in: Biomater. - Phys. Chem. - New Ed., InTech, 2018. https://doi.org/10.5772/intechopen.72247.

[42] C.K. Chua, K.F. Leong, K.H. Tan, F.E. Wiria, C.M. Cheah, Development of tissue scaffolds using selective laser sintering of polyvinyl alcohol/hydroxyapatite biocomposite for craniofacial and joint defects, J. Mater. Sci. Mater. Med. 15 (2004) 1113–1121. https://doi.org/10.1023/B:JMSM.0000046393.81449.a5.

[43] M.S. Wahab, K.W. Dalgarno, R.F. Cochrane, S.H. Member, Development of Polymer

Nanocomposites for Rapid Prototyping Process, Proc. World Congr. Eng. WCE. II (2009).

[44] S. Raynaud, E. Champion, D. Bernache-Assollant, P. Thomas, Calcium phosphate apatites with variable Ca/P atomic ratio I. Synthesis, characterisation and thermal stability of powders, Biomaterials. 23 (2002) 1065–1072. https://doi.org/10.1016/S0142-9612(01)00218-6.

[45] D. Drummer, S. Greiner, M. Zhao, K. Wudy, A novel approach for understanding laser sintering of polymers, Addit. Manuf. 27 (2019) 379–388. https://doi.org/10.1016/j.addma.2019.03.012.

[46] R.D. Goodridge, R.J.M. Hague, C.J. Tuck, An empirical study into laser sintering of ultra-high molecular weight polyethylene (UHMWPE), J. Mater. Process. Technol. 210 (2010) 72–80. https://doi.org/10.1016/j.jmatprotec.2009.08.016.

[47] Y. Khalil, N. Hopkinson, A. Kowalski, J.P.A. Fairclough, Characterisation of UHMWPE polymer powder for laser sintering, Materials (Basel). 12 (2019). https://doi.org/10.3390/ma12213496.

[48] S.E. Ghiasian, K. Lewis, Automated Geometric Correction System for Additive Manufacturing Considering Build Orientation, J. Mech. Des. 143 (2021) 1–30. https://doi.org/10.1115/1.4051353.

[49] F. Calignano, F. Giuffrida, M. Galati, Effect of the build orientation on the mechanical performance of polymeric parts produced by multi jet fusion and selective laser sintering, J. Manuf. Process. 65 (2021) 271–282. https://doi.org/10.1016/j.jmapro.2021.03.018.

[50] K. Senthilkumaran, P.M. Pandey, P.V.M. Rao, Influence of building strategies on the accuracy of parts in selective laser sintering, Mater. Des. 30 (2009) 2946–2954. https://doi.org/10.1016/j.matdes.2009.01.009.

[51] S. Danjou, P. Koehler, Determination of Optimal Build Direction for Different Rapid Prototyping Applications, 14èmes Assises Eur. Du Prototypage Fabr. Rapide. (2009) 24–25.

[52] K. Shahzad, J. Deckers, J.P. Kruth, J. Vleugels, Additive manufacturing of alumina parts by indirect selective laser sintering and post processing, J. Mater. Process. Technol. 213 (2013) 1484–1494. https://doi.org/10.1016/j.jmatprotec.2013.03.014.

[53] S.H. Diermann, M. Lu, Y. Zhao, L.J. Vandi, M. Dargusch, H. Huang, Synthesis, microstructure, and mechanical behaviour of a unique porous PHBV scaffold manufactured using selective laser sintering, J. Mech. Behav. Biomed. Mater. 84 (2018) 151–160. https://doi.org/10.1016/j.jmbbm.2018.05.007.

[54] R.G.T. Fim, A.A. Mascheroni, L.F. Antunes, J.B.E. Engerroff, C.H. Ahrens, P.A.P. Wendhausen, Increasing packing density of Additively Manufactured Nd-Fe-B bonded magnets, Addit. Manuf. 35 (2020) 101353. https://doi.org/10.1016/j.addma.2020.101353.

[55] J.P. Kruth, B. Vandenbroucke, J. Van Vaerenbergh, I. Naert, Digital manufacturing of biocompatible metal frameworks for complex dental prostheses by means of SLS/SLM, Virtual Model. Rapid Manuf. - Adv. Res. Virtual Rapid Prototyp. (2005) 139–145.

[56] S. XiaoHui, L. Wei, S. PingHui, S. QingYong, W. QingSong, S. YuSheng, L. Kai, L. WenGuang, Selective laser sintering of aliphatic-polycarbonate/hydroxyapatite composite scaffolds for medical applications, Int. J. Adv. Manuf. Technol. 81 (2015) 15–25. https://doi.org/10.1007/s00170-015-7135-x.

[57] M.M. Savalani, L. Hao, P.M. Dickens, Y. Zhang, K.E. Tanner, R.A. Harris, The effects and interactions of fabrication parameters on the properties of selective laser sintered hydroxyapatite polyamide composite biomaterials, Rapid Prototyp. J. 18 (2012) 16–27. https://doi.org/10.1108/13552541211193467.

[58] B. Duan, M. Wang, Encapsulation and release of biomolecules from Ca-P/PHBV nanocomposite microspheres and three-dimensional scaffolds fabricated by selective laser sintering, Polym. Degrad. Stab. 95 (2010) 1655–1664. https://doi.org/10.1016/j.polymdegradstab.2010.05.022.

[59] Z. Zeng, X. Deng, J. Cui, H. Jiang, S. Yan, B. Peng, Improvement on selective laser sintering and post-processing of polystyrene, Polymers (Basel). 11 (2019). https://doi.org/10.3390/polym11060956.

[60] N. Raghunath, P.M. Pandey, Improving accuracy through shrinkage modelling by using Taguchi method in selective laser sintering, Int. J. Mach. Tools Manuf. 47 (2007) 985–995. https://doi.org/10.1016/j.ijmachtools.2006.07.001.

[61] C.Y. Wang, Q. Dong, X.X. Shen, Research on warpage of polystyrene in selective laser sintering, Appl. Mech. Mater. 43 (2011) 578–582. https://doi.org/10.4028/www.scientific.net/AMM.43.578.

[62] Y. Shi, Y. Wang, J. Chen, S. Huang, Experimental investigation into the selective laser sintering of high-impact polystyrene, J. Appl. Polym. Sci. 108 (2008) 535–540. https://doi.org/10.1002/app.27686.

[63] S. Changhui, H. Aibing, Y. Yongqiang, W. Di, Y. Jia-kuo, Customized UHMWPE tibial insert directly fabricated by selective laser sintering, Int. J. Adv. Manuf. Technol. 85 (2016) 1217–1226. https://doi.org/10.1007/s00170-015-8046-6.

[64] J.M. K. Manetsberger, J. Shen, Compensation of Non-Linear Shrinkage of Polymer Materials in Selective Laser Sintering, Solid Free. Fabr. Proc. (2000) 298–305. http://utwired.engr.utexas.edu/lff/symposium/proceedingsArchive/pubs/Manuscripts/2000/2000-37-Shen.pdf.

[65] V.E. Beal, R.A. Paggi, G. V. Salmoria, A. Lago, Statistical evaluation of laser energy density effect on mechanical properties of polyamide parts manufactured by selective laser sintering, J. Appl. Polym. Sci. 113 (2009) 2910–2919. https://doi.org/10.1002/app.30329.

[66] Y. Zhao, H. Ma, An investigation of post treatment on properties and structure of ultrahigh molecular weight polyethylene parts prepared by selective laser sintering for biomedical application, (2020) 1484–1495. https://doi.org/10.1002/pat.4878.

[67] M. Rumpler, A. Woesz, J.W.C. Dunlop, J.T. Van Dongen, P. Fratzl, The effect of geometry on three-dimensional tissue growth, J. R. Soc. Interface. 5 (2008) 1173–1180. https://doi.org/10.1098/rsif.2008.0064.

Appendix I

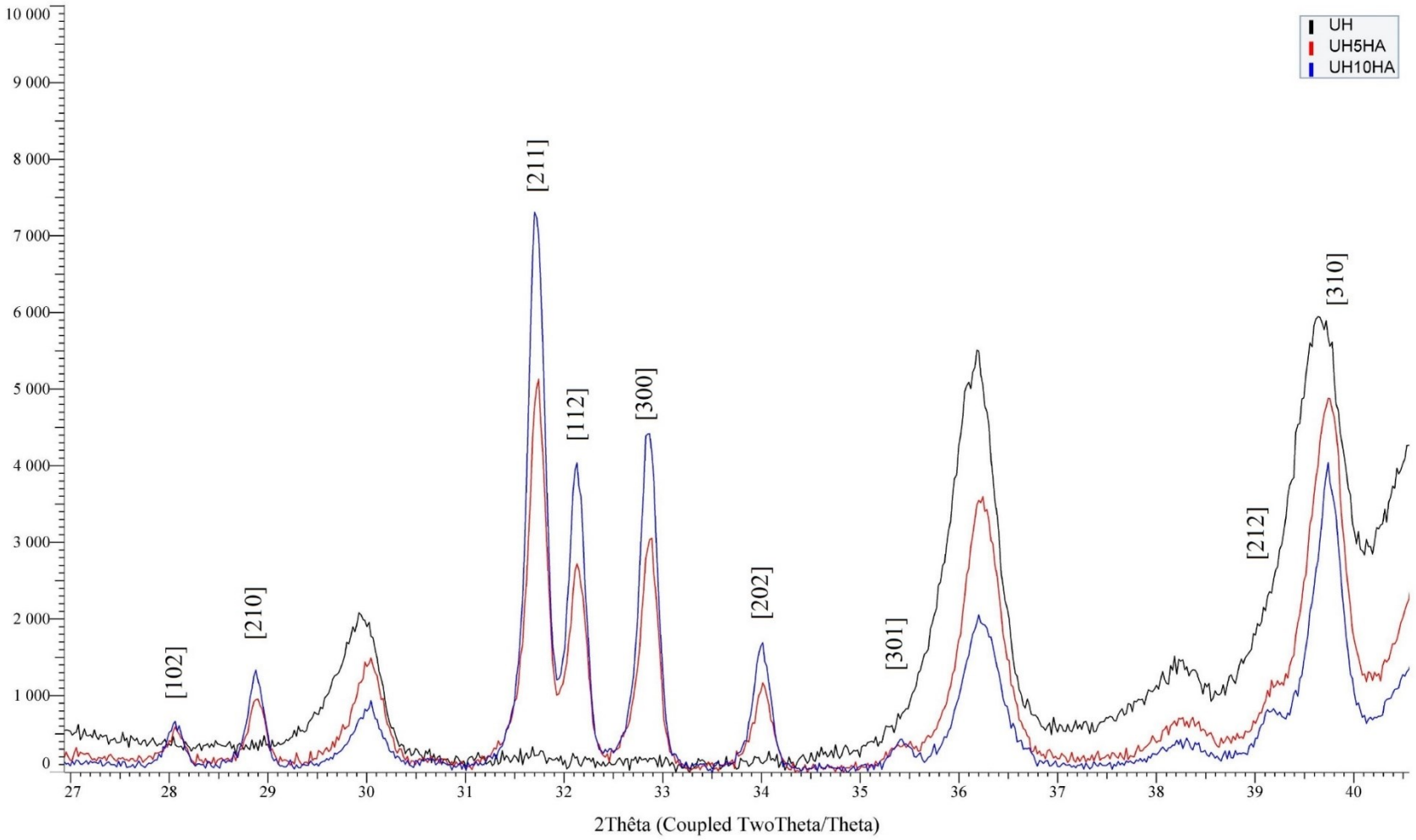
UH
UH5HA
UH10HA
[102]
[210]
[211]
[112]
[300]
[202]
[301]
[212]
[310]
10 000
9 000
8 000
7 000
6 000
5 000
4 000
3 000
2 000
1 000
0
27
28
29
30
31
32
33
34
35
36
37
38
39
40
2Thêta (Coupled TwoTheta/Theta)

Appendix II

UH SAMPLES

UH samples length (mm)		Laser speed (mm/s) 750	600	450
Laser power (W)	15	-	-	34.15 ± 0.08
	20	-	34.13 ± 0.08	34.10 ± 0.30
	25	34.00 ± 0.12	34.25 ± 0.15	34.52 ± 0.06

UH samples width (mm)		Laser speed (mm/s) 750	600	450
Laser power (W)	15	-	-	4.88 ± 0.09
	20	-	4.75 ± 0.07	4.92 ± 0.07
	25	4.78 ± 0.14	5.00 ± 0.09	5.14 ± 0.08

UH samples thickness (mm)		Laser speed (mm/s) 750	600	450
Laser power (W)	15	-	-	1.53 ± 0.09
	20	-	1.56 ± 0.07	1.65 ± 0.11
	25	1.55 ± 0.12	1.60 ± 0.12	1.62 ± 0.08

UH-05HA SAMPLES

UH5HA samples length (mm)		Laser speed (mm/s) 750	600	450
Laser power (W)	15	34.21 ± 0.06	34.19 ± 0.08	34.44 ± 0.02
	20	34.22 ± 0.15	34.46 ± 0.02	34.66 ± 0.02
	25	34.31 ± 0.05	-	-

UH5HA samples width (mm)		Laser speed (mm/s) 750	600	450
Laser power (W)	15	4.79 ± 0.08	4.87 ± 0.10	5.02 ± 0.07
	20	4.89 ± 0.10	5.05 ± 0.07	5.34 ± 0.14
	25	5.00 ± 0.08	-	-

UH5HA samples thickness (mm)		Laser speed (mm/s) 750	600	450
Laser power (W)	15	1.38 ± 0.16	1.47 ± 0.05	1.46 ± 0.10
	20	1.47 ± 0.11	1.43 ± 0.08	1.43 ± 0.07
	25	1.50 ± 0.12	-	-

UH-10HA SAMPLES

UH10HA samples length (mm)		Laser speed (mm/s) 750	600	450
Laser power (W)	15	33.59 ± 0.30	34.12 ± 0.18	34.54 ± 0.16
	20	34.29 ± 0.19	34.45 ± 0.08	34.77 ± 0.21
	25	34.60 ± 0.15	-	-

UH10HA samples width (mm)		Laser speed (mm/s) 750	600	450
Laser power (W)	15	4.69 ± 0.13	4.91 ± 0.18	5.27 ± 0.19
	20	4.97 ± 0.15	5.19 ± 0.15	5.70 ± 0.16
	25	5.27 ± 0.06	-	-

UH10HA samples thickness (mm)		Laser speed (mm/s) 750	600	450
Laser power (W)	15	1.60 ± 0.12	1.40 ± 0.16	1.33 ± 0.17
	20	1.51 ± 0.14	1.42 ± 0.10	1.36 ± 0.13
	25	1.51 ± 0.13	-	-

Appendix III

Parameters	UH	UH5HA	UH10HA
750 x 15 (ED = 0.500 J/mm^3)	-	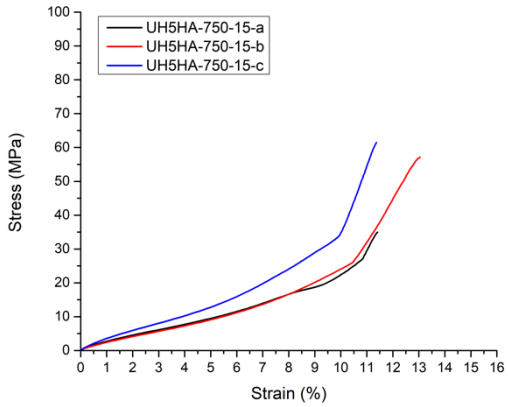	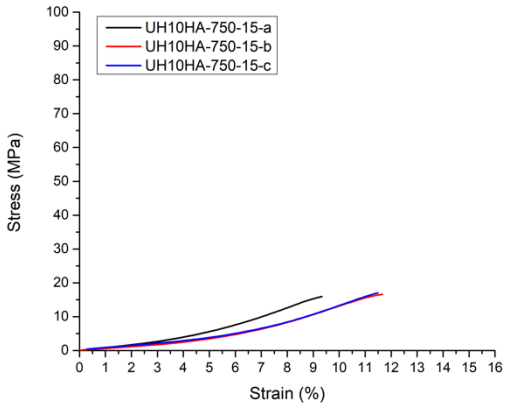
750 x 20 (ED = 0.667 J/mm^3)	-	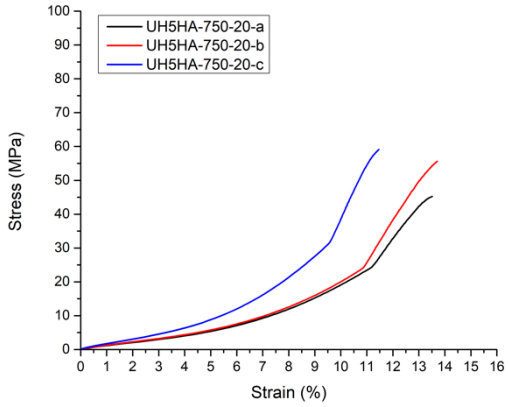	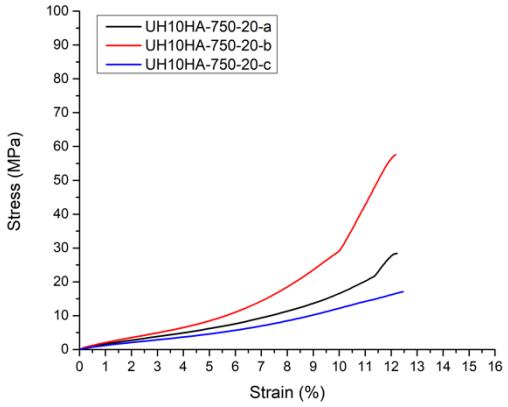

750 x 25 (ED = 0.833 J/mm^3)	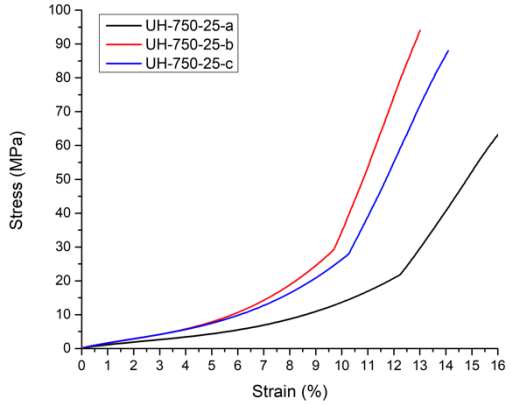	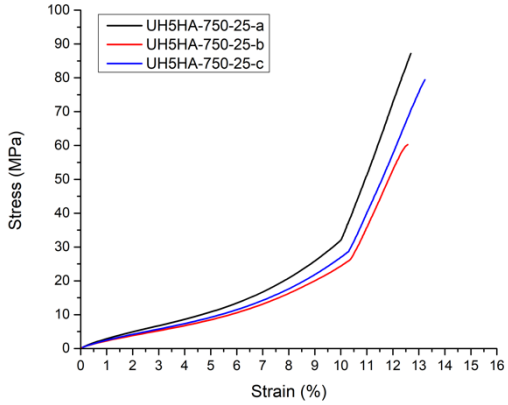	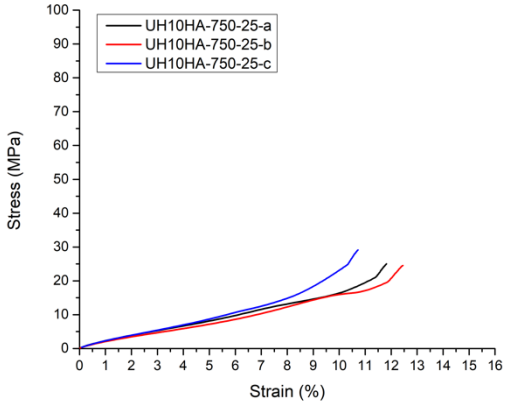
600 x 15 (ED = 0.625 J/mm^3)	-	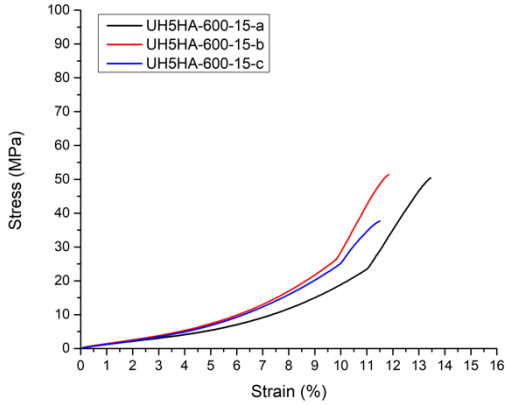	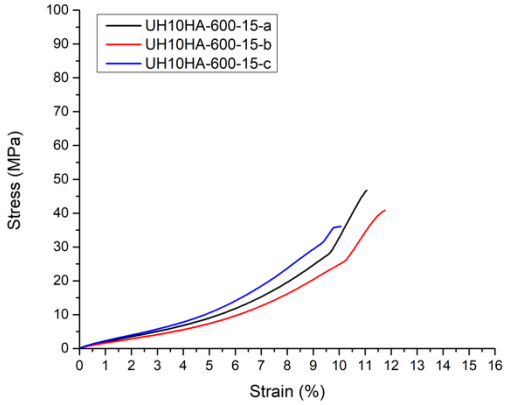

600 x 20 (ED = 0.833 J/mm^3)	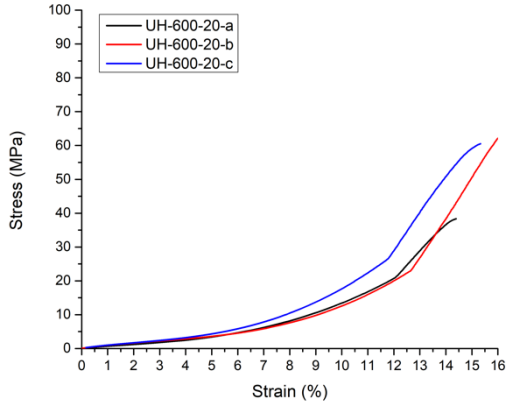	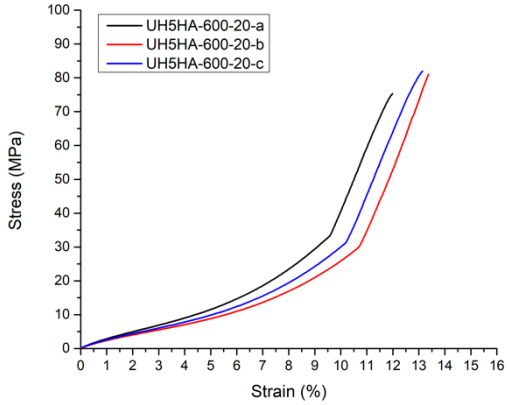	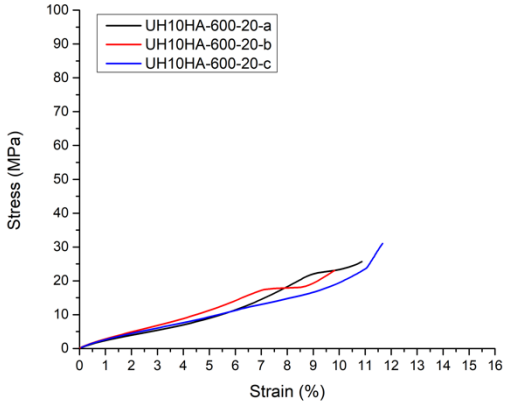
600 x 25 (ED = 1.042 J/mm^3)	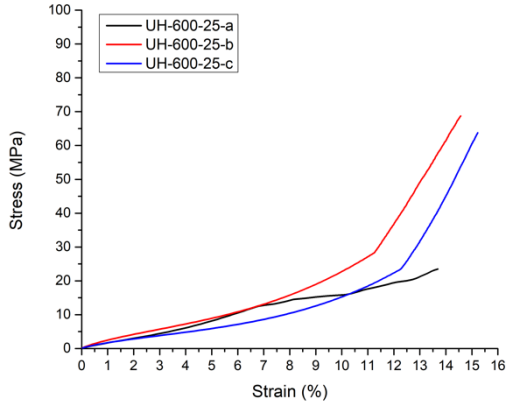	-	-

450 x 15 (ED = 0.833 J/mm^3)	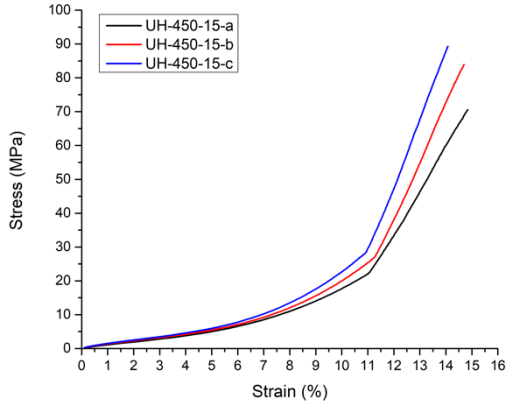	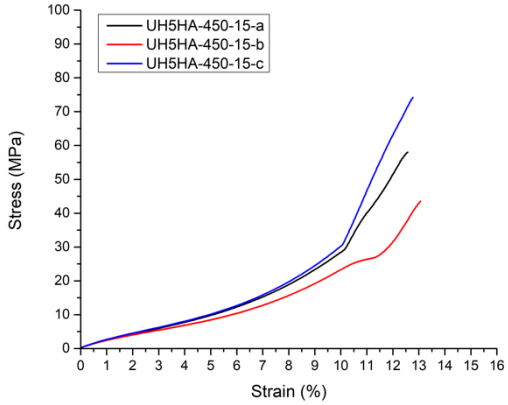	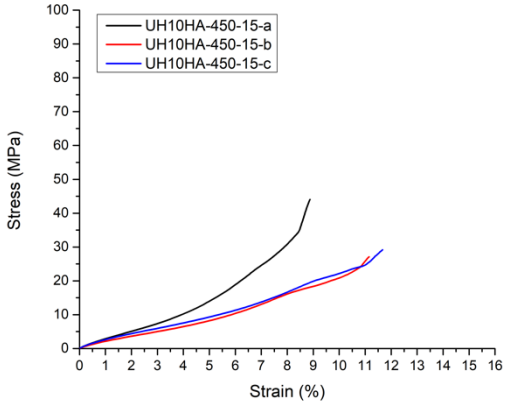
450 x 20 (ED = 1.111 J/mm^3)	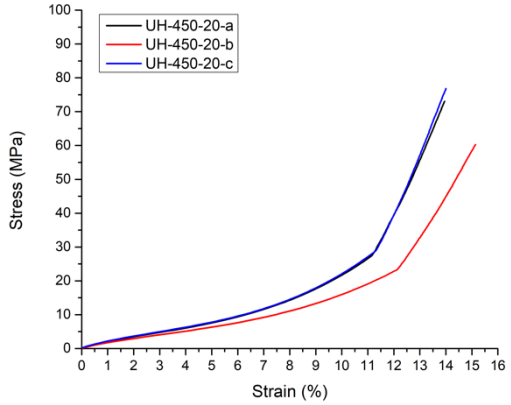	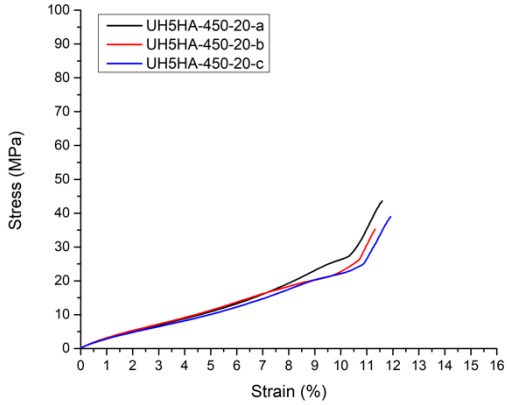	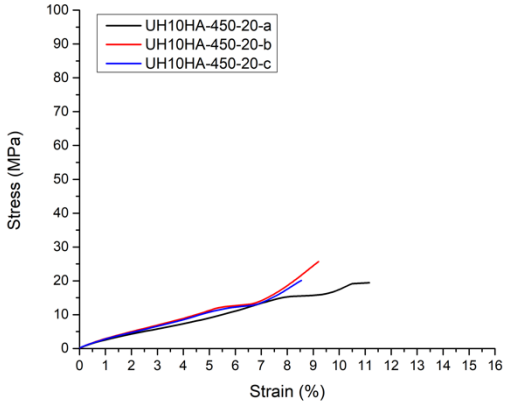

450 x 25 (ED = 1.389 J/mm^3)	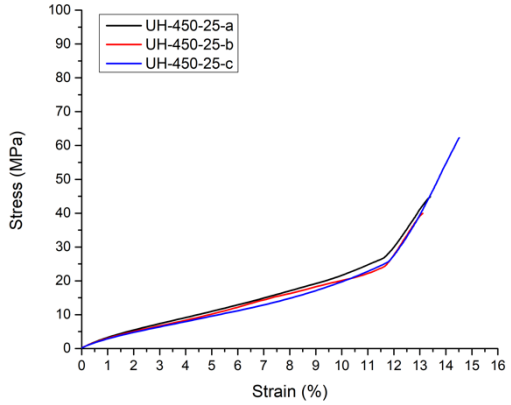	-	-

Conclusions of Chapter 4

Results have shown the capability of the SLS process to fabricated rectangular and cylindrical samples of UHMWPE/SDHA composites. The addition of SDHA particles have ameliorated powder flowability and increased the SLS sintering window. Indeed, SLS processing of UHMWPE is challenging, however, a better UHMWPE powder preparation and the employment of precise SLS equipment would be favourable for better results.

Mechanical properties have shown the great influence of SDHA content on strength values, moreover, SLS processing parameters also play an important role. For a better understanding of mechanical performance and the suitability of UHMWPE/HA composites to fabricate implantable devices, further mechanical assays should be conducted. Ultimately, pieces simulating the desired design should be fabricated, evaluating dimensional variation and mechanical properties.

Preliminary biological assays confirmed the non-toxicity and the support pre-osteoblast attachment of UHMWPE after SLS processing, either, sample surface topography has influenced cell behaviour. Nevertheless, SDHA particles were also revealed to be advantageous for UHMWPE processing and their use in more suitable SLS processing polymers should be explored. This would expand the potential of use to other types of implants.

CHAPTER 5
General Conclusions and Final Considerations

UHMWPE/HA composite samples were successfully produced by the selective laser sintering (SLS) technique, whereas the UHMWPE served as a flexible matrix to add SDHA particles to enhance bioactivity. Some of the fabricated rectangular samples achieved mechanical strength values compatible with the range of cortical bone. Likewise, the biological response of *in vitro* assays has shown the capability of using SLS-manufactured UHMWPE/HA composites to be used for implantable devices.

The submitted review article (Chapter 2) has extracted information from the bibliography regarding SLS processing of polymer/Ca-P composites. This work has summarized relevant information from different stages of SLS processing: material selection, mixture, employed equipment and processing parameters. Results have shown the novelty of using SDHA particles in composite mixtures as SLS feedstock. Likewise, morphological features of spray-dried particles demonstrate suitable characteristics for SLS processing. It was possible to observe the capability of the SLS technique to produce controlled porosity devices, in different ranges of size and materials combination. With the appropriate combination of materials and processing parameters, it is possible to fabricate diversified implantable devices.

Chapter 3 presented a screening method for the spray drying process intending to produce suited particles for SLS feedstock. Experiments indicated the importance of the suspension preparation and the selection of proper processing parameters. Finally, additional experiments have increased powder production efficiency without losing the desirable morphological features. In this work, spherical HA particles in the range of 15 to 25 μm were obtained with good process efficiency, demonstrating the aptitude of the spray drying process for preparing SLS feedstock materials.

Further bibliographic research, detailed at the end of Chapter 2, has demonstrated challenges associated with processing UHMWPE and its limitations. These aspects were evidenced in Chapter 4 while processing UHMWPE and UHMWPE/SDHA powders. Considerable dimension variation and narrow sintering window are the main drawbacks when SLS processing UHMWPE. The addition of SDHA has slightly contributed to a wider sintering window, however, UHMWPE is still highly influenced by thermal gradients while processing by SLS. To assess this issue, an accurate selection of processing parameters and precise SLS equipment is required.

Mechanical properties of the SLS fabricated samples have shown great dependency on processing parameters, moreover, lower ultimate strength is associated with higher SDHA content. Still, values compatible with cortical bone were achieved for most of the fabricated samples, except for UH10HA. The SLS fabricated samples were shown to be non-toxic, seem not to inhibit cell growth and were able to support pre-osteoblast attachment but with lower efficiency than pure HA dense disks. Surface finishing of the samples has impacted bone cell biology and further experiments must be assessed.

Future works should investigate the influence of SDHA on other polymers, preferably those which have better SLS processability such as polyamide (PA), polycaprolactone (PCL) and polylactide acid (PLA). Likewise, evaluate the feasibility and usefulness of manufacturing pieces using different contents of SDHA powder. Supplementary biological assays with more replications should also be conducted for a better understanding and more representative results. Finally, doped HA particles have shown very promising results and benefits for biological use; therefore, the spray drying process and SLS should also be evaluated.

RESUMO EXPANDIDO

SINTERIZAÇÃO SELETIVA A LASER DE BIOCOMPÓSITOS UHMWPE/HA PARA APLICAÇÕES EM TECIDO ÓSSEO

Introdução

Em virtude da disponibilidade de implantes personalizáveis, com geometrias complexas e combinação de diferentes tipos materiais, esses dispositivos promovem recuperação mais rápida, aumentando a qualidade de vida dos pacientes. Consequentemente, processos de manufatura aditiva (MA) têm sido estudados para solucionar diferentes problemáticas relacionadas à regeneração de tecidos ósseos. Isso se faz necessário quando há diagnóstico de patologias, como osteoporose, tumor, infecção, fraturas e desordens genéticas, que prejudicam ou impossibilitam o processo de recuperação natural e necessitam de intervenção cirúrgica.

Para tal, a técnica mais utilizada e com altas taxas de sucesso é o enxerto ósseo autógeno, no qual se retira um bloco ósseo do próprio paciente, com dimensões compatíveis ao local a ser efetuado o reparo. Dentre os fatores limitantes desse método, destaca-se a impossibilidade de recuperação de grandes defeitos ósseos, necessitando-se de outras técnicas para estes casos. Amplamente utilizados na regeneração do tecido ósseo, arcabouços tridimensionais porosos, conhecidos como *scaffolds*, são estruturas que mimetizam a matriz extracelular do tecido ósseo, servindo de alternativa para o enxerto ósseo.

O tecido ósseo humano possui uma complexa estrutura vascularizada, sendo composto de uma porção orgânica, com fibrilas de colágeno, e outra inorgânica, contendo cristais de fosfato de cálcio. Nesse sentido, a combinação de biopolímeros e biocerâmicos mostra-se oportuna devido à associação de propriedades fortemente desejadas, especialmente de biocompatibilidade e osteocondutividade.

Biocerâmica, em particular hidroxiapatita (HA), já é amplamente utilizada para implantes ósseos, por possuir características de osteocondução e biocompatibilidade. Entretanto, desafios no processamento desse tipo de material dificulta a obtenção de implantes personalizados.

Polímeros biocompatíveis propiciaram soluções para implantes devido às características de maior processabilidade. Diversos polímeros são empregados como matéria-prima, como é o caso do polietileno de ultra alto peso molecular (*Ultra High Molecular Weight Polyethylene*, UHWMPE), utilizado há décadas para implantes de quadril, joelho e ombro. Considerado de difícil processamento devido ao alto peso molecular por métodos convencionais, a MA se apresenta como alternativa para obtenção de peças, como por exemplo via sinterização seletiva a laser, que viabiliza o processamento deste material para obtenção de implantes customizáveis.

O processamento via sinterização seletiva a laser (*Selective Laser Sintering*, SLS) consiste na obtenção de peças 3D a partir da energia fornecida por um feixe de laser, que sinteriza as partículas depositadas sucessivamente em camadas. Esse processo é favorecido caso os materiais possuam uma combinação de características, sendo altamente desejável a preparação da matéria prima a ser utilizada.

Um dos processos que podem ser utilizados para modificar propriedades morfológicas das partículas de HA é a atomização (ou *spray drying*, SD), que permite a obtenção de partículas esféricas e com tamanho controlado. Partículas de HA obtidas por *spray drying* (SDHA) apresentam características morfológicas mais apropriadas para serem processadas via SLS, quando comparadas com partículas de HA sintetizadas.

Dessa forma, julga-se que a combinação de biocompósitos UHMWPE/SDHA utilizando o processo de SLS, seja apropriada para fabricação de dispositivos implantáveis para regeneração de tecido ósseo.

Objetivos

O objetivo geral deste trabalho é produzir e caracterizar amostras de UHMWPE/SDHA obtidas pelo processo de SLS.

Para tal, os objetivos específicos do trabalho proposto contemplam:

- Síntese e caracterização de pó nanométrico de HA estequiométrico.
- Investigar a aptidão do processo de *spray drying* para obter partículas de HA com característica morfológica esférica e gama de tamanho entre 15 e 25 μm.
- Selecionar parâmetros de processamento apropriados para o processamento de amostras UHMWPE/SDHA e verificar se propriedades mecânicas são apropriadas para uso em tecidos ósseos.
- Realizar ensaios biológicos para avaliar a biocompatibilidade das amostras.

Metodologia

A primeira etapa do trabalho envolveu a síntese e preparação do pó de HA. A síntese de HA foi efetuada por meio do processo de co-precipitação, o protocolo consiste na adição controlada de uma solução de fosfato (fosfato diamônico $(NH_4).2HPO_4$) em uma solução de cálcio (obtida a partir da dissolução de nitrato de cálcio: $Ca(NO_3)_2.4H_2O$). A quantidade de reagentes foi calculada para obter-se uma razão molar de Ca/P = 10/6. A síntese foi realizada em atmosfera de argônio, mantendo-se pH = 9 e temperatura de 85 ºC, com tempo de maturação de 100 minutos. Após, o preparado foi centrifugado e lavado com água destilada, secando-se a 100 ºC. O pó obtido foi submetido a um tratamento térmico de 650 ºC durante 30 minutos (rampa de 10 ºC/min) para remover subprodutos da reação.

O processo de síntese resultou pós nanométricos de HA, então submetidos a um processo de *spray drying* para produzir partículas com formato esférico e distribuição controlada de

tamanho de partícula. Para encontrar os parâmetros ideais de processamento, considerando o objetivo de se obter partículas esféricas homogêneas, com diâmetro médio de 15 a 25 μm, foram variados os parâmetros de fabricação por meio de um planejamento fatorial e de uma função de desejabilidade. O equipamento de *spray drying* utilizado possibilitou a variação dos seguintes parâmetros: temperatura de entrada, velocidade de aspiração, taxa de alimentação e pressão de atomização. Além desses, pode-se variar a concentração da suspenção inicial, em termos de quantidade de HA e de ligante (metilcelulose). As partículas de HA recuperadas após o processo de *spray drying* (SDHA) foram submetidas a um tratamento térmico com rampa de 3 °C/min até 500 °C para remoção do ligante, seguido por uma rampa de 10 °C/min até 1000 °C, mantendo-se esta temperatura por 1 h.

Métodos de caracterização como microscópio eletrônico de varredura (JEOL IT300LV e Quanta 450), difração de raios X (D8 Advance, Bruker), espectroscopia de infravermelho por transformada de Fourier, medidas de reologia (AR1500 TA Instruments, US) e análise de distribuição de tamanho de partícula por espalhamento a laser (Partica LA-950 V2, Horiba) foram empregados para as partículas de HA e SDHA.

A segunda parte do projeto contemplou a fabricação de amostras de UHMWPE/SDHA, por meio do processo de SLS, visando aplicações em engenharia de tecido ósseo. Amostras com dimensões de 35 × 5 × 1,40 mm, foram fabricadas utilizando 3 quantidades diferentes, em massa, de SDHA: 0% (UH); 5% (UH5HA) e 10% (UH10HA). Parâmetros de processo foram investigados, utilizando-se um planejamento fatorial com ponto central para avaliar a variação dos parâmetros de potência e velocidades do laser.

As amostras retangulares foram submetidas a análises mecânicas (Q800, TA Instruments) e medidas dimensionais por meio de paquímetro. A partir dos resultados de comportamento mecânico, selecionaram-se parâmetros de processamento para fabricação de amostras cilíndricas (10 × 5 mm) para efetuar análises biológicas de viabilidade e proliferação celular.

Resultados e Discussão

As etapas do trabalho resultaram na elaboração de artigos relacionados às atividades propostas na convenção de cotutela. Uma revisão bibliográfica a partir das bases de dados *Scopus*, utilizando palavras-chave pertinentes ao tema estudado, possibilitou elaborar um artigo com uma visão global da fusão em leito de pó de compósitos de polímeros/fosfato de cálcio.

Na primeira etapa do trabalho, verificou-se a possibilidade de obter partículas de HA com morfologia esférica, distribuição de tamanho de partículas uniforme e com diâmetro médio de 15 a 25 μm. Verificou-se que a modificação dos parâmetros de processo, especificamente taxa de alimentação e pressão de atomização, influenciam diretamente no tamanho das partículas obtidas. Igualmente, na preparação da solução inicial, deve-se atentar para as características reológicas e quantidade de sólido adicionado de modo que não haja aglomerados de HA ou alta viscosidade que impossibilite o processamento.

A segunda etapa do trabalho investigou a fabricação de amostras da mistura de UHMWPE com adição de partículas de SDHA. Os pós foram misturados mecanicamente, em diferentes composições: UH (100% UHMWPE), UH5HA (95% UHMWPE com 5% SDHA) e UH10HA (90% UHMWPE com 10% SDHA). Amostras retangulares (35 × 5 × 1,40 mm) foram fabricadas, variando-se parâmetros de processamento (potência e velocidade do laser) por planejamento fatorial. Propriedades mecânicas e variação dimensional foram avaliadas. Foram selecionados os parâmetros mais apropriados para fabricação de amostras cilíndricas (10 × 5 mm). Análises de viabilidade celular e proliferação foram realizadas.

Os resultados de análise dimensional evidenciaram contração e distorção das amostras fabricadas, fenômeno também observado na bibliografia relacionada. Constatou-se que uma maior densidade de energia propicia a sinterização de partículas localizadas no entorno da amostra, contribuindo para maiores dimensões. Ensaios mecânicos foram representados em

curvas de tensão-deformação, havendo queda de propriedades mecânicas com o aumento da proporção de SDHA na amostra. No entanto, maiores concentrações de SDHA favoreceram resultados de viabilidade e proliferação celular nas amostras.

Considerações Finais

Os resultados obtidos na primeira etapa apontam viabilidade de produção e modificação de características morfológicas apropriadas para sinterização seletiva a laser a partir de partículas nanométricas de hidroxiapatita. Na segunda etapa do trabalho, constatou-se a difícil processabilidade do pó de UHMWPE. Assim, o aumento da porção de SDHA nas amostras prejudica propriedades mecânicas. No entanto, a adição das partículas de SDHA demonstrou-se benéfica em relação à processabilidade dos materiais e em relação a atividade e proliferação celular.

Palavras-chave: *spray drying*; UHMWPE; hidroxiapatita; sinterização seletiva a laser; engenharia de tecido ósseo.

RESUMÉ ÉTENDU

FRITTAGE SÉLECTIF PAR LASER DE BIOCOMPOSITES UHWMPE/HA POUR L'INGÉNIERIE DU TISSU OSSEUX

Introduction

La possibilité de fabriquer des implants personnalisables, avec des géométries complexes et présentant différentes combinaisons de matériaux est devenu important pour la médicine. Ces dispositifs favorisent une récupération plus rapide, ce qui améliore la qualité de vie des patients. Les procédés de fabrication additive (FA) peuvent être utilisés pour résoudre différents problèmes liés à la régénération du tissu osseux. En effet, cela est nécessaire lorsqu'il y a un diagnostic de pathologies, telles que les tumeurs, les infections, les fractures et les troubles génétiques, qui altèrent ou rendent impossible le processus naturel de récupération et nécessitent une intervention chirurgicale.

A cet effet, la technique la plus utilisée, et avec des taux de réussite élevés, est la greffe osseuse autogène, dans laquelle un bloc osseux est retiré du patient, avec des dimensions compatibles avec l'emplacement à réparer. Parmi les facteurs limitants de cette méthode, l'impossibilité de récupérer des défauts osseux importants en particulier nécessite l’utilisation de techniques alternatives. Largement utilisés dans la régénération du tissu osseux, les architectures poreuses tridimensionnelles sont des structures qui imitent la matrice extracellulaire du tissu osseux ; ce sont des alternatives à la greffe osseuse.

Le tissu osseux humain possède une structure vascularisée complexe. Il est composé d'une partie organique, avec des fibrilles de collagène, et d'une partie inorganique, contenant des cristaux de phosphate de calcium. C’est pourquoi, l'association de biopolymères et de biocéramiques s'avère opportune, notamment du fait de la combinaison de leur propriétés.

Les biocéramiques phosphocalciques, particulièrement l'hydroxyapatite (HA), sont largement utilisées pour la fabrication d'implants osseux, en raison de leurs propriétés d'ostéoconduction et de biocompatibilité. Cependant les défis liés à la mise en forme de ce type de matériau rend difficile l'obtention d'implants personnalisés.

Les polymères biocompatibles fournissent des solutions pour l'élaboration ces implants personnalisés en raison de processabilité plus élevées. Plusieurs polymères sont utilisés comme matière première. On peut citer par exemple le polyéthylène à haut poids moléculaire (*Ultra High Molecular Weight Polyethylene*, UHWMPE). Il est utilisé depuis des décennies pour les parties travaillant en friction dans les implants de hanche, de genou et d'épaule. En raison de son poids moléculaire élevé le UHWMPE est considéré comme difficile à mettre en forme à l'aide les méthodes conventionnelles. Le frittage sélectif par laser (*Selective Laser Sintering*, SLS), qui est une méthode de fabrication additive (FA), se présente comme une alternative pour l'obtention de pièces car il permet une mise en forme du matériau et l'obtention d'implants personnalisables.

Le processus de frittage sélectif par laser consiste à obtenir des pièces 3D à partir de l'énergie fournie par un rayon laser, qui fritte les particules déposées successivement en couches. Ce processus est favorisé si les matériaux ont une combinaison de caractéristiques précise (particules sphériques avec un dispersion de taille contrôlé). Une préparation préalable de la matière première à utiliser est donc nécessaire.

L'atomisation (ou *spray drying*, SD) permet de maîtriser les propriétés morphologiques des particules d'HA. Cette méthode permet, à partir des particules d'HA synthétisées, d'obtenir des particules de taille et de morphologie maîtrisées. Les particules d'HA obtenues par *spray drying* (SDHA) ont les caractéristiques nécessaires pour une utilisation par procédé SLS.

Les poudres de biocomposites UHMWPE/SDHA obtenues et mises en forme par SLS, permettent la fabrication de dispositifs implantables pour la régénération du tissu osseux.

Objectifs

L'objectif général de ce travail est de produire et de caractériser des échantillons UHMWPE/SDHA obtenus par le procédé SLS. À cette fin, les objectifs spécifiques des travaux proposés comprennent :

- La synthèse et la caractérisation de poudre stœchiométrique d'HA nanométrique.
- L'étude de la capacité du procédé d'atomisation à produire des particules d'HA sphériques avec une gamme de taille comprise entre 15 et 25 μm.
- De sélectionner les différents paramètres de fabrication par SLS adaptés à la fabrication d'échantillons UHMWPE/SDHA et évaluer si les propriétés mécaniques sont appropriées pour des applications en substitution osseuse.
- D'évaluer *in vitro* la biocompatibilité des échantillons.

Méthodologie

La première étape du travail impliquait la synthèse et la préparation de la poudre de HA. La synthèse de HA a été réalisée par coprécipitation en voie liquide. Le protocole consiste en l'ajout contrôlé d'une solution de phosphate diammonique ($(NH_4).2HPO_4$) à une solution de calcium, obtenue à partir de la dissolution de nitrate de calcium ($Ca(NO_3)_2.4H_2O$). La quantité des réactifs a été calculée pour obtenir un rapport molaire de Ca/P = 10/6. La synthèse a été réalisée sous atmosphère d'argon, en maintenant pH = 9 et une température de 85 °C, avec un temps de maturation de 100 minutes. Ensuite, la préparation a été centrifugée et lavée avec de l'eau distillée puis séchée à 100 °C. La poudre obtenue a été soumise à un traitement thermique à 650 °C pendant 30 min, avec une rampe de 10 °C/min, pour éliminer les sous-produits de réaction.

La synthèse a abouti à des poudres de HA nanométriques, qui ont ensuite été soumises à un procédé d'atomisation afin de produire des particules de forme sphérique avec une distribution granulométrique contrôlée. L'objectif était d'obtenir des particules sphériques de distribution granulométrique homogène et d'un diamètre moyen de 15 à 25 µm.

L'étude des paramètres procédés a été faite à l'aide d'un plan factoriel et les conditions optimisées ont été mises en évidence grâce à une fonction de désirabilité. D'une part, l'équipement d'atomisation utilisé a permis de faire varier les paramètres suivants : température d'entrée, vitesse d'aspiration, débit d'alimentation et pression d'atomisation. D'autre part, la concentration de la suspension initiale, c'est-à-dire la quantité de poudre d'HA et de liant (méthylcellulose), a été optimisée. Les particules d'HA obtenues après le processus d'atomisation (SDHA) ont consolidé par traitement thermique avec une rampe de 3 °C/min jusqu'à 500 °C pour éliminer le liant, suivi d'une rampe de 10°C/min jusqu'à 1000 °C en maintenant cette température pendant 1 heure.

Les particules d'HA et de SDHA ont été caractérisées par microscopie électronique à balayage (JEOL IT300LV et Quanta 450), diffraction des rayons X (D8 Advance, Bruker), spectroscopie infrarouge à transformée de Fourier et granulométrie laser (Partica LA -950 V2, Horiba). Des études rhéologiques ont également été conduites (AR1500 TA Instruments, US).

La deuxième partie du projet comprenait la fabrication d'échantillons UHMWPE/SDHA, *via* le procédé SLS. Des échantillons mesurant 35 mm × 5 mm × 1,40 mm ont été fabriqués en utilisant 3 pourcentages massiques différents de SDHA : 0 % (UH), 5% (UH5HA) et 10% (UH10HA). Les paramètres procédés ont été étudiés à l'aide d'un plan factoriel à point central afin d'évaluer l'influence de la puissance et de la vitesse du laser.

Les propriétés mécaniques des échantillons rectangulaires obtenus ont été évaluées (Q800, TA Instruments) et des mesures dimensionnelles réalisées en utilisant un pied à coulisse digital. Les paramètres permettant d'obtenir les résultats mécaniques les plus probant ont

ensuite été utilisés pour la réalisation d'échantillons cylindriques (10 mm × 5 mm) destinés aux analyses biologiques de viabilité et de prolifération cellulaire.

Résultats et discussion

Les étapes du travail ont abouti à la rédaction et à la soumission de trois articles scientifiques liés aux activités proposées dans l'accord de cotutelle de thèse. Une revue bibliographique depuis la base de données *Scopus*, en utilisant des mots clés pertinents par rapport à la thématique étudiée, a permis la rédaction d'un article permettant d'avoir une vue globale de la fusion en lit de poudre de composites polymère/phosphate de calcium.

Dans la première étape du travail, la possibilité d'obtenir des particules d'HA de morphologie sphérique, une distribution granulométrique uniforme et un diamètre moyen de 15 à 25 µm par atomisation a été vérifiée. Il a été constaté que la modification des paramètres du procédé, notamment la vitesse d'alimentation et la pression d'atomisation, influencent directement la taille des particules obtenues. De même, lors de la préparation de la solution initiale, il est important de prêter aux caractéristiques rhéologiques de la suspension (viscosité trop élevée) et à la quantité de solide ajoutée afin de limiter la formation d'agglomérats d'HA qui rendent le procédé irréalisable.

La deuxième étape du travail a porté sur la fabrication d'échantillons composites UHMWPE / particules de SDHA. Différentes compositions de poudres ont été mélangées mécaniquement : UH (100% UHMWPE), UH5HA (95% UHMWPE avec 5% SDHA) et UH10HA (90% UHMWPE avec 10% SDHA). Des échantillons rectangulaires (35 mm × 5 mm × 1,40 mm) ont été fabriqués, en faisant varier les paramètres de processus (puissance et vitesse du laser) par un plan factoriel. Les propriétés mécaniques et la variation dimensionnelle ont été évaluées. Les paramètres les plus appropriés pour la fabrication d'échantillons cylindriques (10

mm × 5 mm) ont été sélectionnés. Des analyses de viabilité cellulaire et de prolifération ont été effectuées.

Les résultats de l'analyse dimensionnelle ont montré une contraction et une distorsion des échantillons fabriqués, un phénomène également observé dans la bibliographie. Il a été constaté qu'une densité d'énergie plus élevée permet une meilleure cohésion des particules situées en périphérie de l'échantillon, contribuant à des dimensions plus grandes. Les tests mécaniques ont été représentés à l'aide de courbes contrainte-déformation. Une altération des propriétés mécaniques lié à une augmentation de la proportion de SDHA dans l'échantillon a été observées. Cependant, des concentrations plus élevées de SDHA ont favorisé la viabilité et la prolifération cellulaire dans les échantillons.

Conclusion

Les résultats obtenus démontrent la faisabilité de la production par atomisation de particules d'hydroxyapatite nanométriques de morphologie contrôlée adaptées au processus de frittage sélectif par laser. L'élaboration de composite UHMWPE /HA par SLS, il a été constaté qu'une quantité importante de SDHA dans les échantillons altère les propriétés mécaniques. Cependant, l'ajout de particules de SDHA permet d'améliorer la processabilité SLS des matériaux ainsi que la biocompatibilité des composites.

Mots-clés : *spray drying* ; UHMWPE ; hydroxyapatite ; frittage sélectif par laser ; ingénierie du tissu osseux.